2009-09-25

Pore Size Characterization of Monolithic Capillary Columns Using Capillary Flow Porometry

Yan Fang
Brigham Young University - Provo

PORE SIZE CHARACTERIZATION OF MONOLITHIC CAPILLARY COLUMNS USING CAPILLARY FLOW POROMETRY

by

Yan Fang

A dissertation submitted to the faculty of

Brigham Young University

in partial fulfillment of the requirements for the degree of

Doctor of Philosophy

Department of Chemistry and Biochemistry

Brigham Young University

December 2009

BRIGHAM YOUNG UNIVERSITY

GRADUATE COMMITTEE APPROVAL

of a dissertation submitted by

Yan Fang

This dissertation has been read by each member of the following graduate committee and by majority vote has been found to be satisfactory.

Date	Milton L. Lee, Chair
Date	H. Dennis Tolley
Date	Steven W. Graves
Date	Steven R. Goates
Date	David V. Dearden

BRIGHAM YOUNG UNIVERSITY

As chair of the candidate's graduate committee, I have read the dissertation of Yan Fang in its final form and have found that (1) its format, citations and bibliographical style are consistent and acceptable and fulfill university and department style requirements; (2) its illustrative materials including figures, tables, and charts are in place; and (3) the final manuscript is satisfactory to the graduate committee and is ready for submission to the university library.

Date	Milton L. Lee Chair, Graduate Committee

Accepted for the Department

David V. Dearden
Graduate Coordinator

Accepted for the College

Thomas W. Sederberg
Associate Dean, College of Physical and Mathematical Sciences

ABSTRACT

PORE SIZE CHARACTERIZATION OF MONOLITHIC CAPILLARY COLUMNS USING CAPILLARY FLOW POROMETRY

Yan Fang

Department of Chemistry and Biochemistry

Doctor of Philosophy

A simple capillary flow porometer (CFP) was assembled for pore structure characterization of monolithic capillary liquid chromatography columns based on ASTM standard F316-86. Determination of differential pressures and flow rates through dry and wet samples provided the necessary information to determine the through-pore throat diameter, bubble point pore diameter, mean flow pore diameter, and pore distribution. Unlike measurements in bulk using traditional techniques to provide indirect information about the pore properties of monolithic columns, monoliths can be characterized in their original chromatographic forms with this system.

The performance of the new CFP was first evaluated by characterizing the pore size distributions of capillary columns packed with 3, 5, and 7 μm diameter spherical silica particles. The mean through-pore diameters of the three packed columns were measured to be 0.5, 1.0 and 1.4 μm, which are all smaller than the pore diameters calculated from a close-packed arrangement (i.e., 0.7, 1.1 and 1.6 μm), with distributions ranging from 0.1 -

0.7, 0.3 - 1.1 and 0.4 - 2.6 μm, respectively. This is reasonable, since visual inspection of SEM images of the particles showed relatively large fractions of smaller than specified particles in the samples. Typical silica monoliths were fabricated via phase separation by polymerization of tetramethoxysilane (TMOS) in the presence of poly(ethylene glycol) (PEG). The mean pore diameter and pore size distribution measured using the CFP system verified that a greater number of pores with small throat diameters were prepared in columns with higher PEG content in the prepolymer mixture. SEM images also showed that the pore diameters of monoliths fabricated in bulk were found to be smaller than those in monoliths synthesized by the same procedure, but confined in capillary tubes.

The CFP system was also used to study the effects of column inner diameter and length on pore properties of polymeric monoliths. Typical monoliths based on butyl methacrylate (BMA) and poly(ethylene glycol) diacrylate (PEGDA) in capillary columns with different inner diameters (i.e., 50 to 250 μm) and lengths (i.e., 1.5 to 3.0 cm) were characterized. The mean pore diameters and the pore size distributions indicated that varying the inner diameter and/or the length of the column affected little the pore properties. The latter finding is especially important to substantiate the use of CFP for determination of monolithic pore structures in capillaries. The results indicate that the through-pores are highly interconnected and, therefore, pore structure determinations by CFP are independent of capillary length.

A negatively charged polymer monolith based on BMA, ethylene glycol dimethacrylate (EDMA) and 2-acryloylamido-2-methylpropanesulfonic acid monomer (AMPS), was successfully prepared in silica sacrificial layer, planar (SLP) microchannels.

Extraction of FITC (fluorescein 5-isothiocyanate) labeled phenylalanine and capillary electrochromatography (CEC) of FITC labeled glycine using this monolithic stationary phase were demonstrated.

ACKNOWLEDGEMENTS

I remember fondly the first day when I arrived at Brigham Young University five years ago, which seems just like yesterday. As I recall the past years at BYU, I am very grateful to many people who have given me support in my studies and everyday life. Without them, I could not have gone so far away from home and accomplished my cherished degree.

First, I would like to give my sincere appreciation and best wishes to my advisor, Dr. Milton L. Lee, for his guidance, patience, encouragement and support. Being mentored by him through these years has been a great pleasure and fortune for me, which has helped me overcome difficulties many times. Dr. Lee is not only a very successful scientist but also a considerate person. His character will greatly affect me in my future career and life.

Second, I would like to sincerely thank all of my other committee members: Dr. H. Dennis Tolley, Dr. Steven W. Graves, Dr. Steven R. Goates and Dr. David V. Dearden , for their time, instruction, and suggestions during my progress reports and preparation of this dissertation.

Third, I appreciate the help, discussions and friendships of the former and current members in our group and some close friends: Dr. Binghe Gu, Dr. Nosa Agbonkonkon, Dr. Shu-ling Lin, Dr. Yansheng Liu, Dr. Aaron Nackos, Lailiang Zhai, Dr. Yue Zhao, Na Li, Peng Xu, Yu Zhang, Miao Wang, Ying Peng, Xin Chen, Dr. Yun Li, Jacoline Murray, Tai Truong, Jesse Contreras, Jie Xuan, Dan Li and Kun Liu. We enjoyed fun and valuable times together during these years at BYU.

Most importantly, I would like to give my deepest love and appreciation to my family members: my husband Yan Li, my parents Xihu Fang and Shuzhen Yuan, my parents in law Ping Li and Xiaoling Li, my brother Zhanbo Fang and my cousin Ming Ma. During these years, they always supported me with true love, understanding and trust. Hence, I always felt happiness in my life and dared to try new things and take challenges to achieve my personal goals.

Finally, I thank the Department of Chemistry and Biochemistry at Brigham Young University for providing me such a great opportunity and generous financial support for my graduate studies. Financial support from the National Institutes of Health and Berkeley HeartLab are also greatly appreciated.

TABLE OF CONTENTS

LIST OF ACRONYMS

AFM	atom force microscpy
AMPS	2-acryloylamido-2-methylpropanesulfonic acid monomer
ASTM	american society for testing and materials
BET	Brunauer, Emmett, Teller
BJH	Barrett, Jovner, Halenda
BMA	butyl methacrylate
CE	capillary electrophoresis
CEC	capillary electrochromatography
CFP	capillary flow porometry
DMPA	2,2-dimethoxy-2-phenyl-acetophenone
DMSO	dimethyl sulfoxide
EDMA	ethylene glycol dimethacrylate
EOF	electroosmotic flow
ESEM	environmental scanning electron microscopy
FEGSEM	field emission gun scanning electron microscopy
FITC	fluorescein 5-isothiocyanate

GC	gas chromatography
Gly	glycine
GMA	glycidyl methacrylate
HPLC	high performance liquid chromatography
ISEC	inverse size-exclusion chromatography
LC	liquid chromatography
LIF	laser induced fluorescence
MIP	mercury intrusion porosimetry
MS	mass spectrometry
MTMS	methyltrimethoxysilane
OTC	open-tubular columns
PECVD	plasma enhanced chemical vapor deposition
PEEK	polyetheretherketone
PEG	poly(ethylene glycol)
PEGDA	poly(ethylene glycol) diacrylate
Phe	phenylalanine
PMMA	poly(methylmethacrylate)

PMT	photomultiplier tube
PNM	pore network model
PPM	parallel pore model
PSD	pore size distributions
SEC	size-exclusion chromatography
SEM	scanning electron microscopy
SFC	supercritical fluid chromatography
SLP	sacrificial layer, planar
***μ*TAS**	micro total analytical system
TEM	transmission electron microscopy
THF	tetrahydrofuran
TMOS	tetramethoxysilane
TPB	total pore blocking
TPM	3-(trimethoxysilyl)propylmethacrylate
UHPLC	ultrahigh pressures liquid chromatography

LIST OF TABLES

LIST OF FIGURES

CHAPTER 1 BACKGROUND AND SIGNIFICANCE

1.1 Miniaturization of Liquid Chromatography Columns

Classical liquid chromatography (LC) has been around for quite a long time. Typically, stainless-steel columns with diameters of 1, 2, and 4.6 mm i.d. and lengths of 10-25 cm are packed with 3, 5, and 7 μm diameter spherical silica particles and used with commercial pumping systems. In order to obtain high chromatographic efficiency, longer columns have been investigated, however, the required pressure to pump the mobile phase through the column is too large to be practical.

Based on chromatographic theory, separation efficiency can be improved if the particle size of the materials used for the stationary phase is reduced. As high performance liquid chromatography (HPLC) developed, the particle size of the packing materials progressively became smaller. In modern HPLC, the stationary phases used are called microparticulate column packings and are uniform, porous, spherical silica particles. C-18 alkyl groups are usually attached on the silica surface to create a bonded phase for reversed phase LC.

Recently, efforts have been made to reduce the diameter of the column itself. The advantages of miniaturization of LC columns are: (1) low consumption of both mobile and stationary phases, (2) better detection sensitivity, (3) high resolution with long columns, (4) applicability of temperature programming, (5) convenience in selection of operating conditions, and (6) coupling with mass spectrometry (MS).[1-4]

When the column dimensions are miniaturized in micro-HPLC, the required amount of stationary phase is small. Therefore, expensive and valuable materials can

be used. Furthermore, toxic, flammable or exotic mobile phases can also be used. The column efficiency is theoretically independent of the column diameter, however, the concentration of solutes eluting from the column is inversely proportional to the square of the inner diameter of the column. Therefore, it is possible to gain better detection limits in micro-HPLC with the use of a concentration-sensitive detector. Since multi-path dispersion can be decreased and the heat generated by the pressure drop can be effectively dissipated in micro-HPLC, high resolution with long columns can be achieved. The small heat capacity of microscale columns also can facilitate the application of temperature programming. When operating conditions need to be optimized for new samples, it is convenient that only a few milliliters of mobile phase are required. In micro-HPLC, the flow rate of the mobile phase is very low, which makes the direct coupling to MS much easier.

Open tubular columns are quite different from conventional packed columns. In these columns, the stationary phase is only coated on the inner surface of the capillary, forming a thin film. Compared with packed columns, open tubular columns provide good permeability, however, due to low solute diffusion in liquids, poor chromatographic efficiency results.

1.2 Packed Capillary LC Columns

According to the inner diameter (i.d.) of the column, packed columns can be classified as large diameter, microbore and packed capillary columns. Large diameter columns are commonly used in LC and supercritical fluid chromatography (SFC). Tubes with i.d. between 2-5 mm and 5-25 cm in length are generally packed with

uniformly sized spherical particles with diameters between 3 and 10 μm. Most of the column tubes are made from stainless steel due to both its high strength under pressure and chemical inertness. Glass or polyetheretherketone (PEEK) are also available for applications in which greater inertness is required, but high pressure is not critical.

Microbore columns filled with 3-10 μm uniform packing materials, typically having 1 mm i.d. and 10-100 cm in length, are also used in LC and SFC applications. Tubing for microbore columns must have a smooth finish with deviations less than 2 μm. Therefore, glass-lined stainless steel tubing is preferred because it not only has a smooth inner surface, but it is also chemically inert and strong enough to withstand high pressures.

Packed capillary columns usually have i.d.s between 20-500 μm and range from 10 to 200 cm in length. In most cases, fused silica tubing is chosen as column material because it has good mechanical strength and flexibility, which makes it easy to handle and strong enough to withstand pressures up to 800 bar. To prepare a capillary column, four steps are required: cutting the fused silica capillary, deactivating the column surface, attaching end frits and fittings, and packing the column. Compared with large diameter and microbore columns, the advantages of capillary columns are their low flow rate, typically 1-10 μL/min, high column efficiency, low heat capacity, improved sensitivity for concentration-sensitive detectors, and ability to analyze small sample amounts. Therefore, they are being used increasingly in LC, SFC, gas chromatography (GC), and multidimensional chromatography.[5]

Particle size, particle configuration, and column diameter play very important roles in determining the separation speed and efficiency. Theoretically, small particles (<3 μm) can facilitate fast and highly efficient separations in HPLC because of the reduced intraparticle mass transfer resistance due to the short diffusion distance and, to a lesser extent, the small contribution of "eddy diffusion" to the plate height.[6-7] However, since the pressure drop along the length of a packed column for optimum linear velocity is inversely proportional to the square of the particle diameter, using very small particles coupled with short analysis time stresses conventional pressure pumping systems because of the higher pressures that are required.[8-13] Therefore, a compromise is necessary between the required column efficiency and the pressure drop in the column, which is accomplished by adjusting the column length. However, in order to separate a wide range of compounds in complex mixtures, obtaining high column efficiency is essential. Highly efficient and rapid separations have recently been achieved by using small particle-packed columns and ultrahigh pressures (UHPLC), electroosmotic flow (capillary electrochromatography, CEC), or by employing monolithic column packings instead of packed particles in HPLC.[14]

1.3 Monolithic Capillary Columns

A monolithic column is defined as a column consisting of single continuous rod that possesses an interconnected skeletal structure with interconnected flow paths (through-pores).[14] In the past ten years, monolithic columns have emerged as a new approach to alleviate the pressure-drop limitation of packed bed columns. Monolithic columns were pioneered by Hjertén et al., Svec and Fréchet, Horvath, and Tanaka,

and have already resulted in a number of well-performing, commercially available polymeric and silica monolith columns.[15-21] In contrast to particle-packed columns, a monolithic column can be formed with small skeletal structure and large through-pores, which can simultaneously reduce both flow resistance and stationary phase support diffusion path length. Therefore, both high permeability and high column efficiency can be realized from a support structure having a large (through-pore-size)/(skeleton-size) ratio, which is not possible with a particle-packed column with a [through-pore (interstitial void)-size]/(particle-size) ratio in the range of 0.25-0.4.[14]

Monolithic silica columns can be prepared either in a mold, such as in a 6-9 mm i.d. glass test tube, or in a fused silica capillary with an i.d. smaller than 250 μm.[14,22,23] Tanaka et al. developed a method to prepare a porous monolith based on hydrolytic polymerization of tetramethoxysilane (TMOS) accompanied with phase separation in the presence of water-soluble organic polymers (such as poly(ethylene glycol), PEG). The morphology of the silica monolith usually has a bimodal structure consisting of micrometer-sized through-pores and meso- or micro-porous skeleton.

The early methods for silica monolith preparation involve gelation followed by further treatment with aqueous ammonium hydroxide solution at 40℃ for 24 h to form mesopores. Later, when the method was optimized, urea replaced ammonium hydroxide. All of the components were mixed together before reaction. In the first 22 h, gelation occurred at 40℃; then, as the temperature was increased to 120℃ for 3 h, mesopores were formed with the generation of ammonia by hydrolysis of urea. In this

way, extra acid washing was avoided and the preparation procedure became simpler. Standard conditions for preparing monolithic silica columns were optimized by Tanaka et al. and are commonly used today. Commercial monolithic silica columns manufactured according to these conditions are also available.

With the use of tetramethoxysilane (TMOS) as the crosslinker, large voids along the wall of a large-diameter capillary cannot be avoided because of serious shrinkage of the silica skeletal structure. The problem can be minimized by attachment of the silica monolith to the wall of a smaller diameter capillary, i.e., 50 or 75 μm diameter. However, if methyltrimethoxysilane (MTMS) is mixed with TMOS in a ratio of 3:1, successful silica monolithic columns with comparable performances can be fabricated in capillaries with inner diameters as large as 200 μm.

Motokawa et al. [24, 25] reported that hybrid-type monolithic silica columns with different domain sizes (i.e., combined distance across one skeletal unit and through-pore, or a unit of network structure after phase separation during formation), can be prepared by adjusting the content of the components in the starting mixture. In this report, keeping all other conditions constant, as the content of PEG was increased from 8.8 to 12.8 g, the domain size of the silica monolithic column was reduced from 10 to 3 μm. The conclusion was that increasing the amount of PEG results in a decrease in the domain size.

Hara et al.[26] also studied the effect of the content of TMOS on domain size. It was found that when the rest of the conditions remained constant, silica monolithic columns with a smaller domain size were prepared with higher TMOS concentration

or with a higher concentration ratio of TMOS to PEG.

Due to their easy preparation, ease of attachment to the glass surface, elimination of packing procedure and excellent performance, polymer monolithic stationary phases in capillary columns have grown in interest in the last few years.[27, 28] Unlike packed columns, polymer monoliths do not need frits to hold them in place, they can be made from a variety of monomers to provide tunable selectivities, they can be cured thermally or with ultraviolet light, and they readily fill the available space during formation. These features make them well fitted for chromatography. [29-36]

Three steps are normally required in the formation of a polymer monolith in both capillary and microchip formats: glass surface modification, polymerization of the monomer reagents, and rinsing out excess reagents and porogens. The presence of silanol groups on the silica capillary column surface favors a variety of chemical reactions, so double bonds can be introduced easily to immobilize the monolith, such as by reacting with 3-(trimethoxysilyl)propylmethacrylate (TPM).[29, 37, 38] Currently, two approaches are usually involved in the synthesis of polymer monoliths. Copolymerization was originally reported and still remains the most popular method, especially for affinity chromatography and enzyme immobilization.[34, 35] Grafting is a newer method developed to introduce new chemistries. Grafting by deep UV has particularly gained popularity recently. Before polymerization, liquid monomer solution is carefully introduced into the surface functionalized fused silica capillary. Under initiation by heat or UV light, the morphology of the porous polymer monolith forms by phase separation that occurs as

the monomers polymerize. As the polymer grows and becomes less polar with the depletion of monomers, its solubility decreases in the surrounding solvent which becomes more polar. As the polymer continues to grow, the solvent-rich and polymer-rich phases separate, thus resulting in an interconnected network of polymer nodules surrounding solvent-filled pores.[39-42] After polymerization, the solvents (porogens) are flushed out of the column to create the porous monolith.

Monolith skeletal porosity is very important in flow-through applications, since large surface area provides more active sites for effective interactions. At the same time, good permeability allows faster separation and low back-pressure. Therefore, both large surface area and good permeability are desirable characteristics of a good quality monolith. The monolith pores can be categorized into three groups based on diameter: macropores (＞ 50 nm), mesopores (2 - 50 nm), and micropores (＜2 nm). Mesopores and micropores are critical to provide high surface area while macropores mainly contribute to permeability. In many cases, a large surface area is not accompanied by good permeability, and vice versa. Therefore, reaching a desirable balance between surface area and pore permeability by optimizing experimental conditions is quite necessary.

Several factors affect the pore size distribution of a polymer monolith, including initiator concentration, total monomer to total porogen ratio, monomer to crosslinker ratio, porogen nature, ratio of porogens, and photopolymerization time. In general, good permeability can be obtained by decreasing the amount of initiator, however, at the cost of longer reaction time. There is also a straightforward method to decrease

the pressure drop in a monolithic column, i.e., decreasing the total monomer to total porogen ratio. Unfortunately, a decrease in the homogeneity and rigidity of the monolith occurs as well. The same will happen when changing the monomer to crosslinker ratio. Studies also show that the smaller the column diameter, the larger the pore size distribution that can be obtained. This is because the heat produced from the reaction can be dissipated faster in a column with small diameter than in one with large diameter. The temperature directly affects the number of nuclei which are generated from the initiator. When the temperature is low, the initiator decomposes slower and produces larger clusters of nuclei. As a result, monoliths with larger pore structure can be created.

As described above, the onset of phase separation (i.e., polymer chain precipitation from the porogen) is critical for controlling the pore size distribution of the resulting monolith. Therefore, the selection of porogens is key to obtaining good permeability. Furthermore, the selection of porogens is unlimited and does not affect the composition and rigidity of the monolith. Porogen mixtures with different solvent strengths are prepared by adjusting the good solvent to poor solvent ratio. In general, good solvents will generate monoliths with small through-pores due to later onset of phase separation, while poor solvents yield monoliths with large through-pores, resulting in good permeability.

1.4 Monoliths in Microfluidic Devices

Adapting current LC methods to the chip format is of interest in the quest for an LC-based micro total analytical system (μTAS). Silicon,[43] polymer,[44] and glass[45] are

three major substrate materials used for microfabrication. The early microdevices were fabricated from silicon because it is widely used in the microelectronics industry, and successful fabrication techniques were established. However, because silicon is not transparent to visible or UV wavelengths for optical detection, it has been replaced by other materials, such as glass and quartz.

Microchips used for the separation of biological molecules have gained much attention due to their distinct advantages, such as fast analysis, small sample consumption, separation and detection in a single device, etc.[46] Separation processes based on electrophoresis or electroosmotic flow in open tubular or surface-modified microchannel formats have been performed for biomolecular separations.[47, 48] Chromatography is more versatile and reliable for protein separation, so efforts have been placed on introducing stationary phases in the channels. Packing columns with particles and attaching retaining frits in a chip are difficult.[49] Open tubular chromatography with polymer coatings on the channel walls continues to suffer from low surface area and, hence, low loading capacity.[48] Casting of soft polymers in chips for electrochromatography and pressure-driven chromatography can provide separations as good as those based on capillaries.[50] A microchip with open segments for sample injection and detection would be desirable for protein separation.

In comparison to silicon and polymer microchips, glass is the dominant material used for microfluidic device fabrication, since it has good optical, mechanical, electrically insulating and thermal properties. Moreover, glass surfaces are easy to modify because surface chemistries have been well-established. Thermal bonding is a

difficult step used in glass microchip fabrication to seal a cover plate to a micromachined substrate for channel enclosure.

The standard surface modification procedure using silane chemistry is employed for attaching monoliths in glass microchip channels. First, to produce as many hydroxyl groups on the surface as possible, the channels are rinsed with acetone and water, followed by activation with 0.2 mol/L NaOH for 30 min. The channels are then washed with water, activated with 0.2 mol/L HCl for 30 min, washed with water and acetone again, and finally dried at 120℃ for 1 h. In a following step, double bonds are introduced by filling a 30 vol. % acetone solution of 3-(trimethoxysilyl)propyl methacrylate in the channels and sealing the channel ends. After reacting for 24 h at room temperature, the solution is washed with acetone, leaving the channels dry for monolith preparation. Monoliths have been successfully prepared in glass microchips for various applications, such as enzymatic microreactor, [51] non-mechanically actuated valve, [52, 53] passive micromixers to enhance mixing efficiency for on-chip labeling reactions, [54, 55] on-chip solid-phase extraction and preconcentration,[56, 57] and fast HPLC separation of proteins and peptides.[58]

Polymer materials are popular for microfabrication since they offer attractive mechanical and chemical properties, low cost, ease of fabrication, biocompatibility, and high flexibility. However, most commercial polymers can adsorb biomolecules through hydrophobic, electrostatic or other interactions, leading to sample loss, analytical irreproducibility, and poor separations. Therefore, efforts have been made to develop strategies for passivating polymer substrates, such as cold plasma

discharge treatment, [59] transamidation using lithiated diamines with subsequent reaction of the amine groups, [60] UV-initiated grafting with ethylene diacrylate, [61] and forming octadecylated surfaces for hot-embossed poly(methylmethacrylate) (PMMA) devices.[62, 63, 64]

1.5 Pore Characterization of Monolithic Columns

Porosity, pore size distribution, surface area, bubble point and mean flow pore size are important characteristics of a porous material. Porosity is the void volume of the porous material usually expressed as the percentage of the total volume. Each porous material has its own specific desired porosity for different applications. A pore cross-section can be circular or irregular. The pore sizes of pores with circular cross-sections are expressed in terms of diameter, while pores with irregular cross-section are defined as the diameter of a circular opening whose perimeter to area ratio is a circular pore at the same location.[65] That is,

$$(\text{Perimeter}/\text{Area})_{\text{pore}} = (\text{Perimeter}/\text{Area})_{\text{circle of diameter d}} \quad (1.1)$$

This is the way that many techniques, such as MIP and BET, measure the diameter of a pore along the channel of the pore. A porous material normally has a range of pore sizes, which may appear in a unimodal or multi-modal distribution.

Pores in porous materials form channels for fluid flow. As shown in Figure 1.1, if a channel starts from one surface and terminates inside the material, such pores are called blind pores. However, if the channel can extend from one free surface to another, the pores are called through-pores. If a pore is completely enclosed inside the material, it is called a closed pore. Closed pores influence the bulk density of the

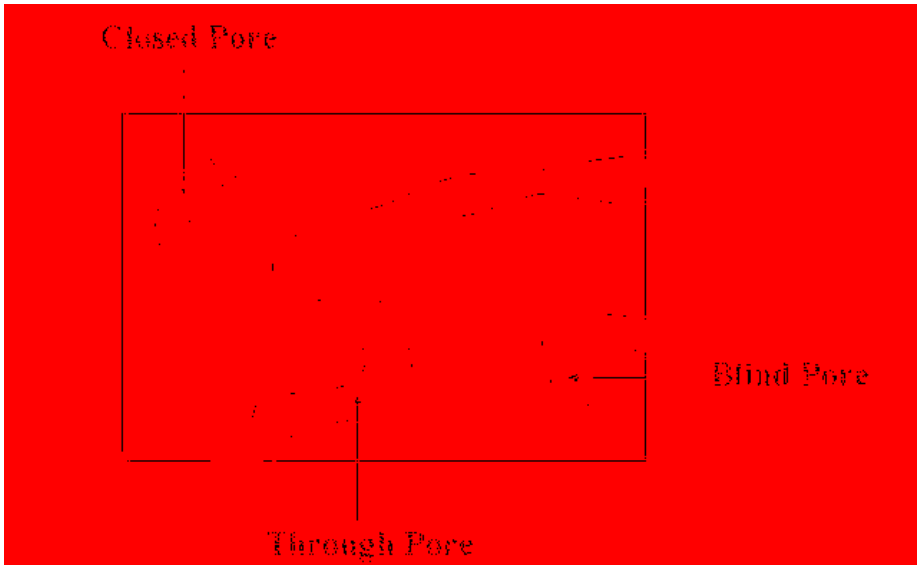

Figure 1.1 Three different kinds of pores.

material. Blind pores influence not only the bulk density of the material, but also the amount of liquid and gas that can be stored in the material. Through-pores are responsible for flow, so they influence the fluid flow rate and the storage capacity for liquids, as well as bulk density.

The surface area of the pore walls is determined by the pore shape, pore size and the roughness of the walls. Pores can be divided into three types based on their sizes, i.e., macropore, mesopore, or micropore. The surface area of closed pores is not useful, contrary to blind and through-pores. The surface area of through-pores, also called envelope surface area, influences flow rate and separation. In a porous material, the largest pore size is often known as the bubble point pore size. The rate of fluid flow is determined by the permeability of the material and can be described in terms of both gas permeability and liquid permeability. The mean flow pore size is taken as a measure of filter performance. All of these barrier properties of porous materials are important for industrial applications.

The morphology and pore structure of porous media are important in the design of separation columns due to their influence on the hydrodynamic properties (e.g., flow properties), thermodynamic properties (e.g., loadability) and mass transfer kinetics (e.g., efficiency). There are two classes of traditional methods for determining pore size and morphology. Microscopic techniques, such as SEM and X-ray analysis, provide actual images of the surface, but no quantitative characterization of the surface area and pore volume. They are also quite involved, time consuming and expensive. However, macroscopic measurement techniques, such

as BET and MIP can determine the macroscopic effects of phenomena occurring in the pore volume and on the pore surface rapidly and inexpensively.[66] SEM, MIP, BET and ISEC (inverse size-exclusion chromatography) are four traditional methods for pore size characterization of packed and monolithic columns, and have been used for decades.[67]

Generally, SEM can provide direct images of monoliths. A monolithic structure with pores and skeleton can be reflected. How well a monolith attaches to the capillary wall also can be observed if the original morphology is not destroyed by the vacuum. Pore size distribution and mean pore diameters can be roughly estimated, and the pore size difference between two monoliths can be observed. Although SEM only provides very limited and rough information about monoliths, it is always chosen by scientists as the first choice and an indispensable method to obtain preliminary structural information about monoliths, because it is simple, fast and easy to perform, and it provides visual information.

Because MIP is a much more accurate and very traditional technique for pore size characterization of a variety of materials, it is used almost as popularly as SEM for characterizing the pore structures of monoliths. MIP tests samples in bulk format and provides information about blind and through-pores based on volume measurements. Mostly, this technique determines macropores and mesopores between 300-0.03 μm diameter. Unavoidably, toxic mercury is used and very high pressure is required.

Another very traditional technique for pore characterization of materials is BET. BET requires bulk samples and can measure blind and through-pores also, based on the determination of surface area. The measurable diameter range is approximately 1-0.0005 μm, so it is usually applied to determine mesopores and micropores.

ISEC is the only chromatographic-based technique that can provide information about mesopore and micropore distributions. An HPLC system, tetrahydrofuran (THF) solvent and polystyrene standards are required to use this technique. Due to the limited information it can provide, ISEC is not used as often as MIP or BET for general purpose pore-size characterization.

Grimes et al.[68] formulated two models, the parallel pore model (PPM) and pore network model (PNM), based on the first moments of the column response to a pulse injection, to measure ISEC curves for six silica monoliths having different macropore and mesopore diameters. PPM and PNM are able to determine the void fractions of the macropores and silica skeleton, the pore connectivity of the mesopores, as well as the pore number distribution and pore volume distribution of the mesopores. They are more applicable for columns with small diameter macropores and/or large macropore void fractions. PPM is an idealization with some limited assumptions, while PNM can be used directly to characterize real porous media.

Guiochon and co-workers[69] investigated the porosities of 4.6 mm i.d. silica monolithic columns using ISEC with polystyrene standards ranging from 550 to 1,860,000 in molecular weight. The study illustrated that in these monolithic columns, the macropore network accounted for approximately 75-80 % of the total porosity

with pore diameters of 0.3 μm and larger, the mesopores represented 10-15 % of the total porosity and their average size was generally between 10-20 nm, and only a small percentage of the total porosity corresponded to micropores. The results indicated that the external and the total porosities of the silica monolithic columns were much higher than those of conventional packed columns.

In MIP and BET testing, bulk samples are usually required. Therefore, a monolith is typically prepared in a small glass vial, transferred to a Soxhlet thimble, placed in a Soxhlet apparatus for extraction with methanol for 12 h, and finally vacuum-dried overnight at 40℃. Using this procedure, Urban et al.[70] studied the pore characteristics of organic-polymer monolithic columns using MIP and ISEC. While keeping the monomer content constant, changes in porous properties with change in the ratio of porogen solvents were measured. MIP measures the entire range of pore sizes and provides more physical information about the monoliths, while ISEC is more applied to determination of mesopores in chromatographic monoliths. Although both techniques seem complementary, a key concern about MIP is the extent to which the porous properties of “dry” monoliths measured by MIP are really indicative of the chromatographic performance under “wet” conditions.

BET was applied by Oxelbark et al.[71] for comparison of bupivacaine imprinted polymers prepared in crushed monolith, microsphere, silica-based composite and capillary monolith formats. Samples in all four formats were prepared in bulk. The specific surface areas were evaluated using BET, the specific pore volumes were determined following the Gurvitch rule (which states that the number of molecules

occluded in a specified porous volume must be related to the respective density),[71] and the average pore diameters were calculated based on the BJH theory (which was developed by Barrett, Joyner and Halenda for calculating the porosity measurements in gas adsorption).[71] The results indicated that the different formats exhibited widely different porosities and specific surface areas in the dry state. The crushed monolith had large pore structure while the microspheres had poorly developed pore structure.

BET and MIP were also combined together by Viklund et al.[72] for studying porous properties of two macroporous organic monoliths photopolymerized in situ: poly(glycidyl methacrylate-*co*-ethylenedimethacrylate) and poly(styrene-*co*-divinylbenzene). The pore size distributions (PSD) were determined using MIP, and the specific surface areas were calculated from the adsorption/desorption isotherms of nitrogen based on BET equations. It was found that the specific surface area of a typical macroporous material was mainly contributed from pores smaller than 50 nm (mesopores and micropores). The porous properties of the monoliths are a direct consequence of the quality of the porogenic solvent, the percentage of cross-linking monomer and the ratio between the monomer and porogen phases.

A triple combination of MIP, BET and ISEC for pore characterization of monoliths was reported by Thommes and co-workers.73 Native and n-alkyl-bonded (n-octadecyl) silica monoliths with mesopore diameters between 10 and 25 nm and macropores in the range of 1.8 to 6.0 μm were selected for study. The results indicated that good agreement between BET and ISEC were obtained for the mesopore size

distribution, but revealed that MIP underestimated the mesopore sizes. However, MIP contributed the macropore size distribution besides providing information on the complete porous structure of the column, including macropores and mesopores. Mercury hysteresis and entrapment in the MIP technique were also confirmed in this study. For some monoliths, there was no entrapment of mercury after extrusion from the mesopore, while a systematic study of many different silica monoliths revealed that through-pores mainly controlled mass transfer and mesopores were responsible for most entrapment behavior. Entrapment happens more likely in a macropore system with heterogeneous and disordered morphology which would restrict mass transfer. The lack of entrapment after extrusion from a mesopore system indicates an ordered, highly porous macropore structure which supports transport properties.

More comprehensive research on pore size characterization of monolithic columns was conducted by Lubda et al.[67] based on applications of MIP, BET, ISEC, SEM and TEM (transmission electron microscopy). Three sets of samples were selected for study. The first set of eight samples had an inner diameter of 4.6 mm, mesopore diameter of 10 nm, and macropore diameter in the range of 1.8 to 7.0 µm. The second set of samples also had an inner diameter of 4.6 mm, but mesopore diameter of 25 nm, and macropore diameter from 1.9 to 7.5 µm. Monoliths in the third set were fabricated in 100 µm i.d. capillaries using the same procedure from which the first two sets were prepared. Polystyrene standards with molecular weights ranging from 484 to 10,300,000 Da were used in ISEC determinations. Therefore, the maximum macropore able to be detected was around 300 nm. Similar porosity was

observed in the first two sets of columns based on ISEC results. In both columns, the percentage of mesopores contributing to the total porosity was constant at approximately 25 %. As the macropore diameters increased from 1.5 to 7.0 µm, the percentage of 300 nm macropores in the total porosity decreased from 8 % to 3 %. However, different from the 4.6 mm i.d. columns, an increase of 3 % to 8 % mesopores was found in the 100 µm i.d. capillary columns. The author believed that this was due to incomplete solidification in the capillary columns. A special sample holder was used in the MIP instrument in this study, so instead of using bulk samples, monolithic columns of 4.6 mm i.d. were directly determined using the MIP technique. Unfortunately, without a reasonable explanation, the results obtained from MIP could not be correlated with what was obtained from ISEC. The minimum pore diameter detectable using a typical MIP instrument with a pressure limitation of 4000 bar is 3.5 nm, so it is evident that any blind or closed pores remained unfilled using mercury intrusion.

To check if there were any large blind or closed pores remaining unfilled and undetected, the author crushed one of the samples after it was analyzed. The comparison indicated that a lower pore volume and a broader distribution of macropores were observed, which could be explained by a reduced percentage of macropores after crushing. For mesopores, a little lower pore volume and the same average pore diameter were observed after crushing. In this study, the surface area was determined using the BET technique. The specific pore volume was deduced according to the Gurvitch rule, and the pore size distribution was calculated according

to the BJH method. Since the BET technique is only able to measure pore diameters smaller than 100 nm, the author was concerned more about the mesopore properties from this technique. The pore size distribution of mesopores measured by MIP was confirmed by the BET results. The SEM images were also applied to confirm the ISEC results. Unfortunately, no pores were found with diameters around 300 nm, which were proposed by ISEC, even with 50,000 times magnification SEM images, or with TEM images. However, a smooth and homogenous pore structure could be observed in both types of images.

As described above, SEM, MIP, BET, and ISEC are popularly applied today for pore size characterizations of monolithic columns, either alone or in combination to complement each other. There are also new techniques, such as atomic force microscopy (AFM),[74] transmission electron microscopy (TEM),[75] and total pore blocking (TPB)[76] which have been developed recently to determine pore characteristics of packed and monolithic columns.

However, due to the limited availability of standards, ISEC is seldom used for the characterization of monolithic columns in recent years. Moreover, since pore size distribution is most meaningful in applications of monolithic columns, surface area from BET is also not of primary interest. As a result, the trend is to combine SEM and MIP for monolith characterization, since SEM can give the direct image of the cross section of a monolithic column, while MIP is able to provide a complete pore size distribution, including macropores and mesopores, although bulk materials must be used for testing.[77-91]

The pore morphology of a packed column is dependent on the particle size used for packing. Therefore, particle size distribution is often determined to characterize a packed column. If pore size distribution is desired, BET and MIP are usually applied.[92-95]

1.6 Pore Characterization Techniques

1.6.1 Scanning Electron Microscopy (SEM)

SEM has been popular for decades for giving a first view of the general structure of materials. This is mainly due to its simplicity. SEM is a non-contact technique. An electron beam scans the sample surface with a high-energy beam of electrons in a raster scan pattern. Signals that contain information about the sample's surface topography, composition and other properties, are produced when electrons interact with atoms that make up the sample, then are collected and detected using an electro-optical lens. In a typical SEM instrument, the electron beam is thermionically emitted from an electron gun fitted with a tungsten filament cathode because tungsten has the highest melting point and lowest vapor pressure of all metals.

Sample preparation is not very complicated for SEM analysis, however, samples should have an appropriate size to fit in the sample chamber and should be mounted rigidly on a sample holder called a sample stub. Conductive (at least at the surface), thermally stable, and relatively flat samples are desirable for SEM determination in order to prevent accumulation of inhomogeneous electrons on the surface. Therefore, metal objects need very little preparation before SEM imaging, except for cleaning and mounting in the sample chamber. For samples such as non-conductive, organic

polymerized monoliths, which are easily charged when scanned by the electron beam, an ultrathin layer of electrically-conducting material, commonly gold, is coated on the sample either by low vacuum sputter coating or by high vacuum evaporation. Besides gold, gold/palladium alloy, platinum, osmium, iridium, tungsten, chromium and graphite,[96] are used in current SEM imaging. These coatings prevent the accumulation of static charge on the samples during electron irradiation. Moreover, they can maximize the signal and improve spatial resolution, especially for samples with low atomic number.

However, even without coating, SEM images of non-conducting samples can be obtained using specialized SEM instrumentation such as the environmental SEM (ESEM) or field emission gun (FEG) SEM operated at low voltage. In ESEM, samples are placed in a relatively high pressure chamber where the working distance is short and the electron optical column is differentially pumped to maintain the appropriate vacuum at the electron gun. If a charge is generated, it will be neutralized in the high pressure region around the sample. At the same time, amplification of the secondary electron signal will be provided. It is difficult to operate low voltage SEM of non-conducting objects in a conventional SEM instrument. Therefore, this technique is only applied in research for samples that are sensitive to the process of applying conductive coatings.

The spatial resolution of SEM depends on the size of the electron spot, the size of the interaction volume, or the extent to which the material interacts with the electron beam. Since all of these factors are large compared to the distances between

atoms, the resolution of SEM is not high enough to image individual atoms such as can be done with transmission electron microscopy (TEM). Details revealing 1-20 nm in size can be reached in the most common or standard detection mode of SEM. A resolution of 0.4 nm can be obtained using the world's highest resolution SEM imstrument.[97]

1.6.2 Mercury Intrusion Porosimetry (MIP)

A non-wetting liquid is a liquid that does not spontaneously flow into pores. Mercury is a non-wetting liquid for most materials. This means that for solid surfaces in equilibrium with gases and liquids, the liquid/solid interfacial free energy is higher than the gas/solid interfacial free energy, and the contact angle is greater than 90°. In this case, mercury will not spontaneously fill the pores of the material. Only when work is done to increase the surface free energy, e.g., by increasing the pressure, can mercury intrude into the pores. The measurement of this increased pressure yields the volume of the intruded mercury, which in turn can be used to determine the pore volume. The pressure required is a function of the pore size. As pores are considered to be cylindrical, the relationship can be expressed by the Washburn equation.[98]

In MIP, a penetrometer, which consists of a glass container with a lid that can be sealed, is usually required to hold the sample during testing. Prior to testing, the penetrometer is weighed and calibrated to provide known parameters for use in later calculations. The penetrometer is generally designed having an open bulbous body at one end of a long stem into which the sample is sealed. When the penetrometer is placed into the porosimeter, mercury is introduced via the stem. Pore size and volume

quantification are accomplished by submerging the sample under a confined quantity of mercury. As the pressure of the mercury is increased hydraulically, a decrease in mercury in the penetrometer stem (which is equal to that pushed into the pores) will be detected based on a capacitance system. As the applied pressure is continually increased, the diameter of the pores which can be filled with mercury become smaller and smaller. Consequently the amount of mercury intruded increases with time and pressure. During this process, data recorded can provide the pore volume distribution directly. If all pores are assumed to be cylindrical, a simple calculation of the dimensional distribution of the pore size is permitted.

Specimens prepared for MIP testing should be dried to remove any moisture from the pores before testing. A dried specimen is loaded into the penetrometer which is weighed before and after loading. Once the penetrometer is placed into the porosimeter, it is filled with mercury. During testing, the pressure is increased and the volume of mercury forced into the pore structure is recorded based on the weight and density of mercury at the experimental temperature.

MIP is usually applied for measuring pore size distribution and total porosity. As described above, the pore size distribution is determined from the volume intruded at each pressure increment. Total porosity is determined from the total volume intruded. In addition to these, it also can provide information about bulk density, hysteresis curve or particle size distribution. As one of its special advantages, MIP can provide the measurement of pore sizes ranging from a few nanometers to several hundred

micrometers, which cannot be realized using most other techniques. Therefore, MIP is widely used for determination of macropore and mesopore size distribution.

Pressurized mercury can only enter the blind and through pores of a sample. Therefore, the volume of intruded mercury measured as a function of pressure represents the cumulative volume of the through pores and blind pores of the sample. Unfortunately, toxic mercury and high pressure are required.

1.6.3 Nitrogen Sorption Porosimetry (BET)

An adsorbed film can form on a clean porous surface when it is exposed to a gas. The extent of adsorption is determined by pressure, temperature, properties of the gas, and properties of the surface. At constant temperature, pressure is the only factor that determines how much of a specific gas can be adsorbed on a specific surface. The measurement of the amount of gas adsorption as a function of pressure can provide information on the characteristics of pore structure.[99, 100] Nitrogen sorption porosimetry measures the specific surface area of pores based on their adsorption/desorption isotherm curves. The amount of gas adsorbed by the sample at a constant temperature as a function of increase in relative pressure is the adsorption isotherm. A desorption isotherm is obtained by reducing the relative pressure at the termination of an adsorption experiment and measuring the amount of adsorbed material left on the sample.

In a typical BET sorptometer, a sample cell is placed inside a Dewar flask containing liquid nitrogen. The sample chamber is connected through valves to reference volume, gas supply, vacuum line, and pressure transducers. A temperature

controller keeps the temperature of the reference volume and connecting lines constant. The sample chamber is able to be heated to any specific temperature under vacuum. For a test, a weighed sample is placed in the sample chamber. The sample chamber is heated and evacuated to remove moisture and adsorbed gases. The desired adsorption temperature is then established in the chamber and the chamber is isolated. The reference volume is pressurized with adsorbate gas and then isolated. The pressure is measured. As the gas is allowed to expand into the sample chamber, the gas pressure is measured after equilibration. The amount of gas adsorbed by the material is calculated. To calibrate the system, an experiment without the sample is performed. Based on the change in pressure and the volume of the system the change in the amount of gas is measured.[101]

Using BET (Brunauer, Emmett, and Teller) theory and its derivations, the BJH (Barrett, Jovner, and Halenda) method, and the Kelvin equation, it possible to compute surface area, pore diameter, and pore volume of porous materials by measuring relative vapor pressure and the amount of vapor condensed in the pores.[102,103]

Nitrogen is widely used for gas adsorption because its interaction constant in BET theory is neither too large for localized adsorption nor too small for lateral movement of molecules on a surface (16.2×10^{-16} cm^2/molecule). Nitrogen adsorption usually measures pore sizes in the range of approximately 0.00035-0.2 μm. Since gas molecules are capable of accessing the through-pores as well as blind pores, gas molecules can be adsorbed on the surfaces of them and they can be characterized.

However, because closed pores are not accessible, they can never be determined unless the sample is crushed and the pores opened to the gas. Irregular pores are assumed to be spherical pores for computation of specific surface area and pore size distribution in the BET method as in the MIP technique. Due to the small range of pore size detectable, nitrogen adsorption porosimetry is mainly used for characterizing mesopores. The BET sorptometer is compact, inexpensive, and easy to use, and it requires minimal maintenance.

1.6.4 Inverse Size-exclusion Chromatography (ISEC)

Size-exclusion chromatography (SEC) is one of the applications of liquid chromatography, however, is different from the other modes since it does not depend on chemical interaction. The separation mechanism of SEC is a sieving process. Although molecule size is correlated to molecular mass for compounds of a given structure, the primary factor controlling retention in SEC is actually the "hydrodynamic volume" of the molecules. Compounds with larger structures are eluted earlier that those with smaller structures because smaller molecules are more easily trapped in the pores. Correlations between retention data and molecular size have been derived in SEC.[104-108]

ISCE uses the correlations in SEC to derive information on the structure of pores of a column from the retention data of a series of known probe compounds. This makes ISEC the only chromatographic-based technique for the characterization of pore distribution and total porosity of separation columns. However, pure size-exclusion data are required in the use of ISEC. This means that there should be

no adsorption of the probe compounds on the surface of the adsorbent studied, or the mobile phase should be at least as strongly adsorbed as the probe samples used. The solid matrix should be rigid and should not shrink or swell when the eluent is changed. The temperature and mobile phase flow-rate must remain constant during the whole experiment.[109, 110]

In a typical ISEC experiment, polystyrene standards with narrow molecular mass distribution starting from 201, 2,460, 6,400, 13,200, 19,300, 44,100, 75,700, 151,500, 223,200, 560,900, 1,045,000, 1,571,000 up to 1,877,000 can be used. The pore size distribution can be derived based on the simple correlation of $M_w = 2.25(10d)^{1.7}$. Here, M_w is the molecular mass of the polystyrene standard and d represents the diameter of the polystyrene standard in nm. Hence, as polystyrene standards are used, the limitation in pore size measurable using ISEC is from 1.4 to 304 nm.[34] Traditional HPLC equipment can be used to perform measurements of retention volumes of different molecules during size-exclusion separation. After a separation is accomplished, the retention volume for each standard is calculated. While each standard has a known molecular weight, an ISEC curve representing the relationship between $\log M_w$ and the retention volume can be plotted. If the M_w is further correlated to the diameter of the polystyrene standards, the pore size distribution determined by the column can be described by the percentage of the accumulated pore volume and the corresponding pore diameter. Based on retention behavior and some defined correlations, the porosity characteristics of a column can be calculated.[67]

ISEC can be used to obtain three-dimensional porosity properties of packed or monolithic columns, while imaging techniques can only provide information about pore surfaces. However, ISEC conditions, such as the use of THF as solvent, do not represent typical chromatographic conditions. Columns can be contaminated or destroyed in an ISEC measurement. Furthermore, there is limited availability of standards within a limited molecular weight range.

1.6.5 Atomic Force Microscopy (AFM)

AFM is a direct probe technique that allows study of surface morphology based on deflection of a flexible tip during scanning movement on a surface. Usually, AFM can be operated in three modes: contact, non-contact and intermittent (tapping).

A study was recently reported concerning the pore size characterization of a monolith for electrochromatography via AFM in air and liquid phase.[74] A distinct advantage presented in this work is that AFM can characterize samples that are either dry or wet, so the surface of a monolith can be studied under conditions similar to those used in a chromatographic separation. Compared to ISEC, AFM is a more direct imaging technique, and compared to SEM, it permits more accurate detection of surface roughness, both in depth and in the z direction. When imaging structures are similar in size or smaller than the radius of the tip, care must be paid to avoid contacting the surface with the side of the tip, which leads to erroneous measurements.

1.6.6 Transmission Electron Microscopy (TEM)

To observe the cross section of a porous column using TEM, special considerations must be paid to the preparation of the sample. The porous skeleton should be embedded in a matrix in order to preserve its structure and to prevent it from being damaged during microtomation. In most cases, samples for TEM must be microtomed and stained to increase the contrast.[66] The presence of silica from the capillary should be avoided since it will damage the blades used in conventional microtomes. Second, a staining step is required to increase the contrast. Recently, Courtois et al.[75] reported an assessment of the macroporous structure of monolithic columns using TEM. In this work, a new methodology was developed for sample preparation. The steps included *in situ* embedding of the monolith in a contrast resin, followed by dissolution of the fused-silica tubing, further encasement of the resin-embedded monolith, and microtomy. Computational assessment of the pore structure was obtained from transmission electron micrographs.

TEM requires only a small sample for analysis. However, the specific operating conditions make sample preparation quite complicated.

1.6.7 Total Pore Blocking (TPB)

TPB is a new method reported recently by Cabooter et al. to determine the external porosity of packed and monolithic columns.[76] It is actually a pore filling process. Four steps are involved. In step 1, the column is thoroughly rinsed with isopropanol. In step 2, isopropanol is gradually replaced by a hydrophobic solvent, which fills the column, both inside and outside the pores. In step 3, the hydrophobic

solvent occupying the interstitial space is pushed out of the column by a hydrophilic buffer, while that inside the pores remains. This occurs because of the strong hydrophobic character of the inside of the pores, (i.e., coatings such as C18 or C8), and the immiscibility of the hydrophobic solvent and hydrophilic buffer flowing outside the pores. As a result, the pores of the column become totally blocked by the hydrophobic solvent. In the last step, a non-retained tracer molecule with low M_w, such as uracil, is injected into the column. The measured retention time theoretically corresponds to the volume of the interstitial space from which the hydrophobic solvent was removed, thereby, giving the external porosity of the column.

TPB makes it possible to determine the interstitial volume and external porosity of a column from the elution time of a small tracer molecule by blocking the internal pores with a hydrophobic solvent. The retention of small molecules leads to accurate determination since small molecules are able to penetrate every corner of the interstitial space. However, incomplete filling of the pores, leakage of blocking agent during the experiment, presence of non-removed hydrophobic liquid occupying the small corners of the interstitial space, and dead time repeatability are concerns associated with this method.

1.6.8 Capillary Flow Porometry (CFP)

The CFP technique was developed for the evaluation of pore structure characteristics of filter materials, such as non-woven and woven filtration media.[65, 99, 102, 111-118] It is basically an extrusion method.

A wetting liquid is a liquid that can wet a solid surface spontaneously. Figure 1.2 illustrates a drop on a surface that does not spontaneously wet the surface.

Here,

$$\gamma_{\text{solid/gas}} - \gamma_{\text{solid/liquid}} = \gamma \cos\theta \qquad (1.2)$$

where θ is the contact angle and γ is the surface tension. A wetting liquid can spontaneously fill pores, but cannot flow along the surface spontaneously due to surface tension, the interfacial free energy of liquid/solid being less than that of gas/solid ($0^0 \le \theta \le 90^0$). To remove the wetting liquid out of the pores, work must be done to increase the surface free energy of liquid/solid. That is

$$pdV=(\gamma_{\text{solid/gas}} - \gamma_{\text{solid/liquid}})\, dS \qquad (1.3)$$

where p is the differential pressure, dV is the increase in volume of gas in the pores, and dS is the increase in solid/gas interfacial area and the corresponding decrease in solid/liquid interfacial area. Based on Equations 1.1 to 1.3, if a gas is used to displace the liquid from the pores, the needed pressure for the gas to flow through the pores is given by

$$P = 4\gamma\cos\theta/d \qquad (1.4)$$

where d is the pore diameter. For low surface tension wetting liquids, θ can be taken as zero. Based on Equation (1.4), the largest pores will be purged at the lowest pressure, while the smallest pores require the highest pressure.

The CFP technique uses an inert, non-reacting gas to detect a pore when gas flows through the sample due to the removal of the liquid at a specific differential pressure. This pore size value actually represents the diameter at the most

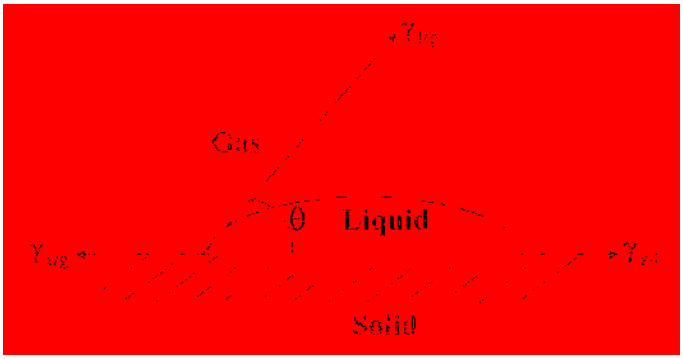

Figure 1.2 Relationship between contact angle and wettability of a solid surface

.

constricted part of a through-pore, where the differential pressure is at a maximum. Based on measurements of differential pressures and flow rates though wet and dry samples, a wide variety of through-pore characteristics, including largest pore diameter (bubble point), throat pore diameter, mean flow pore diameter, pore distribution, gas permeability and liquid permeability, can be computed. In addition, toxic liquids and high pressures are not required, and short test duration is experienced. Theoretically, any wetting liquid with known surface tension can be used with the CFP technique. A disadvantage is that blind and closed pores cannot be determined with this technique.

CFP detects the presence of a pore when gas flows through that pore, which happens only when the pressure is high enough to displace liquid from the most constricted part of the pore. Consequently, pore diameter calculated from the pressure is the diameter of the pore at its most constricted point. Thus, each pore is detected as a single pore of diameter equal to the diameter at the most constricted part of the pore. Based on ASTM (American Society for Testing and Materials) standards,[119] the parameters for CFP characterizations are defined as follows:

Filter flow % (FF %) = 100 × wet flow/dry flow

Incremental Filter flow% (ΔFF %) = current FF % – previous FF %

Incremental pore diameter (Δd) = previous diameter – current diameter

Relative pore size distribution portion = ΔFF %/Δd

Mean value diameter = 1/2 (previous diameter + current diameter).

Wet curve = gas flow rate through the wet sample as a function of the differential pressure

Dry curve = gas flow rate through the dry sample as a function of the differential pressure

Half-dry curve = half of the gas flow rate through the dry sample as a function of the differential pressure

There are four options to characterize a sample using CFP: wet up/dry down, wet up/dry up, dry up/wet up, and wet up/calculate dry. Wet up/dry down means the wet curve is determined with the pressure increasing, followed by the dry curve with the pressure decreasing. Wet up/dry up means the wet curve is determined with the pressure increasing, and then the dry curve with the pressure increasing. Dry up/wet up means the dry curve is determined with the pressure increasing, followed by the wet curve with the pressure increasing. Wet up/calculate dry means that no data for the dry curve is obtained, which can be drawn as a straight line passing through the first and last point on the wet curve.[120-122]

Dry up/wet up is the most accurate option for characterizing a porous material because, if the wet curve is determined first, the non-removed wetting liquid will always bring error to the following dry curve. However, for some samples which cannot be dried, testing the wet curve is a good start.

To obtain dry and wet curves is the main purpose in a CFP experiment. On the basis of these two curves, a series of parameters are computed. The pore diameter is calculated from the differential pressure according to Equation 1.4. Although each

pore may have many pore diameters, CFP only measures the most constricted point. Therefore, each of the diameters computed actually represents the most constricted cross-section of a pore, which is called the throat pore diameter. The bubble point (indicating the largest pore diameter) is the pressure at which the first air bubbles start to form on the sample. It is given as the pressure at which the wet curve deviates from the x-axis. The pressure where the dry and half-dry curves intersect gives the mean flow diameter. Pore size distribution is computed based on the relationship: Pore distribution = Increment FF%/(previous diameter – current diameter). The dry curve represents gas permeability and the wet curve represents liquid permeability. Since all data are obtained based on flow rate, full characterization of the pore structures of separation columns in their actual chromatographic forms can be achieved, which makes CFP a desirable technique.

The column must be wetted before measuring with CFP. Based on the principle of CFP, selection of the wetting liquid is critical for the experiment. For CFP applications, a good wetting liquid should have low surface tension and high vapor pressure. Low surface tension is beneficial for rapid and complete pore filling, while high vapor pressure is important for stability and purity of the filling. Either of the two characteristics of a wetting liquid could affect the speed and accuracy of a CFP determination. Table 1.1 shows the minimum pore size detectable using different wetting liquids.

Table 1.1 Minimum pore size detectable in CFP using different wetting liquids.[a]

Fluid	Surface tension, dynes/cm	Minimum pore diameter, µm
Water	72.0	0.15
Mineral oil	34.7	0.07
Petroleum distillate	30.0	0.06
Denatured alcohol	22.3	0.05
Silwick[b]	20.1	0.04
Porewick[c]	16.0	0.03
Galwick[d]	15.9	0.03

[a] for 200 psi porometer

[b] Silwick: silicone

[c] Porewick: a non-volatile perfluorinated liquid, C5-C18

[d] Galwick: propene, 1,1,2,3,3,3-hexaflouro, oxidized, polymerized

1.7 Significance and Content of this Dissertation

Increasing attention is being paid to the development of new monolithic materials for liquid chromatographic columns, concentration membranes, sample extractors and bioreactors. Compared with traditional packed beds for CEC and HPLC, the main advantage of monolithic columns is their high permeability to liquid flow, which can increase mass transfer rates and improve separation efficiency.

The porosity of packed and monolithic capillary columns is mainly determined by the through-pores, whereas the micropores and mesopores in the skeletal structure contribute to surface area. Both of these must be optimized for use in flow-through applications because the pore size distribution of the column is critical for each application and a column is useful only if it possesses the desired surface structure. The pore size distribution of a column is usually measured using bulk techniques such as MIP, BET, etc. Many studies have focused on pore size characterization of the monoliths; however, very few techniques can provide the pore size characteristics of the stationary phase in its chromatographic form (i.e., packed or continuous within the column). CFP has proven to be an efficient pore size characterization methodology for filter materials. My research centered on extending the application of CFP to packed and monolithic separation columns. The main aim of this dissertation is to build a reliable technique based on CFP to measure the pore size distribution of capillary separation columns in their real chromatographic forms. As more natural and accurate information is provided on

the pore structure of monolithic columns, better evaluation and understanding of them should be obtained. As a result, easier control and design of desirable porous structures for different applications can be reached, which will in turn create better use of monolithic columns in liquid chromatography.

Chapter 2 reports a new CFP system assembled from a simple microflow meter and a commercial digital pressure controller. The mean through-pore diameter and pore size distribution of three packed columns containing standard silica particles (3, 5, 7 μm diameter) and three typical silica monoliths prepared in 50 μm i.d. fused silica capillaries via phase separation by polymerization of tetramethoxysilane (TMOS) in the presence of poly(ethylene glycol) (PEG), were characterized using the home-built CFP system. It was verified that a greater number of pores with small throat diameters were prepared in columns with higher PEG content in the prepolymer mixture. SEM images show that the pore diameters of monoliths fabricated in bulk were smaller than those in monoliths synthesized by the same procedure, but confined in capillary tubes. In Chapter 3, the new CFP system was applied to study the effect of column diameter and length on pore properties of polymeric monoliths based on glycidyl methacrylate (GMA) and poly(ethylene glycol) diacrylate (PEGDA). The pore size distributions indicated that change in column length and inner diameter had little effect on pore structure. Chapter 4 reports the preparation of a monolithic structure in a sacrificial layer, planar (SLP) microfluidic device. The channels of SLP devices were constructed on the surface of glass or quartz substrates using a procedure quite different from the traditional fabrication methods. The dimensions of the channels

were much smaller than traditional glass microchips (10 μm in width and 0.9 cm long). A polymeric monolith with negative charge was successfully prepared in the microfluidic channels and amino acid extraction was obtained based on an ion exchange mechanism. Chapter 5 proposes future research directions for the new CFP method and for monolithic SLP microfluidic devices.

1.8 References

1. Gilbert, M. T. High Performance Liquid Chromatography; Wright: Bristol 1987.
2. Lindsay, S. High Performance Liquid Chromatography; Wiley: New York 1992.
3. Ishii, D. Introduction to Microscale High-Performance Liquid Chromatography; VCH: New York 1988.
4. Kucera, P. Microcolumn High-performance Liquid Chromatography; Elsevier: New York 1984.
5. Kennedy, R. T.; German, I; Thompson, J. E.; Witowski, S. R. *Chem. Rev*. **1999**, *99*, 3081-3131.
6. Takeuchi, T. *Chromatography* **2005**, *26 (1)*, 7-10.
7. Wu, N.; Collins, D.C.; Lippert, J.A.; Xiang, Y.; Lee, M.L. *J. Microcol. Sep.* **2000**, *12 (8)*, 462-469.
8. Tolley, L.; Jorgenson, J.W.; Moseley, M.A. *Anal. Chem*. **2001**, *73*, 2985-2991.
9. Xiang, Y.; Yan, B.; Yue, B.; McNeff, C.V.; Carr, P.W.; Lee, M.L. *J. Chromatogr. A* **2003**, *983*, 83-89.
10. Xiang, Y.; Yan, B.; McNeff, C.V.; Carr, P.W.; Lee, M.L. *J. Chromatogr. A* **2003**, *1002*, 71-78.
11. Wu, N.; Lippert, J.A.; Lee, M.L. *J. Chromatogr. A* **2001**, *911*, 1-12.
12. Gong, Y.; Xiang, Y.; Yue, B.; Xue, G.; Bradshaw, J.S.; Lee, H.K.; Lee, M.L. *J. Chromatogr. A* **2003**, *1002*, 63-70.
13. Crescentini, G.; Bruner, F.; Mangani, F.; Guan, Y. *Anal. Chem*. **1988**, *60*, 1659-1662.

14. Svec, F., Tennikova, T.B., Deyl, Z. Monolithic Materials: Preparation, Properties and Applications; Elsevier: Amsterdam, 2003.

15. Desmet, G.; Cabooter, D.; Gzil, P.; Verelst, H.; Mangelings, Y.V.H.; Clicq, D. *J. Chromatogr. A* **2006**, *1130*, 158-166.

16. Hjertén, S.; Liao, J. L.; Zhang, R. *J. Chromatogr.* **1989**, *473*, 273-280.

17. Svec, F.; Fréchet, J. M. J. *Anal. Chem.* **1992**, *64*, 820-822.

18. Gusev, I.; Huang, X.; Horvath, C. *J. Chromatogr. A* **1999**, *855*, 273-290.

19. Minakuchi, H.; Nagayama, H.; Soga, N.; Ishizuka, N.; Tanaka, N. *Anal. Chem.* **1996**, *68*, 3498-3501.

20. Minakuchi, H.; Nakanishi, K.; Soga, N.; Ishizuka, N.; Tanaka, N. *J. Chromatogr. A* **1998**, *797*, 121-131.

21. Oberarcher, H.; Premstaller, A.; Huber, C.G. *J. Chromatogr. A* **2004**, *1030*, 201-208.

22. Ikegami, T.; Dicks, E.; Kobayashi, H.; Morisaka, H.; Tokuda, D.; Cabrera, K.; Hosoya, K.; Tanaka, N. *J. Sep. Sci.* **2004**, *27*, 1292-1302.

23. Eeltink, S.; Decrop, W.M.C.; Rozing, G.P.; Schoenmakers, P.J.; Kok, W.Th. *J. Sep. Sci.* **2004**, *27***,** 1431-1440.

24. Fujimoto, C. *J. High Resolut. Chromatogr.* **2000**, *23 (1)*, 89-92.

25. Ishizuka, N.; Minakuchi, H.; Nakanishi, K.; Soga, N.; Hosoya, K.; Tanaka, N. *J. High Resolut. Chromatogr.* **1998**, *21*, 477-479.

26. Hara, T.; Kobayashi, H.; Ikegami, T.; Nakanishi, K.; Tanaka, N. *Anal. Chem.* **2006**, *78*, 7632-7642.

27. Yang, Y.; Donald R. Lynch, Jr. *LCGC LC Column Technology Supplement* **2004**, *June*, 34-38.

28. Motokawa, M.; Kobayashi, H.; Ishizuka, N.; Minakuchi, H.; Nakanishi, K.; Jinnai, H.; Hosoya, K.; Ikegami, T.; Tanaka, N. *J. Chromatogr. A* **2002**, *961*, 53-63.

29. Vidič, J.; Podgornik, A.; Štrancar, A. *J. Chromatogr. A* **2005**, *1065*, 51-58.

30. Svec, F.; Peters, E. C.; Sýkora, D.; Fréchet, J. M. J. *J. Chromatogr. A* **2000**, *887*, 3-29.

31. Zou, H.; Huang, X.; Ye, M.; Luo, Q. *J. Chromatogr. A* **2002**, *954*, 5-32.

32. Ngola, S. M.; Fintschenko, Y.; Choi, W.; Shepodd, T. J. *Anal. Chem.* **2001**, *73*, 849-856.

33. Palm, A.; Novotny, M. V. *Anal. Chem.* **1997**, *69*, 4499-4507.

34. Gu, B.; Armenta, J. M.; Lee, M. L. *J. Chromatogr. A* **2005**, *1079*, 382-391.

35. Armenta, J. M.; Gu, B.; Humble, P. H.; Thulin, C. D.; Lee, M. L. *J. Chromatogr. A* **2005**, *1097*, 171-178.

36. Gu, B.; Chen, Z.; Thulin, C. D.; Lee, M. L. *Anal. Chem.* **2006**, *78*, 3509-3518.

37. Courtois, J.; Szumski, M.; Byström, E.; Iwasiewicz, A.; Shchukarev, A.; Irgum, K. *J. Sep. Sci.* **2006**, *29***,** 14-24.

38. Rohr, T.; Hilder, E. F.; Donovan, J. J.; Svec, F.; Fréchet, J. M. J. *Macromolecules* **2003**, *36*, 1677-1684.

39. Elicabe, G. E.; Larrondo, H. A.; Williams, R. J. J. *Macromolecules* **1998**, *31*, 8173-8182.

40. Kiefer, J.; Hilborn, J. G.; Manson, J. A. E.; Leterrier, Y.; Hedrick, J. L. *Macromolecules* **1996**, *29*, 4158-4160.

41. Kiefer, J.; Hedrick, J. L.; Hilborn, J. G. *Adv. Polym. Sci.* **1999**, *147*, 161-247.

42. Svec, F.; Peters, E. C.; Sykora, D.; Yu, G.; Fréchet, J. M. J. *J. High Resolut. Chromatogr.* **2000**, *23*, 3-18.

43. Minakuchi, H.; Nagayama, H.; Soga, N.; Ishizuka, N.; Tanaka, N. *Anal. Chem.* **1996**, *68*, 3498-3501.

44. Minakuchi, H.; Nakanishi, K.; Soga, N.; Ishizuka, N.; Tanaka, N. *J. Chromatogr. A* **1998**, *797*, 121-131.

45. Oberarcher, H.; Premstaller, A.; Huber, C. G. *J. Chromatogr. A* **2004**, *1030*, 201-208.

46. Wu, N.; Lippert, J. A.; Lee, M. L. *J. Chromatogr. A* **2001**, *911*, 1-12.

47. Gong, Y.; Xiang, Y.; Yue, B.; Xue, G.; Bradshaw, J. S.; Lee, H. K.; Lee, M. L. *J. Chromatogr. A* **2003**, *1002*, 63-70.

48. Crescentini, G.; Bruner, F.; Mangani, F.; Guan, Y. *Anal. Chem.* **1988**, *60*, 1659-1662.

49. Vlakh, E. G.; Tennikova, T. B. *J. Sep. Sci.* **2007**, *30*, 2801-2813.

50. Desmet, G.; Cabooter, D.; Gzil, P.; Verelst, H.; Mangelings, Y. V. H.; Clicq, D. *J. Chromatogr. A* **2006**, *1130*, 158-166.

51. Peterson, D. S.; Rohr, T.; Svec, F.; Fréchet, J. M. J. *Anal. Chem.* **2002**, *74*, 4081-4088.

52. Luo, Q.; Mutlu, S.; Gianchandani, Y. B.; Svec, F.; Fréchet, J. M. J. *Electrophoresis* **2003**, *24*, 3694-3702.

53. Yu, C.; Mutlu, S.; Selvaganapathy, P.; Mastrangelo, C. H.; Svec, F.; Fréchet, J. M. J. *Anal. Chem.* **2003**, *75*, 1958-1961.

54. Mair, D. A.; Schwei, T. R.; Dinio, T. S.; Svec, F.; Fréchet, J. M. J. *Lab Chip*, **2009**, *9*, 877-883.

55. Rohr, T.; Yu, C.; Davey, M. H.; Svec, F.; Fréchet, J. M. J. *Electrophoresis* **2001**, *22*, 3959-3967.

56. Yu, C.; Davey, M. H.; Svec, F.; Fréchet, J. M. J. *Anal. Chem.* **2001**, *73*, 5088-5096.

57. Peterson, D. S.; Rohr, T.; Svec, F.; Fréchet, J. M. J. *Anal. Chem.* **2003**, *75*, 5328-5335.

58. Levkin, P. A.; Eeltink, S.; Stratton, T. R.; Brennen, R.; Robotti, K.; Yin, H.; Killeen, K.; Svec, F.; Fréchet, J. M. J. *J. Chromatogr. A* **2008**, *1200*, 55-61.

59. Liston, E.; Martinu, L.; Wertheimer, M. *J. Adhes. Sci. Technol.* **1993**, *7*, 1091-1127.

60. Henry, A. C.; Tutt, T. J.; Galloway, M.; Davidson, Y. Y.; McWhorter, C. S.; Soper, S. A.; McCarley, R. L. *Anal. Chem.* **2000**, *72*, 5331-5337.

61. Stachowiak, T. B.; Rohr, T.; Hilder, E. F.; Peterson, D. S.; Yi, M.; Svec, F.; Fréchet, J. M. J. *Electrophoresis* **2003**, *24*, 3689-3693.

62. Soper, S. A.; Henry, A. C.; Vaidya, B.; Galloway, M.; Wabuyele, M.; McCarley R. L. *Anal. Chim. Acta* **2002**, *470*, 87-99.

63. Stachowiak, T. B.; Svec, F.; Fréchet, J. M. J. *J. Chromatogr. A* **2004**, *1044*, 97-111.

64. Chen, G.; Svec, F.; Knapp, D. R. *Lab Chip*, **2008**, *8*, 1198-1204.

65. Jena, A. K.; Gupta, K. M. *Inter. Nonwovens J.*, **2003**, *Fall*, 45-53.

66. Liang, C.; Dai, S.; Guiochon, G. *Anal. Chem.* **2003**, *75*, 4904-4912.

67. Lubda, D.; Lindner, W.; Quaglia, M.; Hohenesche, C. F.; Unger, K. K. *J. Chromatogr. A* **2005**, *1083*, 14-22.

68. Grimes, B. A.; Skudas, R.; Unger, K. K.; Lubda, D. J. M. *J. Chromatogr. A* **2007**, *1144*, 14-29.

69. Al-Bokari, M.; Cherrak, D.; Guiochon, G. *J. Chromatogr. A* **2002**, *975*, 275-284.

70. Urban, J.; Eeltink, S.; Jandera, P.; Schoenmarkers, P. J. *J. Chromatogr. A* **2008**, *1182*, 161-168.

71. Oxelbark, J.; Legido-Quigley, C.; Aureliano, C. S. A.; Titirici, M.; Schillinger, E.; Sellergren, B.; Courtois, J.; Irgum, K.; Dambies, L.; Cormack, P. A. G.; Sherrington, D.C.; Lorezi, E. D. *J. Chromatogr. A* **2007**, *1160*, 215-226.

72. Viklund, C.; Pontén, E.; Glad, B.; Irgum, K.; Hörstedt, P.; Svec, F. *Chem. Mater.* **1997**, *9*, 463-471.

73. Thommes, M.; Skudas, R.; Unger, K. K.; Lubda, D. J. M. *J. Chromatogr. A* **2008**, *1191*, 57-66.

74. Cabral, J. L.; Bandilla, D.; Skinner, C. D. *J. Chromatogr. A* **2006,** *1108*, 83-89.

75. Courtois, J.; Szumski, M.; Georgsson, F.; Irgum, K. *Anal. Chem.* **2007**, *79*, 335-344.

76. Cabooter, D.; Lynen, F.; Sandra, P.; Desmet, G. *J. Chromatogr. A* **2007**, *1157*, 131-141.

77. Courtois, J.; Byström, E.; Irgum, K. *Polymer* **2006**, *47*, 2603-2611.

78. Krajnc, P.; Leber, N.; Štefanec, D.; Kontrec, S.; Podgorink, A. *J. Chromatogr. A* **2005**, *1065*, 69-73.

79. Laschober, S.; Sulyok, M.; Rosenberg, E. *J. Chromatogr. A* **2007**, *1144*, 55-62.

80. Yao, K.; Yun, J.; Shen, S.; Wang, L.; He, X.; Yu, X. *J. Chromatogr. A* **2006**, *1109*, 103-110.

81. Unger, K. K.; Skudas, R.; Schulte, M. M. *J. Chromatogr. A* **2008**, *1184*, 393-415.

82. Svec, F.; Fréchet, J. M. J. *Macromolecules* **1995**, *28*, 7580-7582.

83. Hemström, P.; Nordborg, A.; Irgum, K.; Svec, F.; Fréchet, J. M. J. *J. Sep. Sci.* **2006**, *29*, 25-32.

84. Gu, C.; Lin, L.; Chen, X.; Jia, J.; Ren, J.; Fang, N. *J. Chromatogr. A* **2007**, *1170*, 15-22.

85. Dorsey, J. G.; Cooper, W. T.; Siles, B. A.; Foley, J. P.; Barth, H. G. *Anal. Chem.* **1998**, *70*, 591R-644R.

86. Levkin, P. A.; Eeltink, S.; Stratton, T. R.; Brennen, R.; Robotti, K.; Yin, H.; Killeen, K.; Svec, F.; Fréchet, J. M. J. *J. Chromatogr. A* **2008**, *1200*, 55-61.

87. Svec, F.; Huber, C. G. *Anal. Chem.* **2006**, *78*, 2100-2107.

88. Yu, C.; Svec, F.; Fréchet, J. M. J. *Electrophoresis* **2000**, *21*, 120-127.

89. Yu, C.; Xu, M.; Svec, F.; Fréchet, J. M. J. *Monolithic Polymers* **2001**, *40*, 755-769.

90. Mair, D. A.; Geiger, E.; Pisano, A. P.; Fréchet, J. M. J.; Svec, F. *Lab Chip*, **2006**, *6*, 1346-1354.

91. Yang, H.; Shi, Q.; Tian, B.; Xie, S.; Zhang, F.; Yan, Y.; Tu, B.; Zhao, D. *Chem. Mater.* **2003**, *15*, 536-541.

92. Kennedy, R. T.; German, I.; Thompson, J. E.; Witowski, S. R. *Chemical. Reviews* **1999**, *99*, 3081-3132.

93. Kirkland, J. J.; Truszkowski, F. A.; Ricker, R. D. *J. Chromatogr. A* **2009**, *965*, 25-34.

94. Damelson, N. D.; Kirkland, J. J. *Anal. Chem.* **1997**, *59*, 2501-2506.

95. Loh, K.; Wang, D. I. C. *J. Chromatogr. A* **1995**, *718*, 239-255.

96. Suzuki, E.; *Journal of Microscopy* **2002**, *208*, 153-157.

97. Danilatos, G. D. *Advances in Electronic and Electron Physics* **1988**, *71*, 109-250.

98. Abell, A. B.; Willis, K. L.; Lange, D. A. *Journal of Colloid and Interface Science*, **1999**, *211*, 39-44.

99. Jena, A. K.; Gupta, K. M. *J. Power Sources* **1999**, *80***,** 46-52.

100. Kington, G. L.; Aston, J. G. *J. Am. Chem. Soc.* **1951**, *73 (5)*, 1934-1936.

101. Fagerlund, G. *Material Constructions* **1973**, *6*, 239-245.

102. Jena, A. K.; Gupta, K. M. *Fluid/Particle Sep. J.* **2002**, *14 (3)***,** 227-241.

103. Barrett, E.; Joyner, L.; Halenda, P. *J. Am. Chem. Soc.* **73**, 373-380 (1951).

104. Miller, J. Chromatography: Concepts and Contrasts; Wiley: New York 1988.

105. Provder, T. Size Exclusion Chromatography: Methodology and Characterization: Polymers and Related Materials; American Chemical Society: Washington, DC 1984.

106. Provder, T. Detection and Data Analysis in Size Exclusion Chromatography; American Chemical Society: Washington, DC 1986.

107. Yau, W. W., Kirkland, J. J., Bly, D. D. Modern Size-exclusion Liquid Chromatography; Wiley: New York 1979.

108. Van Kreveld, M. E.; Van Den Hoed, N. J. *J. Chromatogr.* **1973**, *83*, 111-129.

109. Halász, I.; Martin, K. *Angew. Chem. (Int. Engl.)* **1978**, *17*, 901-908.

110. Al-Bokari, M.; Cherrak, D.; Guiochon, G. *J. Chromatogr. A* **2002**, *975*, 275-284.

111. Gupta, V; Jena, A. *Advances in Filtration and Separation Technology* **1999**, *13b*, 833-844.

112. Jena, A. K., Gupta, K. M., *J. Power Sources* **1999**, *80 (1 & 2)*, 46 - 52.

113. Gigova, A., *J. Power Sources* **2006**, *158*, 1054 - 1061.

114. Jena, A. K., Gupta, K. M., *American Ceramic Society Bulletin* **2003**, *82*, 9401 - 9406.

115. Sanders, H., Jena, A.K., *Ceramic Industry* **2000**, *150*, 26 - 29.

116. Gupta, N., Jena, A., Gupta, K., *Ceramic Industry* **2001**, *151*, 24 - 29.

117. Rideal, G., *Filtration News* **2004**, *July/August Issue*, 8 - 12.

118. Jena, A., Gupta, K., *INTC* **2000**, 10.0 - 10.11.

119. ASTM Procedure F316-86: “Standard Test Method for Pore Size Characteristics of Membrane Filters by Bubble Point and Mean Flow Pore Test”, February 21, 1986.

120. Jena, A., Gupta, K., *International Wovens J.* **2005**, *Summer Issue*, 26 - 30.

121. Mayer, E., *Filtration News* **2002**, *September/Octuber Issue*, 12 - 24.

122. De Bruyne, M. A. A.; De Bruyne, R. J. E.; De Moor, R. J. G. *International Endodontic Journal* **2006**, *39*, 493-501.

CHAPTER 2 SIMPLE CAPILLARY FLOW POROMETER FOR CHARACTERIZATION OF CAPILLARY COLUMNS CONTAINING PACKED AND MONOLITHIC SILICA BEDS

2.1 Introduction

The morphologies and pore structures of porous media are important in the design of chromatographic columns due to their influence on hydrodynamic properties (e.g., flow properties), thermodynamic properties (e.g., loadability) and mass transfer kinetics (e.g., efficiency). There are two classes of traditional methods for determining pore size and morphology. Microscopic techniques, such as scanning electron microscopy (SEM) and X-ray analysis, provide actual images of the surface, but no quantitative characterization of the surface area and pore volume. They are also quite involved, time consuming and expensive. However, macroscopic measurement techniques, such as BET and MIP can rapidly and inexpensively determine the macroscopic effects of phenomena occurring in the pore volume and on the pore surface. SEM, MIP, BET and ISEC (Inverse size-exclusion chromatography) are four traditional methods for pore size characterization of packed and monolithic columns, which have been used for decades.[1, 2] Newer techniques, such as atomic force microscopy (AFM),[3] transmission electron microscopy (TEM),[4] and total pore blocking (TPB)[5] have been developed recently to determine pore characteristics of packed and monolithic columns.

A major question associated with the most popular methods for pore structure characterization, such as MIP and BET, is how relevant the determined pore size properties are to the chromatographic performance of the columns, especially since

the measurements are made on representative bulk materials not in a column format. Although ISEC can be used to obtain three-dimensional porosity properties of packed or monolithic columns in their chromatographic forms, ISEC conditions, such as the use of THF as solvent, do not represent typical chromatographic conditions. Columns can be contaminated or destroyed during an ISEC experiment. Furthermore, there is limited availability of appropriate standards.

Capillary flow porometry (CFP) is basically an extrusion method, and was developed for the evaluation of pore structure characteristics of filter materials, such as membranes, textile materials, ceramic components, and filtration media.[6-16] Porosity, pore size distribution, surface area, largest pore diameter (bubble point) and mean flow pore size are important characteristics of porous materials. Porosity is the void volume of the porous material usually expressed as the percentage of the total volume. Each porous material has its own desired porosity for specific applications.

Current capillary flow porometers were built primarily based on ASTM (American Society for Testing and Materials) standard F316, as shown schematically in Figure 2.1.[17] In this setup, a sample, for example, a piece of filter paper that is thoroughly wetted, is mounted in the holder before testing. Gas flow through the sample is measured at specific pressures using a rotameter. The relationship between pressure and gas flow rate provides the pore structure characteristics of the sample. Pore sizes are typically reported as pore diameters. This is straightforward for pores with circular cross-sections. Pores with irregular cross-sections are defined according to the diameter of a circular opening whose perimeter to area ratio is a circular pore at

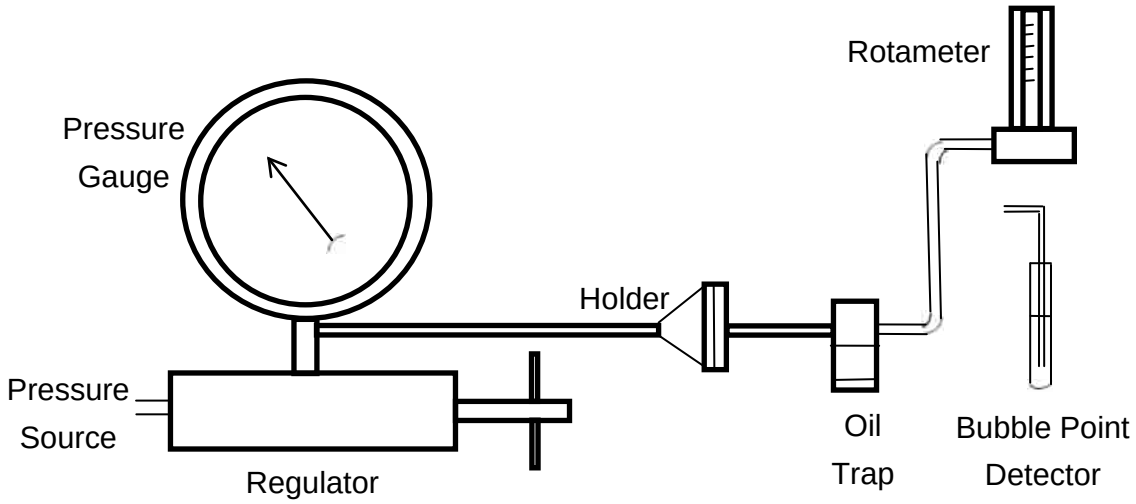

Figure 2.1. Schematic for one filter holder in ASTM standard F316-86.

the same location.[18] That is,

$$\text{(Perimeter/Area)}_{\text{pore}} = \text{(Perimeter/Area)}_{\text{circle of diameter d}} \quad (2.1)$$

A key factor in the CFP technique is the selection of wetting liquid. A good wetting liquid should wet the surface of the porous materials spontaneously and possess relatively low surface tension. Figure 1.2 illustrates a drop on a surface that does not spontaneously wet the surface.[6]

Here,

$$\gamma_{\text{solid/gas}} - \gamma_{\text{solid/liquid}} = \gamma \cos\theta \quad (2.2)$$

where θ is the contact angle and γ is the surface tension. A wetting liquid can spontaneously fill pores but cannot flow along the surface spontaneously due to surface tension, the interfacial free energy of liquid/solid being less than that of gas/solid ($0^0 \le \theta \le 90^0$). To remove the wetting liquid from the pores, work must be done to increase the liquid/solid surface free energy. That is,

$$PdV = (\gamma_{\text{solid/gas}} - \gamma_{\text{solid/liquid}})\, dS \quad (2.3)$$

where P is the differential pressure, dV is the increase in volume of gas in the pores, and dS is the increase in solid/gas interfacial area and corresponding decrease in solid/liquid interfacial area. Based on Equations 2.1 to 2.3, if a gas is used to displace the liquid from the pores, one can show that the needed pressure for the gas to flow through the pores is given by [6]

$$P = 4\gamma\cos\theta/d \quad (2.4)$$

where d is the pore diameter. For low surface tension wetting liquids, θ can be taken as zero. Based on Equation 2.4, the largest pores will be purged at the lowest pressure, while the smallest pores require the highest pressure.

Basically, CFP detects the presence of a pore when gas flows through that pore, which happens only when the pressure is high enough to displace the wetting liquid from the most constricted part of the pore. Consequently, the pore diameter calculated from the pressure (i.e., Equation 2.4), is the diameter of the pore at its most constricted point. Based on measurements of differential pressures and flow rates through wet and dry samples, a variety of through-pore characteristics can be computed. Since the data used are based on flow rate, characterization of the pore structures of chromatographic columns in their actual forms can be achieved, which makes CFP an attractive technique.

Unfortunately, the current commercial capillary flow porometers are designed to evaluate filter materials with large area dimensions and high flow rates. Initial evaluation of such a system in my work to characterize the pore characteristics of monolithic capillary columns led to many difficulties, primarily due to the required low flow rate.

In this work, I designed and constructed a capillary flow porometer for pore size characterization of capillary columns. Three packed columns containing different sizes of silica particles and three silica monolithic columns were characterized using the home-built capillary flow porometer. A variety of through-pore characteristics, such as bubble point, throat pore diameter, mean flow pore diameter, pore

distribution, gas permeability, and liquid permeability, were obtained. Therefore, each of the diameters computed actually represents the most constricted cross-section of a pore, which is called the throat pore diameter. The bubble point (indicating the largest pore diameter) is the pressure at which the first air bubbles start to form from a sample. It is given as the pressure at which the wet curve deviates from the x-axis.

The distribution of pore sizes gives the relative proportion of pores of each size. From Equation 2.4 we see that for a particular pore, the “size” is the diameter at the most constricted point of the pathway described by the pore. This diameter is determined by the amount of work necessary to push the wetting liquid through the pore.

The relative proportion of pores of a particular diameter is measured by comparing the flow rate through the capillary at the pressure associated with the specific diameter relative to the flow rate under dry conditions at that same pressure. If there is only one pore at a specific diameter, then the wetting agent will clear at the appropriate pressure, as given by Equation 2.4. However, an increase in flow rate with the opening of a single pore will be nominal. If, however, there are many pores of this diameter, the increase in flow rate will be larger. Thus the determination of the relative proportion entails determining the proportion of pores that are cleared of wetting agent at each specific pressure. Using Equation 2.4, we can determine the diameter for each specific pressure.

The relative flow rate is determined by comparing the flow rate under wet conditions with those under dry conditions. Specifically, the ASTM standard defines the filter flow for CFP as [17]

Filter flow % (FF %) = 100 × wet flow/dry flow (2.5)

From this we determine that the incremental flow is

Incremental Filter flow % (ΔFF %) = current FF % – previous FF % (2.6)

Incremental pore diameter (Δd) = previous diameter – current diameter (2.7)

The pore distribution is thus the increase in incremental flow relative to the increase in diameter:

Relative pore size distribution portion = Δ FF %/Δd (2.8)

The diameters are calculated using Equation 2.4. The value for each diameter pore interval corresponds to the pore size distribution for that interval:

Mean value diameter = 1/2 (previous diameter + current diameter) (2.9)

2.2 Experimental

2.2.1 Sample preparation

Silica particle packed columns. A high pressure packing system was used for packing columns.[19] Briefly, a Model DSF-150-C1 air-driven pneumatic amplifier pump (Haskel, Burbank, CA, USA) was used to drive the packing slurry through the column. One end of a 150 μm i.d. fused silica capillary was connected to a Valco 1/16'' union (Valco, Houston, TX, USA) with a section of PEEK tubing (Upchurch, Oak Harbor, WA, USA) and a stainless steel frit (0.5 μm pore size) (Upchurch, Oak Harbor, WA, USA) to retain the particles in the capillary. The other end of the

capillary was connected to a modified Swagelok reducing union, which acted as the packing material reservoir, and was connected to the Haskel pump via 1/8'' o.d. tubing.

Slurries of silica particles were made by mixing approximately 30 mg (more than enough for packing) of 3, 5 or 7 μm diameter silica particles in 200 μL of isopropanol. Then the slurry was transferred to the packing reservoir. Liquid carbon dioxide from a gas cylinder was used to drive the silica particle slurry into the capillary column. Particles were held by the stainless steel frit (0.5 μm pore size) in the column during packing. Both the column and the reservoir were placed in an ultrasonic bath (Branson Ultrasonic, Danbury, CT, USA) that was set at room temperature and turned on from the beginning until the column was completely filled. The nitrogen gas pressure for driving the liquid carbon dioxide was increased gradually up to 10,000 psi to maintain a constant filling rate during the entire experiment. The filling process required approximately 2 h, however, the column was left overnight to depressurize.[19] After packing, frits were sintered at both ends of the columns using a capillary burner (Innova Tech, Ellicott City, MD, USA).

Silica monolithic columns. Silica monolithic columns (i.e., A, B and C, Table 2.1), were prepared in 50 μm i.d. fused silica capillaries based on the conditions reported by Tanaka et al.[19] Before preparation, 50 μm i.d. fused silica capillary tubes (Polymicro, Phoenix, AZ, USA) were pretreated with 1 mol/L NaOH solution at 40 °C for 3 h, washed with water and acetone, and then dried. Tetramethoxysilane (TMOS, Aldrich, St. Louis, MO, USA) was added to a solution of poly(ethylene

Table 2.1. Reagent composition and reaction temperature for the preparation of monolithic silica columns.

Column	PEG (g)	TMOS (mL)	Urea (g)	AcOH (mL)	Temperature (°C)
A	8.8	40	9.0	100	40
B	12.4	40	9.0	100	30
C	12.8	40	9.0	100	30

glycol) (PEG, M_W = 10,000, Sigma, St. Louis, MO, USA) and urea in 0.01 M acetic acid and stirred at 0 °C for 45 min. The resulting homogeneous solution was introduced into the pretreated fused silica capillary tube, and allowed to react at 40 °C. Gelation occured within 2 h and the gel was subsequently aged overnight at the same temperature. Then the silica monolithic column was treated at a higher temperature (120 °C) for 3 h to complete mesopore formation from ammonia generated by the hydrolysis of urea, followed by washing with water and methanol. After drying, heat-treatment was carried out at 330 °C for 25 h, resulting in decomposition of organic moieties in the capillary. Table 2.1 lists the reagent mixture compositions and temperatures for the experimental columns.

Bulk silica monoliths. Three bulk silica monolithic samples representing each capillary sample A, B and C were prepared also. Briefly, a bulk sample was prepared in a small 5 mL glass vial, transferred to a 10 mL Soxhlet thimble, placed in a Soxhlet apparatus to extract with methanol for 12 h, and finally vacuum-dried for 5 h at 60 °C.

2.2.2 Scanning electron microscopy

The morphologies of the packed columns, monolithic columns and bulk monoliths were visualized using a scanning electron microscope (FEI Philips XL30 ESEM FEG, Hillsboro, OR, USA). A small section (2 cm) of each capillary column was cut and the cross sectional area was scanned. A section of the bulk monolith was placed on a mold and its surface was scanned.

2.2.3 Capillary flow porometry

A home-built gas flow meter was designed to measure the micro flow rates generated during the experiments. As shown in Figure 2.2, the flow meter was made from a small graduated pipette. The small end of the pipette was sealed using a high temperature flame, and the sealed pipette was filled with water and inverted with the open end submerged in a dish containing water. A 50 cm × 530 μm i.d fused silica capillary was connected at one end to a gas source. The other end of the capillary was inserted into the open end of the seated pipette. A stop watch was used to time the displacement of water in the pipette in order to calculate the gas flow rate.

Pressure control was provided by using a digital pressure controller (Alicat Scientific, Tucson, AZ, USA). The pressure was controlled accurately (± 0.25%). One end of the sample was connected to the output port of the pressure controller, while the other end was connected to the fused silica capillary inserted in the inverted pipette. When pressure was applied, the gas flow rates through the dry and wet samples were measured using the home-built microflow meter.

The dry up/wet up measurement method was applied in this work, which means that a dry curve was determined with the pressure increasing followed by a wet curve with the pressure increasing. Galwick was used as the wetting liquid (surface tension: 16.0 dynes/cm) for all of the wet curve experiments. Generally, the dry curve was measured first by increasing the nitrogen gas pressure at specific pre-set points through a 1.5 cm long dry sample. The sample was then filled with Galwick by purging with the liquid for approximate 0.5 h using a syringe pump

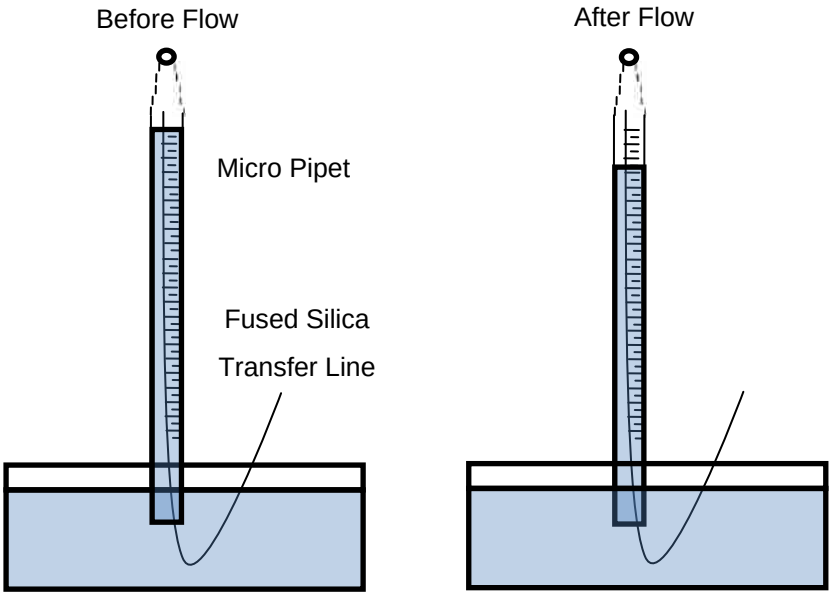

Figure 2.2. Schematic of the home-built microflow meter.

(Harvard Apparatus, Holliston, MA, USA) at a rate of 0.1 µL/min. After the sample was thoroughly wetted, the wet curve was obtained by measuring nitrogen gas flow rate through the sample as the pressure was increased. Typically, to obtain a stable flow rate (i.e., when the pores at a specific pressure are completely cleared of the wetting liquid), approximately 20 h was required for the first applied pressure. This was because the gas flow rate was very low and only a small number of pores were opened. However, at higher pressure when more pores were opened, the equilibration time could be as short as several minutes. Table 2.2 and 2.3 lists the repetitions of measurements made to the dry and wet curves.

2.3 Results and Discussion

2.3.1 Pore size characterization of silica particle packed columns

Wet, dry and half-dry curves. CFP measures the gas flow rate through dry/wet monoliths at specific differential pressures. The relationship between gas flow rate and differential pressure, called the dry/wet curve, can be obtained in sequence. The pore diameter is calculated from the differential pressure according to Equation 2.4. Although each pore may have a range of diameters, CFP only measures the most constricted part, which is called the throat pore diameter.

Based on the definition of the dry curve, the half-dry curve is half of the gas flow rate through the dry sample as a function of differential pressure. The pressure where the wet and half-dry curves intersect gives the mean flow pore diameter.

Figure 2.3 shows representative wet, dry, and half-dry curves of packed columns containing 3, 5 and 7 µm diameter silica particles determined by CFP. At a

Table 2.2. Repetitions for CFP determination of silica particle packed column samples.

Particle diameter (µm)	Column					
	1		2		3	
	Dry	Wet	Dry	Wet	Dry	Wet
3	3/1 [a]	1/3 [b]	3/1	1/3	3/1	1/3
5	3/1	1/3	3/1	1/3	3/1	1/3
7	3/1	1/3	3/1	1/3	3/1	1/3

[a] 3 determinations (i.e. 3 repetitions) of the total curve with 1 measurement of flow for each set pressure.

[b] 1 determination of the total curve with 3 repetition measurements of flow for each set pressure.

Table 2.3. Repetitions for CFP determination of silica monolithic column samples.

Monolith type	Column					
	1		2		3	
	Dry	Wet	Dry	Wet	Dry	Wet
A	3/1 [a]	1/3 [b]	3/1	1/3	3/1	1/3
B	3/1	1/3	3/1	1/3	3/1	1/3
C	3/1	1/3	3/1	1/3	3/1	1/3

[a] 3 determinations (i.e. 3 repetitions) of the total curve with 1 measurement of flow for each set pressure.

[b] 1 determination of the total curve with 3 repetition measurements of flow for each set pressure.

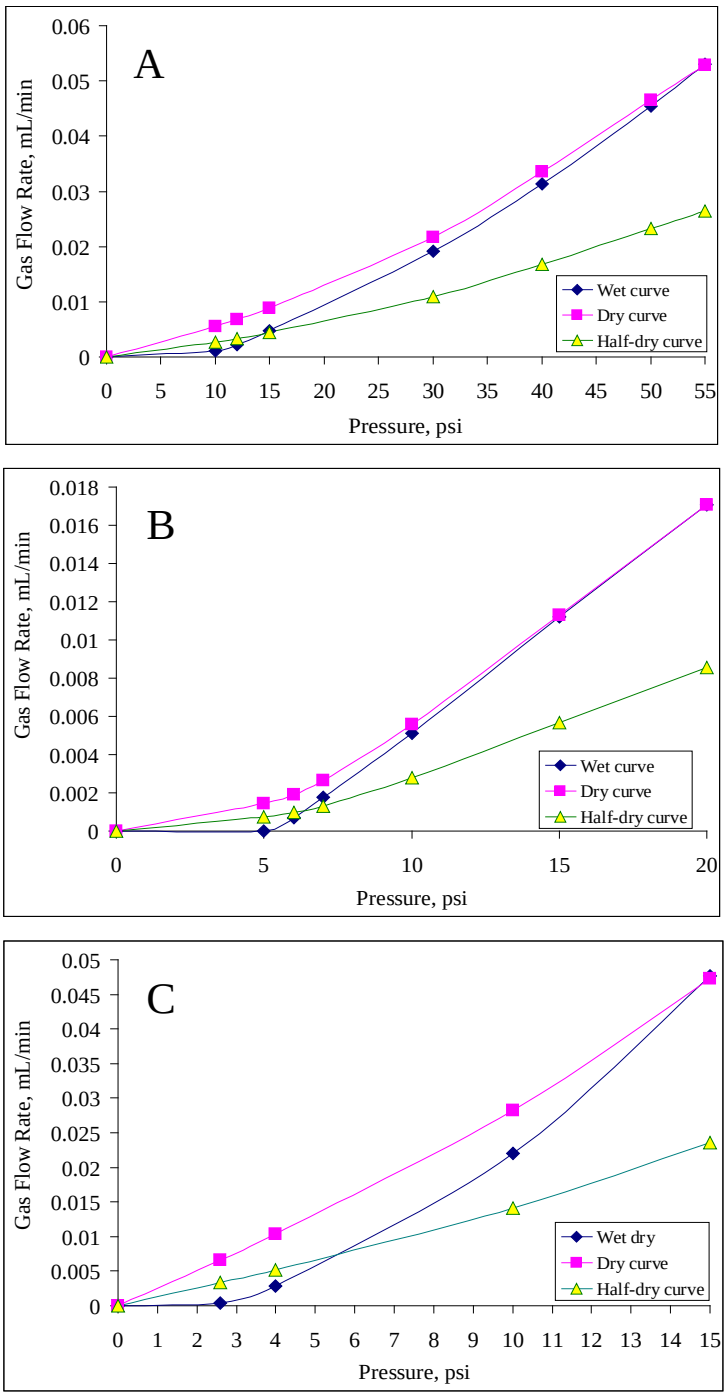

Figure 2.3. Wet, dry and half-dry curves for packed columns containing (A) 3,

(B) 5 and (C) 7 μm diameter particles measured using CFP.

specific differential pressure, the gas flow rate through a wet sample is always smaller than that through the corresponding dry sample until finally the two curves meet together, when all wetting liquid in the through pores is pushed out of the sample.

Table 2.4 summarizes the mean pore diameters obtained from CFP for packed columns containing 3, 5 and 7 µm particles. These values of 0.5 ± 0.02, 1.0 ± 0.17, and 1.4 ± 0.01 µm, respectively, are all smaller than pore diameters calculated from a close-packed arrangement (i.e., 0.7, 1.1 and 1.6 µm). This difference is most likelydue to the fact that the packing materials in the packed column segments were sintered at both ends to retain the particles inside the capillary. Since CFP only detects the most constricted part of a through-pore diameter, the sintered sections led to smaller mean pore diameters. Figure 2.4 are the SEM images of the three packed columns.

Cumulative filter flow. Figure 2.5 shows representative cumulative filter flows for columns packed with 3, 5 and 7 µm particles as determined using CFP. It is evident that all samples finally reached 100% cumulative filter flow. However, the minimum pressure to empty all through-pores in a column depended on the specific column pore characteristics. Due to its very large pores, the column packed with 7 µm particles only required 15 psi gas pressure to purge all of the wetting liquid from its pores, while 20 and 55 psi gas pressures, respectively, were required for columns packed with 5 and 3 µm particles.

Table 2.4. CFP determinations of mean pore diameter compared to calculated pore diameter for packed columns.

Particle diameter (µm)	Column mean pore diameter (µm)			Average	RSD (%)	Calculated [a] (µm)
	1	2	3			
3	0.52	0.48	0.55	0.52	6.75	0.68
5	1.04	1.02	0.96	1.01	4.12	1.13
7	1.45	1.35	1.40	1.40	3.33	1.59

[a]Calculated from close-packed arrangement.

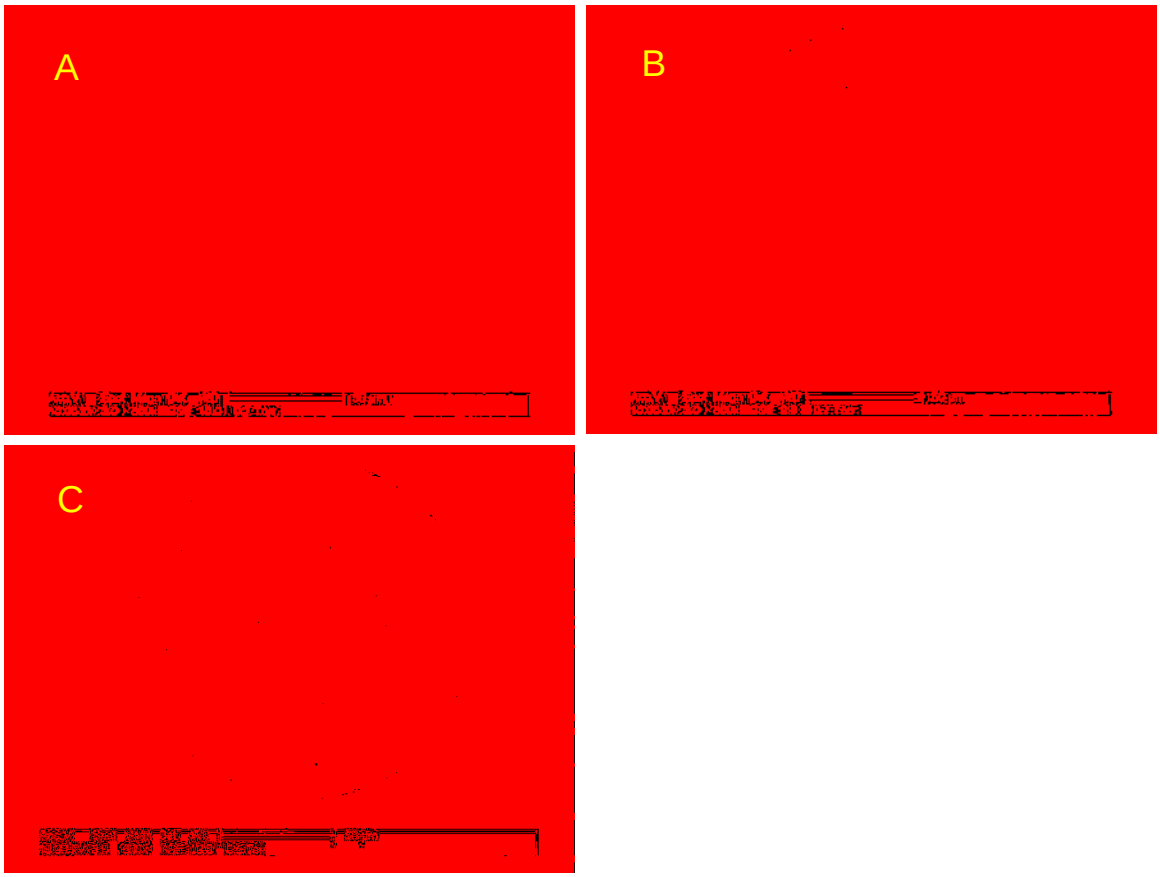

Figure 2.4. Scanning electron micrographs of columns packed with silica particles (A) 3 µm, (B) 5 µm, and (C) 7 µm diameter in 150 µm i.d. capillaries (500× magnification).

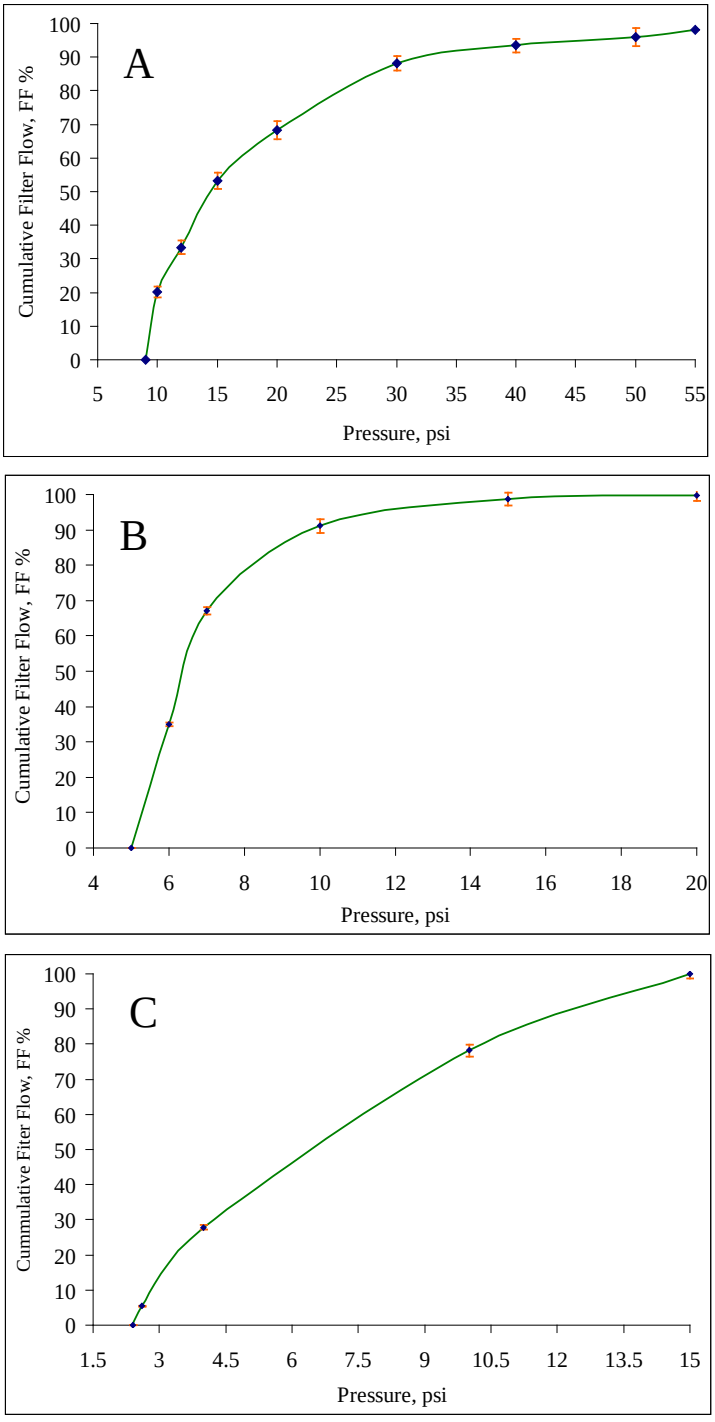

Figure 2.5. Cumulative filter flows for columns packed with (A) 3, (B) 5 and (C) 7 µm particles measured using CFP.

Pore size distribution. Figure 2.6 shows representative curves of the pore size distributions for columns packed with 3, 5 and 7 μm particles as determined by CFP. The area under the distribution curve in any pore size range is the percentage flow in that range. The representative pore size distributions indicate that for 7 μm diameter silica particles, the pores were distributed in a broad range of 0.4 - 2.6 μm. However, for 5 and 3 μm diameter silica particles, the pore size ranges shifted to much smaller values, i.e., 0.3 - 1.1 and 0.1 - 0.7 μm, respectively. Because the particle sizes are not completely uniform, we observed some smaller pores in the column packed with 7 μm particles and some larger pores in the column packed with 5 μm particles. If more measurements had been made to construct the pore size distribution curves, it would be clear whether or not bimodal pore size distributions were presenting for columns packed with 5 and 7 μm particles.

2.3.2 Pore size characterization of silica monolithic columns

The average through-pore diameters of silica monoliths A, B and C as listed in Table 2.1 were sequentially smaller due to a decrease in concentration of PEG in the prepolymer mixture. This conclusion was initially made from rough measurements of SEM images. Therefore, we used CFP to characterize the through-pore properties and to verify this conclusion.

Wet, dry and half-dry curves. Figure 2.7 shows representative wet, dry and half-dry curves obtained for monoliths A, B and C. Each crossing point of the corresponding wet and half-dry curves gave the mean through-pore diameters for columns A, B and C as 3.9, 1.3 and 0.8 μm (Table 2.5), respectively, which strongly

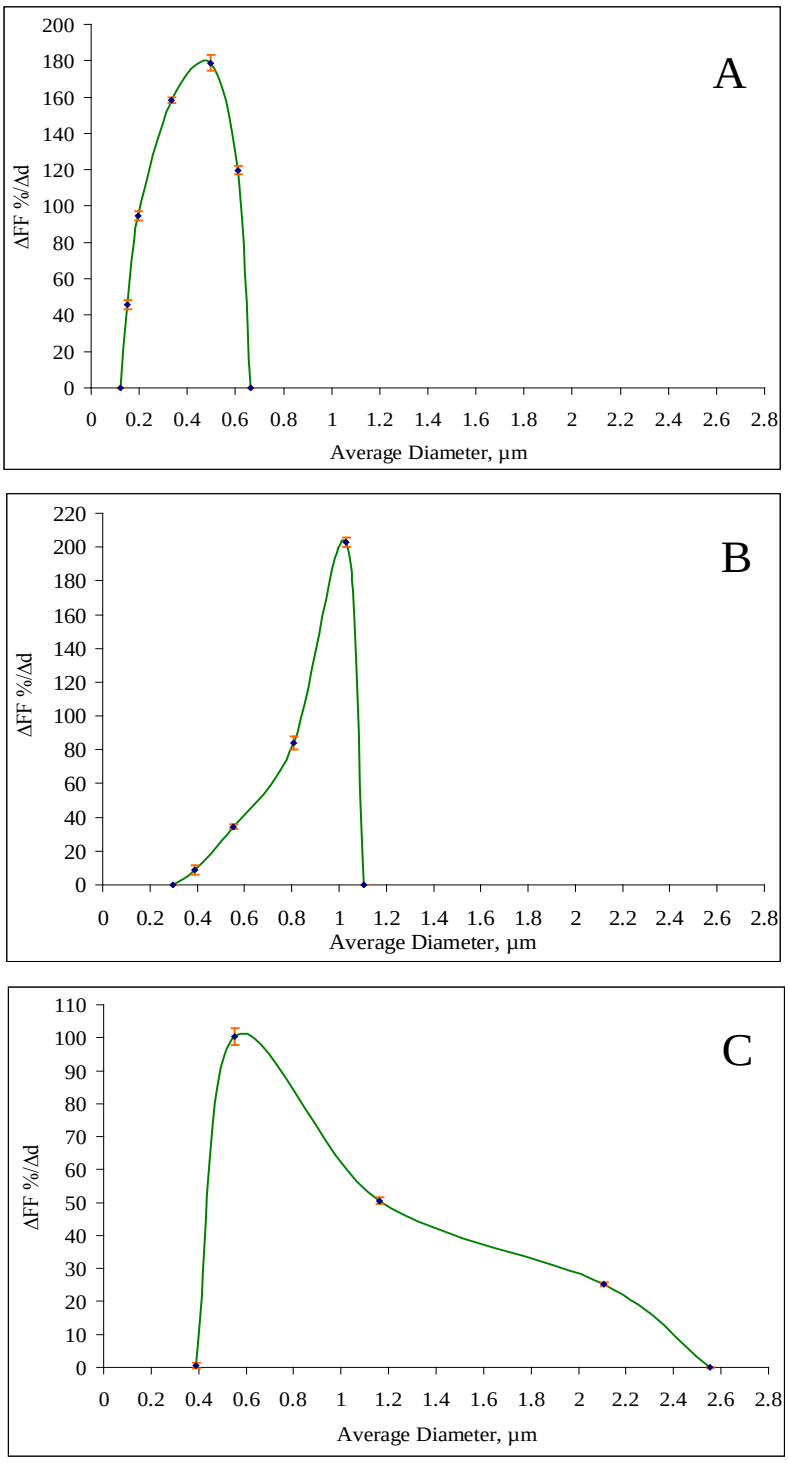

Figure 2.6. Pore size distributions of columns packed with (A) 3, (B) 5 and (C) 7 µm particles determined by CFP.

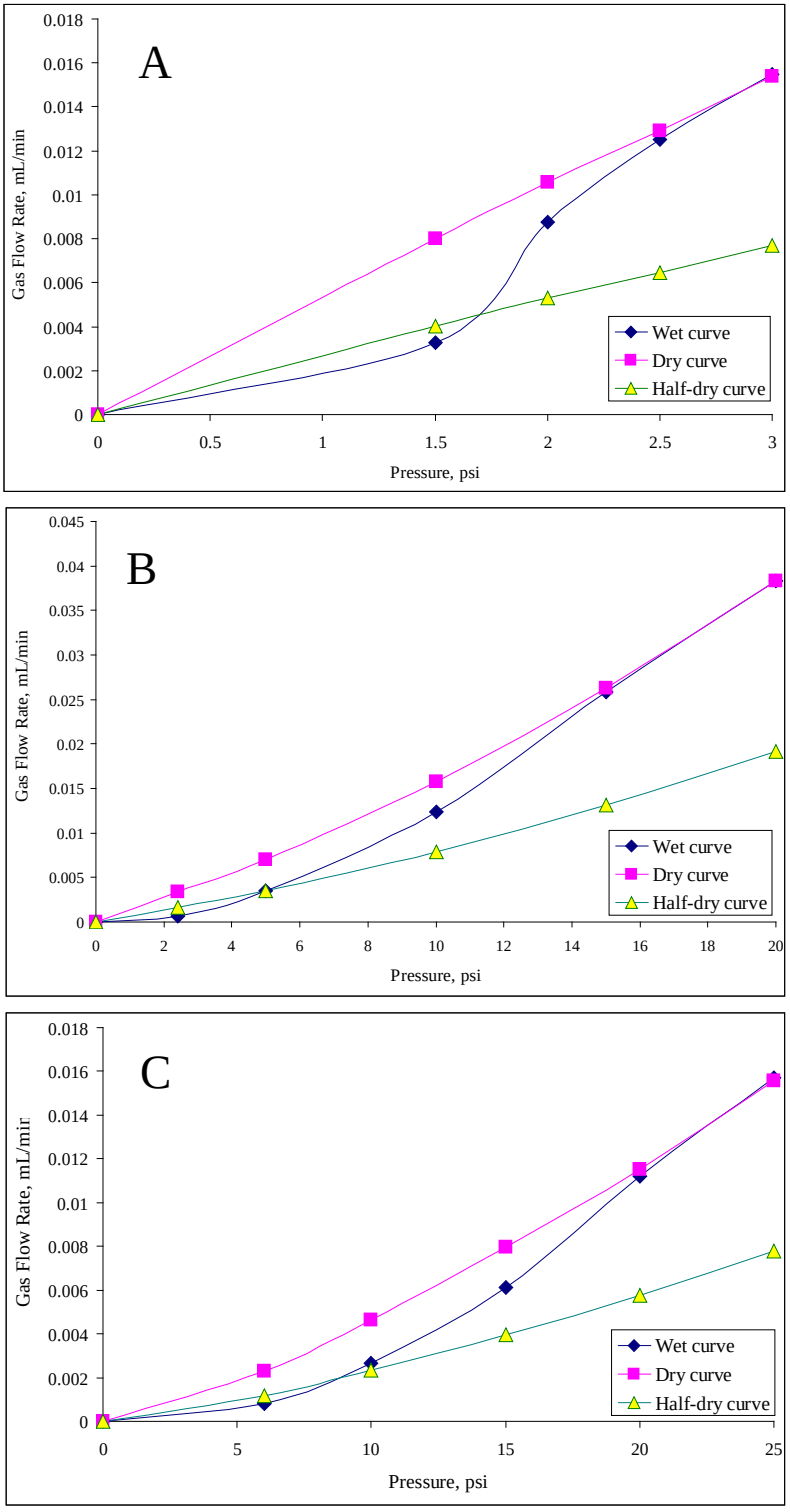

Figure 2.7. Wet, dry and half-dry curves for silica monoliths A, B and C measured using CFP.

Table 2.5. CFP determination of mean pore diameters for silica monolithic columns.

Column	Mean pore diameter (μm)			Average	RSD (%)
	1	2	3		
A	3.92	3.84	3.95	3.90	1.46
B	1.27	1.36	1.30	1.31	3.78
C	0.81	0.83	0.77	0.80	4.25

Cumulative filter flow. Figure 2.8 shows the representative cumulative filter flow curves for the three monolithic columns. As monolith A has the largest through pores, only 3 psi gas pressure was required to purge all of the wetting liquid out of the column. However, much higher pressures, i.e., 20 and 25 psi, respectively, were monoliths B and C, indicating tighter pore structures.

Pore size distribution. Figure 2.9 shows representative curves of the pore size distributions for monoliths A, B and C. Most through-pores in monolith A were between 2.1 - 4.4 μm, explaining the very low back pressure observed for this required for column. Some of the through-pores in column B were as large as 1.0 to 2.8 μm, while some were as small as 0.3 μm. Monolith C gave the smallest pores and narrowest pore size distribution in the range of 0.2 - 1.1 μm.

Comparison of bulk and capillary confined monoliths. Figure 2.10 shows SEM images of monoliths A, B and C synthesized in bulk (right) and in capillaries (left). The left images correspond to the pore properties measured using CFP. Many reports of monolithic columns include pore size properties based on measurements of representative bulk materials with the use of MIP or BET.[20-26] However, when bulk monoliths were fabricated in small glass vials from the same solutions which were used to fabricate monoliths A, B, and C inside capillary tubes, I found that the pore structures were quite different. The SEM images in the left column (in capillary) and right column (in bulk) in Figure 2.10 indicate that monoliths confined in supports the former conclusion regarding the concentration of PEG.

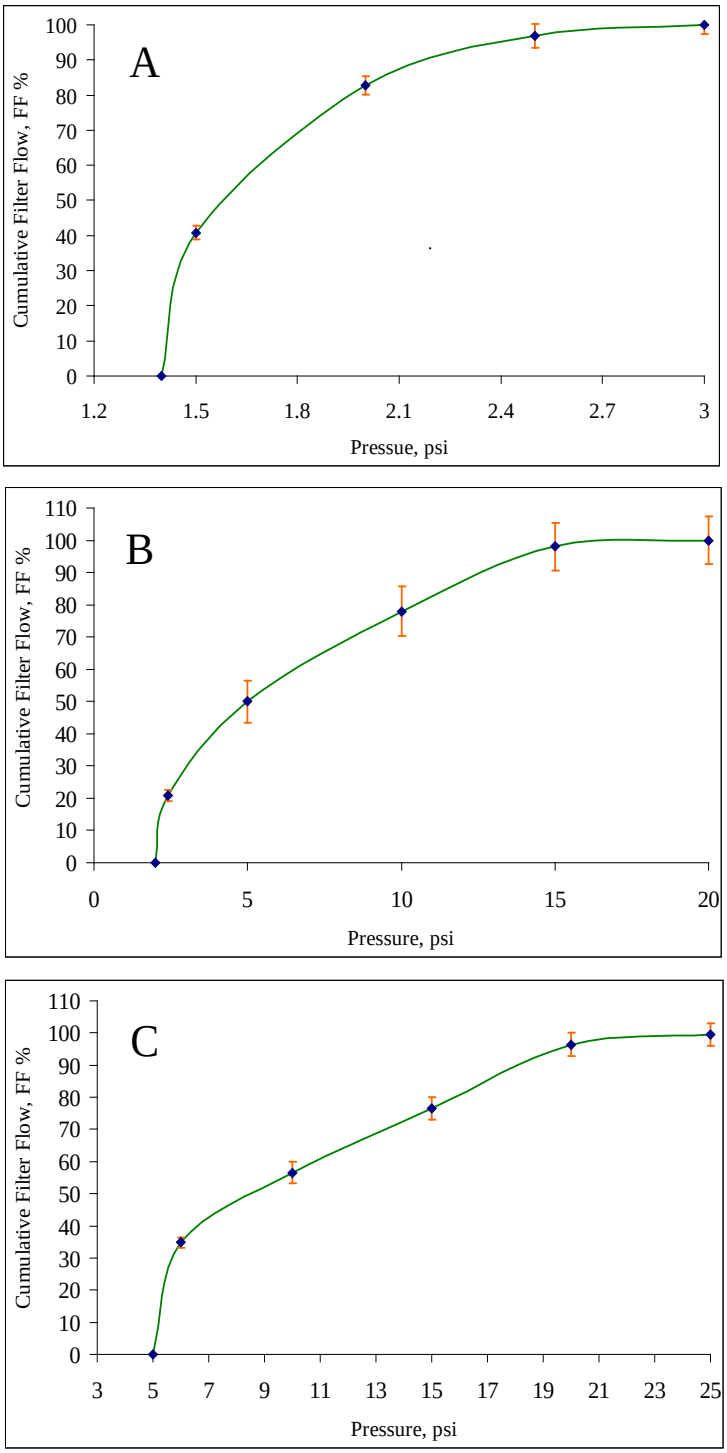

Figure 2.8. Cumulative filter flows for silica monoliths A, B and C measured using CFP.

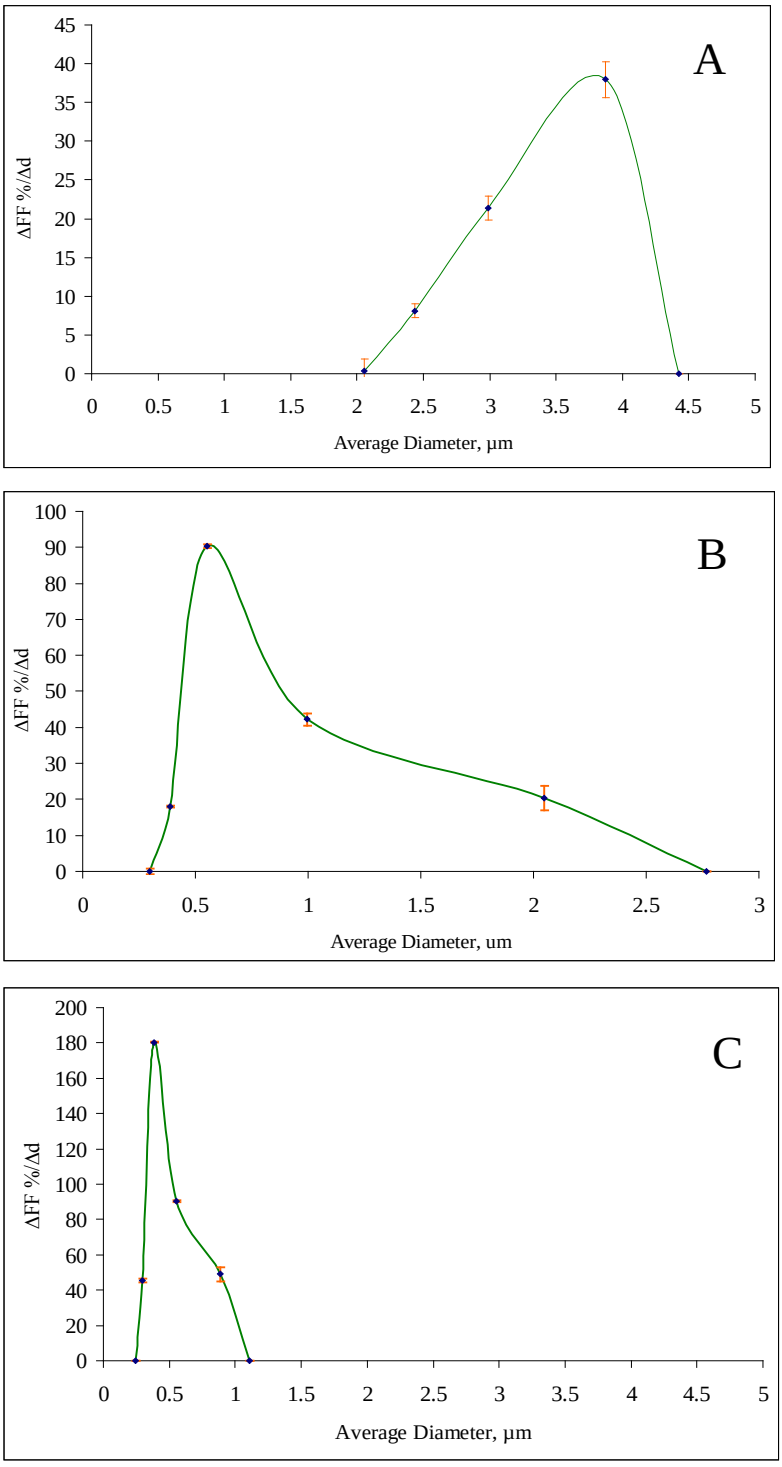

Figure 2.9. Pore size distributions of silica monoliths A, B and C determined by CFP.

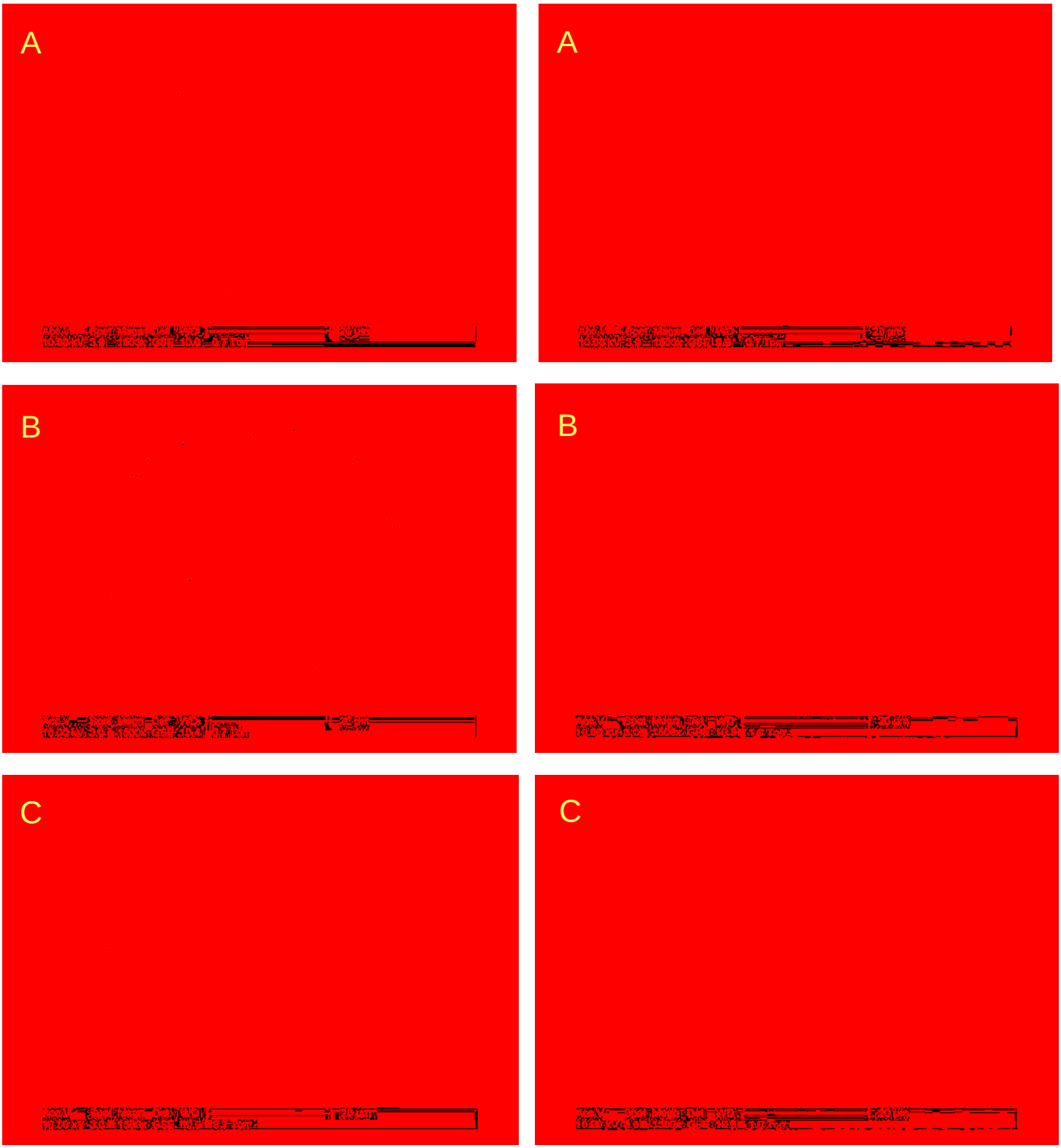

Figure 2.10. SEM images of silica monoliths A, B and C in capillaries (left) and in bulk (right) (1500× magnification).

capillary tubes produced larger pores. This could result because chemical reactions occur in different environments, which can affect conditions, such as pressure, temperature, and heat dissipation. Another reason is that after reaction, the porogens and unreacted prepolymer solutions in the capillary can be flushed out of the column more thoroughly; therefore, a monolith with more open structure would be formed.

2.4 Conclusions

A home-built CFP system was used to characterize the pore structures of silica particle packed and silica monolithic columns. Throat pore diameter, gas and liquid permeability, mean flow pore diameter, cumulative filter flow, and pore size distribution were measured. The mean through-pore diameters of the three packed columns were measured to be 0.5 ± 0.02, 1.0 ± 0.17, and 1.4 ± 0.01 μm, which are all smaller than the pore diameters calculated from a close-packed arrangement (i.e., 0.7, 1.1 and 1.6 μm), with distributions ranging from 0.1 - 0.7, 0.3 - 1.1 and 0.4 - 2.6 μm, respectively. This is reasonable, since visual inspection of SEM images of the particles showed relatively large fractions of smaller than specified particles in the samples.

The measurements verified that the mean pore diameters decreased for three monoliths with increasing concentration of PEG in the reaction mixture. A comparison of SEM images of silica monoliths indicate that monoliths confined in capillary tubes produced larger pores than bulk monoliths fabricated in small glass vials from the same prepolymer solutions.

2.5 References

1. Liang, C., Dai, S., Guiochon, G., *Anal. Chem*. **2003**, *75*, 4904 - 4912.
2. Lubda, D., Lindner, W., Quaglia, M., Hohenesche, C. F., Unger, K. K., *J. Chromatogr. A* **2005**, *1083*, 14 - 22.
3. Cabral, J. L., Bandilla, D., Skinner, C. D., *J. Chromatogr. A* **2006**, *1108*, 83 - 89.
4. Courtois, J., Szumski, M., Georgsson, F., Irgum, K., *Anal. Chem.* **2007**, *79*, 335 - 344.
5. Cabooter, D., Lynen, F., Sandra, P., Desmet, G., *J. Chromatogr. A* **2007**, *1157*, 131 - 141.
6. Gupta, V., Jena, A., *Advances in Filtration and Separation Technology* **1999**, *13b*, 833 - 844.
7. Jena, A. K., Gupta, K. M., *J. Power Sources* **1999**, *80 (1 & 2)***,** 46 - 52.
8. Jena, A. K., Gupta, K. M., *Fluid/Particle Separation J.* **2002**, *14 (3)***,** 227 - 241.
9. Gigova, A., *J. Power Sources* **2006**, *158*, 1054 - 1061.
10. Jena, A. K., Gupta, K. M., *American Ceramic Society Bulletin* **2003**, *82*, 9401 - 9406.
11. Sanders, H., Jena, A.K., *Ceramic Industry* **2000**, *150*, 26 - 29.
12. Gupta, N., Jena, A., Gupta, K., *Ceramic Industry* **2001**, *151*, 24 - 29.
13. Rideal, G., *Filtration News* **2004**, *July/August Issue*, 8 - 12.
14. Jena, A., Gupta, K., *INTC* **2000**, 10.0 - 10.11.
15. Jena, A., Gupta, K., *International Wovens J.* **2005**, *Summer Issue*, 26 - 30.
16. Mayer, E., *Filtration News* **2002**, *September/Octuber Issue*, 12 - 24.

17. ASTM Procedure F316-86: “Standard Test Method for Pore Size Characteristics of Membrane Filters by Bubble Point and Mean Flow Pore Test”, February 21, 1986.

18. Jena, A. K., Gupta, K. M., *Inter. Nonwovens J.* **2003**, *Fall*, 45 - 53.

19. Xiang, Y.; Yan, B.; Yue, B.; McNeff, C.V.; Carr, P.W.; Lee, M.L. *J. Chromatogr. A* **2003**, *983*, 83-89.

20. Motokawa, M., Kobayashi, H., Ishizuka, N., Minakuchi, H., Nakanishi, K., Jinnai, H., Hosoya, K., Ikegami, T., Tanaka, N., *J. Chromatogr. A* **2002**, *961*, 53 - 63.

21. Puy, G., Roux, R., Demesmay, C., Rocca, J.-L., Iapichella, J., Galarneau, A., Brunel, D., *J. Chromatogr. A* **2007**, *1160*, 150 - 159.

22. Yang, H., Shi, Q., Tian, B., Xie, S., Zhang, F., Yan, Y., Tu, B., Zhao, D., *Chem. Mater.* **2003**, *15*, 536 - 541.

23. Grimes, B., Skudas, R., Unger, K., Lubda, D., *J. Chromatogr. A* **2002**, *1144*, 14 - 29.

24. Viklund, C., Pontén, E., Glad, B., Irgum, K., Hörstedt, P., Svec, F., *Chem. Mater.* **1997**, *9*, 463 - 471.

25. Thommes, M., Skudas, R., Unger, K., Lubda, D., *J. Chromatogr. A* **2008**, *1191*, 57 - 66.

26. Unger, K., Skudas, R., Schulte, M., *J. Chromatogr. A* **2008**, *1184*, 393 - 415.

CHAPTER 3 VERIFICATION OF CAPILLARY FLOW POROMETRY FOR PORE SIZE CHARICTERIZATION OF CAPILLARY COLUMNS CONTAINING ORGANIC POLYMER MONOLITHS

3.1 Introduction

As described in detail in Chapter 1, monolithic columns have emerged in recent years as a new column technology to alleviate the pressure-drop limitation of packed bed columns, and many studies have been reported with respect to the development of this new column form.[1-28] However, only a few studies have been reported concerning the effects of inner diameter and column length on pore properties of polymeric monoliths. Gu et al.[29] reported the effect of monolithic column inner diameter on the separation of proteins in capillary liquid chromatography. Polymeric monolithic columns with i.d.s between 100 and 320 μm were systematically studied. The smaller diameter columns were found capable of providing better performance for protein separation due to less flow resistance and an increase in effective diffusion. This conclusion was supported by analysis using the Van Deemter equation, and separation permeability and breakthrough curve data.

As to the effect of column length, it is generally known that longer columns provide greater peak capacity and improve separation resolution. Meent and Jong [30] used two monolithic columns with lengths of 150 and 750 mm separately for liquid-chromatographic analysis of protein tryptic digests with UV and MS detection, and showed that longer monolithic columns provided improved peptide separation and increased the reliability of protein identification. However, it was difficult to find

much information about pore structure characterization of monolithic columns of different lengths.

The performance of the home-made CFP was first evaluated in Chapter 2 by characterizing the pore size distributions of capillary columns packed with 3, 5, and 7 μm particles. Reasonable results were obtained by comparing the mean pore diameter determined using CFP with those calculated from a close-packed arrangement. The mean pore diameter and pore size distribution of typical silica monoliths measured using the CFP system verified that a greater number of pores with small throat diameter were prepared in columns with higher PEG content in the prepolymer mixture.

In this chapter, the new CFP system was applied to study the effects of inner diameter and length on the pore size distributions of organic polymer monoliths in capillary columns based on butyl methacrylate (BMA) and poly(ethylene glycol) diacrylate (PEGDA). Both the homogeneity of the monolith and the reliability of the new CFP system were verified.

3.2 Experimental

Fabrication of monolithic columns. Before synthesis of a monolith, a very general method as reported before was used to functionalize the surface of the UV transparent capillary. First, it was washed with ethanol and deionized water, followed by incubating with 2 M hydrochloric acid for 3 h at 110 °C in a GC oven. Then it was rinsed with ethanol and dried with N_2 at 110 °C overnight in the GC oven. Afterwards, a 15% solution of 3-(trimethoxysilyl)propylmethacrylate in dried toluene

was placed in the capillary overnight at room temperature. After reaction, it was rinsed with toluene and acetone and dried with N_2 overnight in the GC oven.

A prepolymer mixture of 23.9 % GMA, 15.9 % PEGDA, 0.40 % DMPA (2,2-dimethoxy-2-phenyl-acetophenone), 4.98 % methanol and 54.8 % cyclohexanol, was made by weighing each ingredient based on concentration in a 5 mL glass vial. This solution was degassed for approximately 30 s to a clear solution, and then was introduced into the treated capillary by capillary action, followed by exposure to UV light with a cold mirror for approximately 15 min for polymerization. After reaction, the capillary column was flushed with methanol followed by deionized water using a syringe pump to finally open the pores in the skeletal structure of the monolith.

In this work, monoliths were fabricated in 50, 75, 150 and 250 µm i.d. UV transparent capillary columns to study the effect of inner diameter on pore structure. The same monolith was prepared in 75 µm i.d. capillaries in lengths of 1.5, 2.0 and 3.0 cm to explore the effect of length on the pore properties of the columns.

Scanning electron microscopy (SEM). The morphologies of the monolithic columns having different inner diameters were visualized using a scanning electron microscope (FEI Philips XL30 ESEM FEG, Hillsboro, OR, USA). A small section (2 cm) of each capillary column was cut and mounted on a stainless steel sample mold with double-stick tape, and the cross sectional area was scanned.

Determination of pore properties using capillary flow porometry (CFP). As introduced in previous chapters, a home-built gas flow meter was designed to measure the micro flow rates generated during the experiments. The dry up/wet up

measurement method was applied in this work using Galwick [i.e., propene, 1,1,2,3,3,3-hexaflouro, oxidized, polymerized] as the wetting liquid. Table 3.1 and 3.2 lists the repetitions of measurements made to the dry and wet curves.

3.3 Results and Discussion

Effect of column diameter. Figure 3.1 shows SEM images of monolithic columns with inner diameters of 50, 75, 150, and 250 μm. It can be seen that all of the porous monoliths are continuous with micrometer-sized through-pores. However, it is hard to distinguish any difference in pore size only from these SEM images. Fortunately, even in columns with inner diameters as large as 150 and 250 μm, the monoliths were still firmly attached to the column surface. This is one of the advantages of polymeric monoliths compared to inorganic monoliths, especially silica monoliths.

Figure 3.2 shows representative wet, dry and half-dry curves for each of the columns. The half-dry curve was derived from half of the gas flow rate through the dry sample as a function of the differential pressure, which was used to compute the mean pore diameter of the sample. As defined, the pressure where the wet and half-dry curves intersect gives the mean pore diameter. Pressures of 9.88, 9.19, 8.56 and 9.15 psi at the intersecting points of the wet and half-dry curves indicate similar mean pore diameters for all of the columns, regardless of column inner diameter. This is to some degree in accordance with the morphologies observed from the SEM images in Figure 3.1. Table 3.3 lists the mean pore diameters of the columns tested.

Table 3.1. Repetitions for CFP determination of polymeric monolith samples.

Column i.d. (µm)	Column					
	1		2		3	
	Dry	Wet	Dry	Wet	Dry	Wet
50	3/1 [a]	1/3 [b]	3/1	1/3	3/1	1/3
75	3/1	1/3	3/1	1/3	3/1	1/3
150	3/1	1/3	3/1	1/3	3/1	1/3
250	3/1	1/3	3/1	1/3	3/1	1/3

[a] 3 determinations (i.e. 3 repetitions) of the total curve with 1 measurement of flow for each set pressure.

[b] 1 determination of the total curve with 3 repetition measurements of flow for each set pressure.

Table 3.2. Repetitions for CFP determination of polymeric monolith samples.

Column length (cm)	Column					
	1		2		3	
	Dry	Wet	Dry	Wet	Dry	Wet
1.5	3/1 [a]	1/3 [b]	3/1	1/3	3/1	1/3
2.0	3/1	1/3	3/1	1/3	3/1	1/3
3.0	3/1	1/3	3/1	1/3	3/1	1/3

[a] 3 determinations (i.e. 3 repetitions) of the total curve with 1 measurement of flow for each set pressure.

[b] 1 determination of the total curve with 3 repetition measurements of flow for each set pressure.

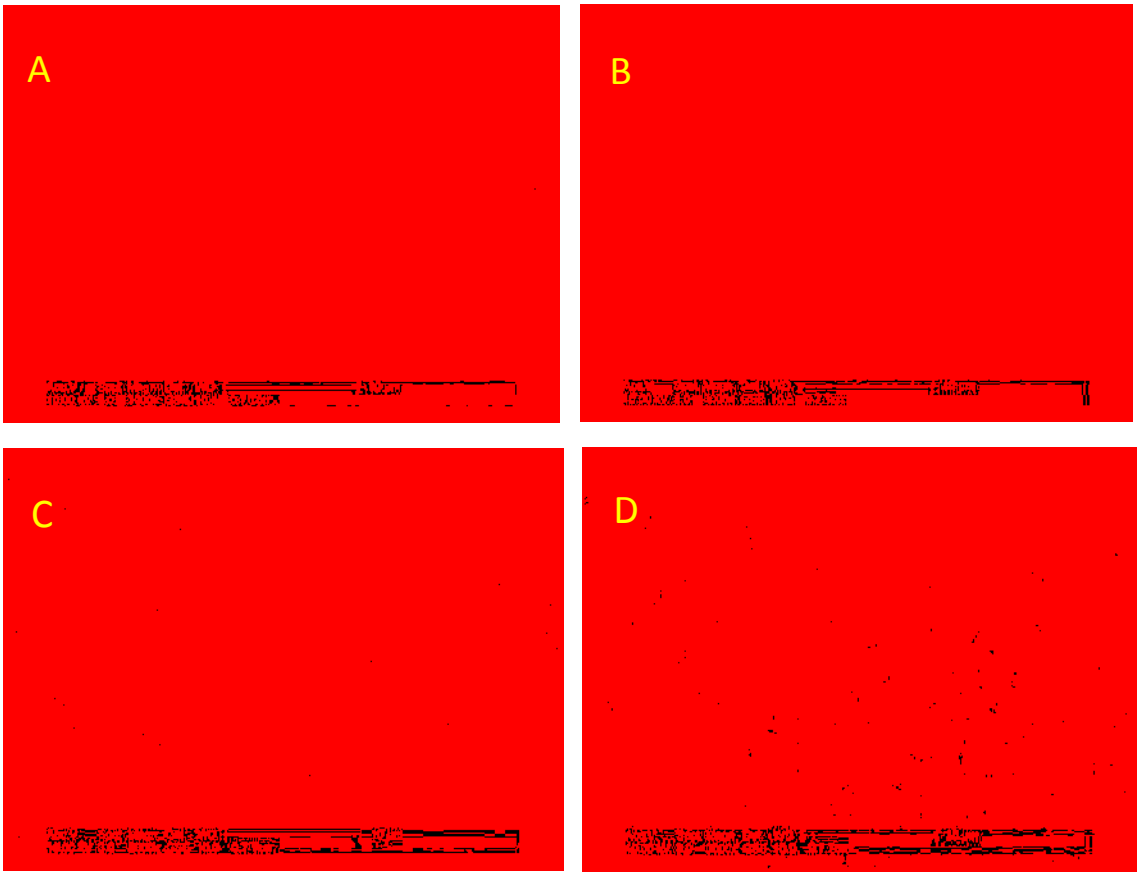

Figure 3.1. Scanning electron micrographs of polymeric monoliths in (A) 50, (B) 75, (C) 150 and (D) 250 μm i.d. capillaries (3000× magnification).

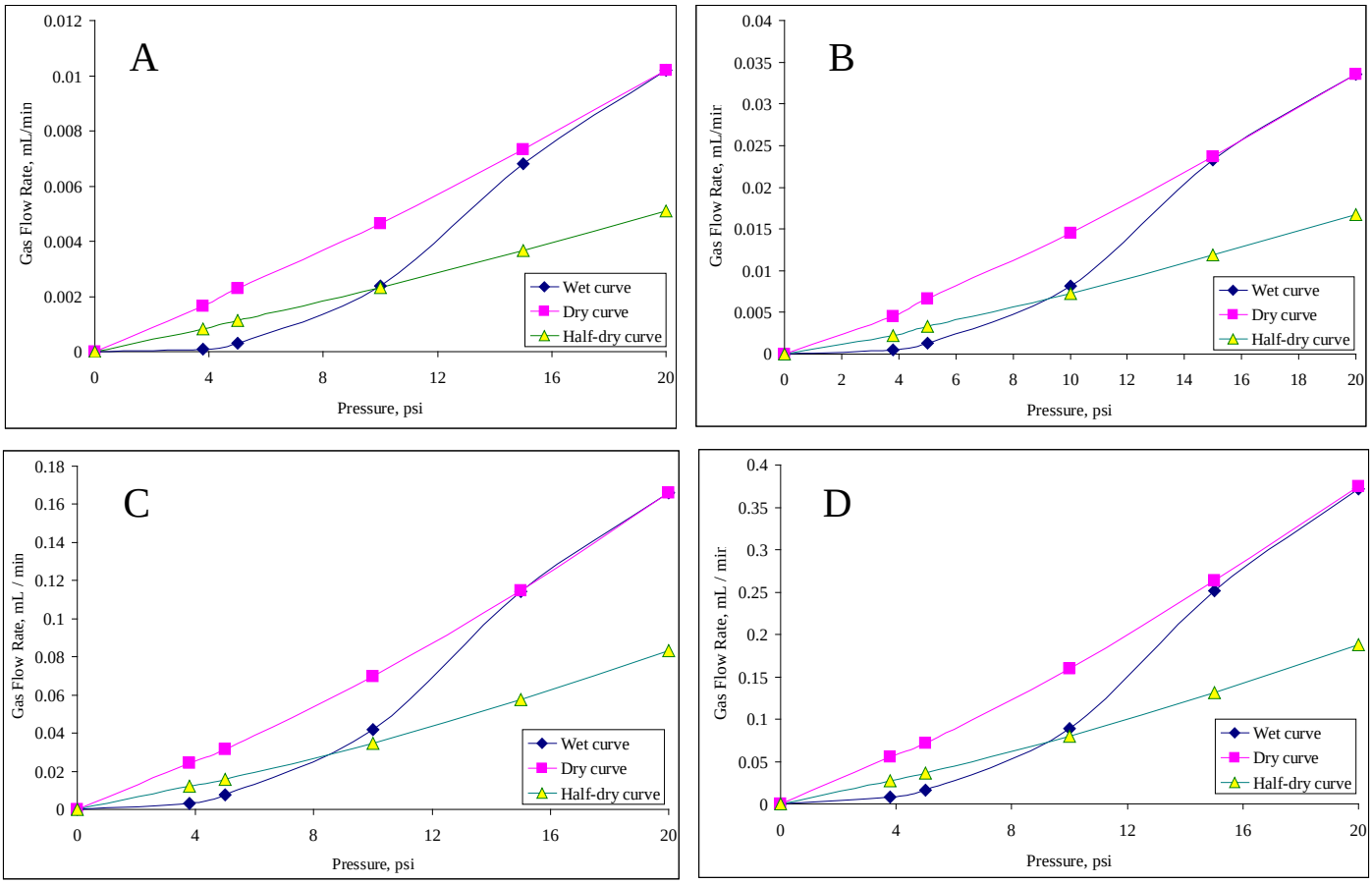

Figure 3.2. Wet, dry and half-dry curves for polymeric monoliths prepared in (A) 50, (B) 75, (C) 150 and (D) 250 µm i.d. capillaries measured using CFP.

Table 3.3. CFP determination of mean pore diameters for polymeric monoliths.

Column i.d. (µm)	Column mean pore diameter (µm)			Average	RSD (%)
	1	2	3		
50	0.67	0.70	0.75	0.71	5.72
75	0.72	0.77	0.80	0.76	5.29
150	0.78	0.72	0.77	0.76	4.25
250	0.73	0.74	0.78	0.75	3.53

Polymeric monoliths can be prepared by free radical polymerization using heat or UV light initiation, however, the latter is commonly preferred. A prepolymer mixture consists of initiator, monomer(s) and porogen(s). Once a certain amount of energy is provided via UV radiation, the initiator which has already been added in the mixture starts to decompose, producing free radicals that initiate the formation of nuclei. As more and more free radicals are liberated, the nuclei become larger until they reach the globular size and finally precipitate. Because monomers are thermodynamically better solvating agents for polymers than porogens, the precipitated nuclei will be surrounded with monomers. Since the concentration of the monomers is higher in the nuclei than in the surrounding solution, polymerization is kinetically preferred in the nuclei. Consequently, as polymers in the nuclei accumulate and the density of the nuclei increase, the whole structure will finally solidify. Initially, the structure is loose with many pores. As polymerization continues, the whole structure grows and crosslinks until a final stable monolith is formed. The temperature controls the decomposition rate of the initiator and, as a result, the concentration of nuclei at any time. If the temperature is low, fewer nuclei will be produced; however, since the concentration of monomers is the same, the individual nuclei will grow larger. Obviously, in a defined volume, the larger the nuclei, the larger the pores that are formed. Therefore, temperature can be applied as a powerful tool to control the pore structure of a monolith.

It is known that polymerization is typically an exothermic process. Heat is released during the preparation of monoliths. If the inner diameter of a column is

large, the generated heat might not be dissipated fast enough. Accumulated heat will increase the decomposition rate of the initiator, which will further increase the number of nuclei formed in a given time. As explained above, since the concentration of monomers is the same, more nuclei will grow to the globular size at once and will not grow very large in the confined space of the column. Consequently, the interstitial voids between the smaller globules will be smaller as well. In the worst case, if the temperature increases too much, it will result in an extremely inhomogeneous structure. Due to this concern, a diameter of 10-25 mm is considered to be the upper limit for preparing monoliths through polymerization.[31, 32] Monoliths prepared in very large columns, e.g., 2.7 mm inner diameter, use methods to control the polymerization temperature.[33-35]

Studies have shown that there is only a very moderate temperature effect on pore size in columns with inner diameters less that 1 mm, as indicated in Figure 3.3.[1] This can explain why a similar mean pore size was determined by CFP for columns with inner diameters from 50 to 250 µm. The heat generated during polymerization can be dissipated well enough in either the 50 or 250 i.d. capillaries. As the curve in Figure 3.3 indicates, there should be a critical inner diameter from which the temperature effect starts to be significant. This diameter may be different for different prepolymer reagents.

Figure 3.4 shows the pore size distributions of columns with different diameters as measured using CFP, which is in accordance with the results in Figures

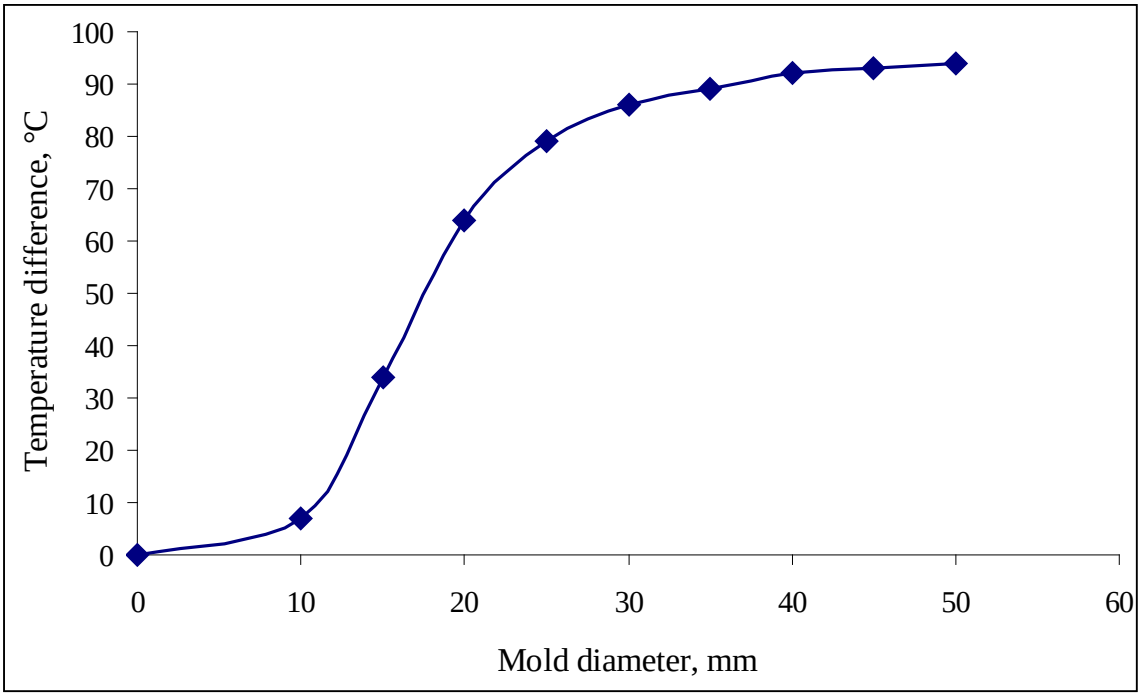

Figure 3.3. Maximum temperature increase of the polymerization mixture placed in molds of different diameters during the polymerization of glycidyl methacrylate-ethylene dimethacrylate monoliths.

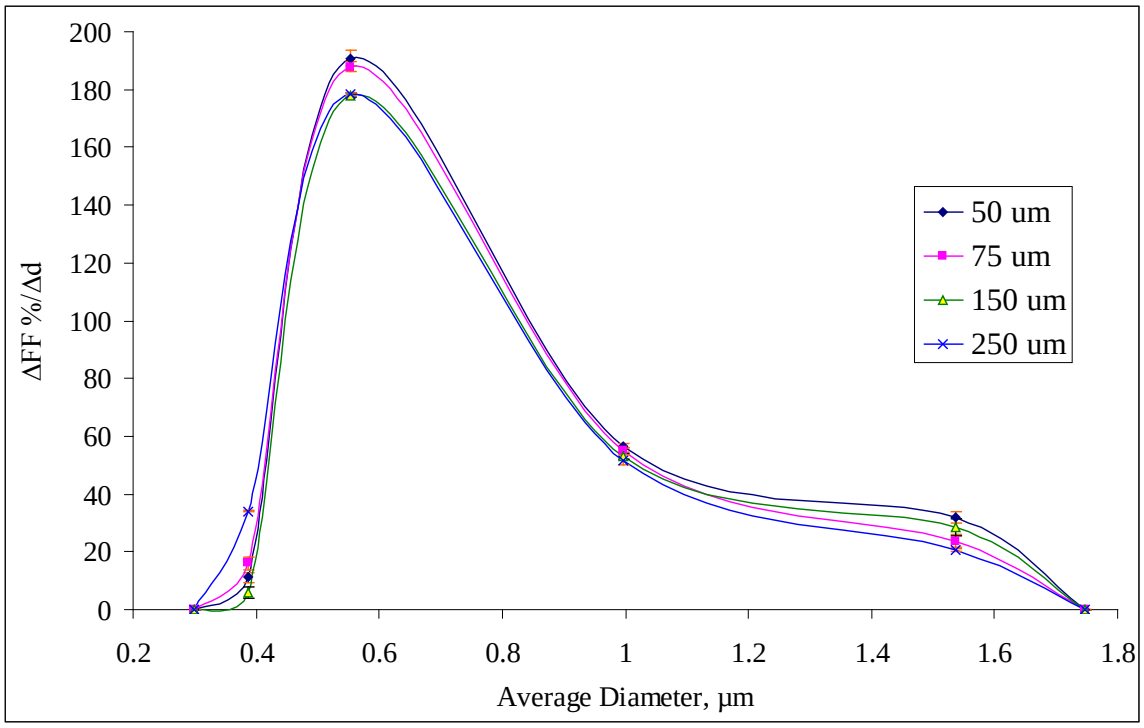

Figure 3.4. Pore size distributions of polymeric monoliths prepared in 50, 75, 150 and 250 i.d. capillaries determined by CFP.

3.1 and 3.2. There is very little difference in pore size distribution among these four columns. Generally, the through-pores are distributed in the range of 0.30-1.75 μm. The monolith prepared in the 50 μm i.d. capillary shows a little higher percentage of larger pores, while the monolith prepared in a 250 μm i.d. capillary has more pores with smaller diameters. Table 3.4 lists the relative standard deviations of the pore size distributions for these four columns.

Effect of length. In order to check the interconnectivity of pores in this polymeric monolithic column, and to further verify the reliability of the new CFP system, monolithic columns with lengths of 1.5, 2.0 and 3.0 were characterized using the home-made CFP. Figure 3.5 shows typical dry and wet curves for these columns. It is very clear that different gas flow rates were measured for both wet and dry curves in columns of different lengths. At constant pressure, the shorter columns gave higher wet and dry flow rates, and the flow rates were proportional to the lengths of the columns. For example, when 10 psi differential pressure was applied, the gas flow rates in the dry and wet samples were 0.0145 and 0.0082 mL/min, respectively, in a 1.5 cm long column, and 0.0066 and 0.0036 mL/min, respectively, in a 3.0 cm long column.

Table 3.5 lists the mean pore diameters for these columns. Although there were differences in the wet and dry flow rates in columns of different lengths, the intersecting points of the wet and half-dry curves for the columns appeared at approximately the same differential pressure of 9.25 psi. This means that these three columns have a similar mean pore diameter of 0.71 μm. Furthermore, all of the dry

Table 3.4. Pore size distributions in different i.d. capillary columns.

Set pressure (psi)	Calculated pore diameter (µm)	ΔFF %/Δd [a]				RSD (%)
		50 µm i.d.	75 µm i.d.	150 µm i.d.	250 µm i.d.	
3.8	1.75	0.00	0.00	0.00	0.00	0.00
5.0	1.54	30.2	21.3	28.7	20.0	20.5
10.0	1.00	56.2	54.6	53.5	50.1	4.82
15.0	0.55	190	189	179	178	3.47
20.0	0.39	12.7	17.5	5.17	34.1	70.6
25.0	0.30	0.01	0.05	0.01	0.04	75.0

[a] ΔFF %/Δd is calculated as described on page 35, where d is derived from the set pressure as given by Equation 2.4 in Chapter 2.

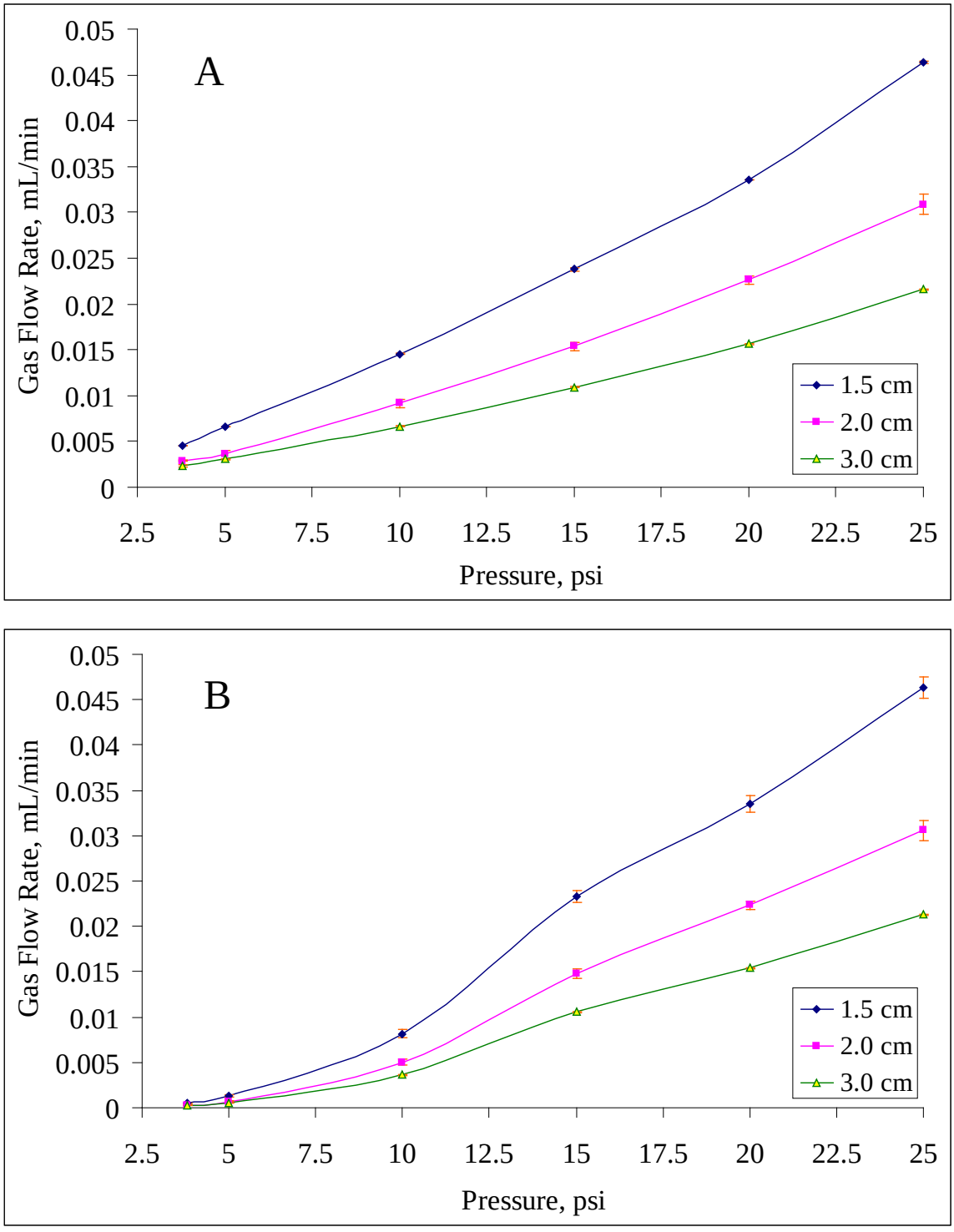

Figure 3.5. Comparisons of (A) dry and (B) wet curves for 1.5, 2.0 and 3.0 cm long polymeric monoliths determined using CFP.

Table 3.5. CFP determinations of mean pore diameters for polymeric monoliths.

Column length (cm)	Column mean pore diameter (μm)			Average	RSD (%)
	1	2	3		
1.5	0.72	0.73	0.72	0.72	0.80
2.0	0.72	0.71	0.70	0.71	1.41
3.0	0.71	0.71	0.69	0.70	1.64

and wet curves converged to the same differential pressure, 25 psi, corresponding to a pore diameter of 0.27 µm, which is the smallest through-pore size detectable in this monolith using CFP.

The pore size distribution for each of the columns is shown in Figure 3.6. They all have remarkably similar shape and range. Even though different gas flow rates were measured for these columns, both dry and wet curves changed together, resulting in a similar ratio between the wet and dry curves at every differential pressure for all columns. Consequently, the computed pore size distributions for all of the columns are identical in the range of 0.30 to 1.75 µm. Since in most cases the three different length columns were cut from the middle sections of a longer column, the pore size distributions indicate that the pore morphology was consistent along the length of the column, and the through-pores were highly interconnected.

3.4 Conclusions

In this work, a typical monolithic stationary phase based on BMA and PEGDA was synthesized for study of the effects of column inner diameter and length on monolith pore properties using CFP methodology. Four columns with inner diameters of 50, 75, 150 and 250 µm were fabricated, and the 75 µm i.d. column was cut into three shorter columns with lengths of 1.5, 2.0 and 3.0 cm. The mean pore diameters and the pore size distributions indicated that similar pore structures were obtained in all columns studied. Heat generated during polymerization was easily dissipated through the capillary walls. Therefore, temperature effects were not significant.

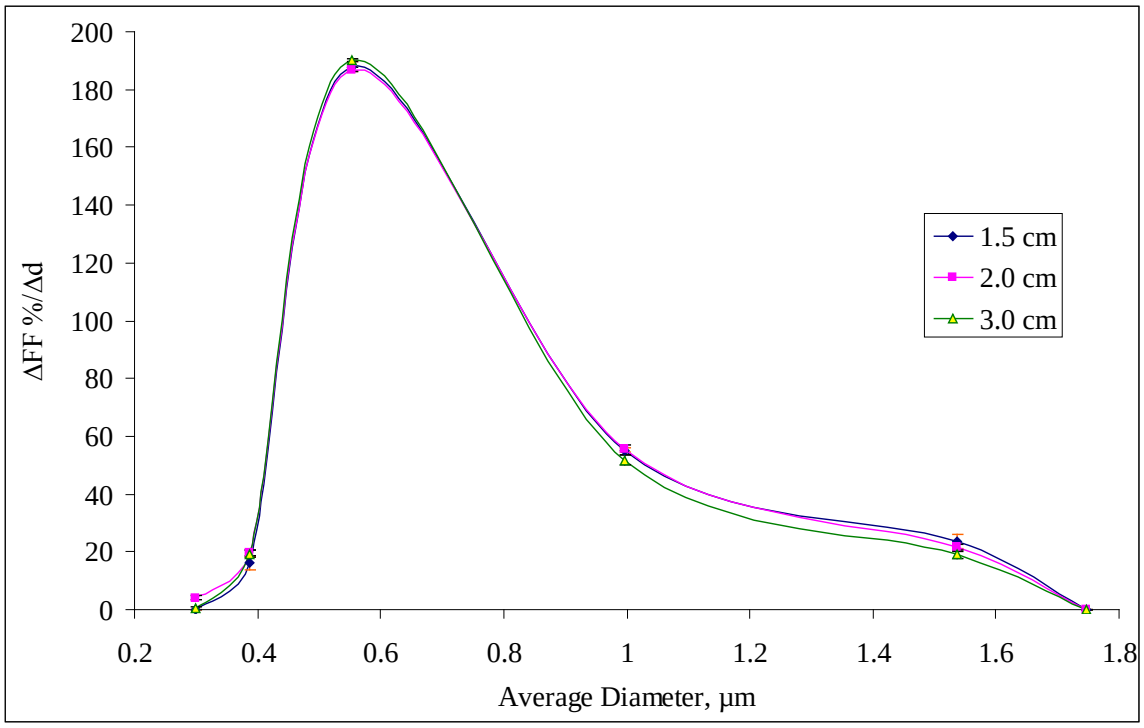

Figure 3.6. Pore size distributions of 1.5, 2.0 and 3.0 cm long polymeric monolithic column segments determined by CFP.

The mean pore diameters and the pore size distributions also showed that the pore properties of the three columns with different lengths were identical, which verified that the pores in the monolith were highly interconnected and the pore structures were uniform. Therefore, it is not necessary to use precise capillary lengths for CFP determinations. Most importantly, this finding validates the use of CFP for determination of monolithic pore structures directly in capillary columns.

3.5 References

1. Svec, F., Tennikova, T.B., Deyl, Z. Monolithic Materials: Preparation, Properties and Applications; Elsevier: Amsterdam, 2003.
2. Desmet, G.; Cabooter, D.; Gzil, P.; Verelst, H.; Mangelings, Y.V.H.; Clicq, D. *J. Chromatogr. A* **2006**, *1130*, 158-166.
3. Hjertén, S.; Liao, J. L.; Zhang, R. *J. Chromatogr.* **1989**, *473*, 273-280.
4. Svec, F.; Fréchet, J. M. J. *Anal. Chem.* **1992**, *64*, 820-822.
5. Gusev, I.; Huang, X.; Horvath, C. *J. Chromatogr. A* **1999**, *855*, 273-290.
6. Minakuchi, H.; Nagayama, H.; Soga, N.; Ishizuka, N.; Tanaka, N. *Anal. Chem.* **1996**, *68*, 3498-3501.
7. Minakuchi, H.; Nakanishi, K.; Soga, N.; Ishizuka, N.; Tanaka, N. *J. Chromatogr. A* **1998**, *797*, 121-131.
8. Oberarcher, H.; Premstaller, A.; Huber, C.G. *J. Chromatogr. A* **2004**, *1030*, 201-208.
9. Yang, Y.; Donald R. Lynch, Jr. *LCGC LC Column Technology Supplement* **2004**, *June*, 34-38.
10. Motokawa, M.; Kobayashi, H.; Ishizuka, N.; Minakuchi, H.; Nakanishi, K.; Jinnai, H.; Hosoya, K.; Ikegami, T.; Tanaka, N. *J. Chromatogr. A* **2002**, *961*, 53-63.
11. Vidič, J.; Podgornik, A.; Štrancar, A. *J. Chromatogr. A* **2005**, *1065*, 51-58.
12. Svec, F.; Peters, E. C.; Sýkora, D.; Fréchet, J. M. J. *J. Chromatogr. A* **2000**, *887*, 3-29.

13. Zou, H.; Huang, X.; Ye, M.; Luo, Q. *J. Chromatogr. A* **2002**, *954*, 5-32.

14. Ngola, S. M.; Fintschenko, Y.; Choi, W.; Shepodd, T. J. *Anal. Chem.* **2001**, *73*, 849-856.

15. Palm, A.; Novotny, M. V. *Anal. Chem.* **1997**, *69*, 4499-4507.

16. Gu, B.; Armenta, J. M.; Lee, M. L. *J. Chromatogr. A* **2005**, *1079*, 382-391.

17. Armenta, J. M.; Gu, B.; Humble, P. H.; Thulin, C. D.; Lee, M. L. *J. Chromatogr. A* **2005**, *1097*, 171-178.

18. Gu, B.; Chen, Z.; Thulin, C. D.; Lee, M. L. *Anal. Chem.* **2006**, *78*, 3509-3518.

19. Courtois, J.; Szumski, M.; Byström, E.; Iwasiewicz, A.; Shchukarev, A.; Irgum, K. *J. Sep. Sci.* **2006**, *29***,** 14-24.

20. Rohr, T.; Hilder, E. F.; Donovan, J. J.; Svec, F.; Fréchet, J. M. J. *Macromolecules* **2003**, *36*, 1677-1684.

21. Elicabe, G. E.; Larrondo, H. A.; Williams, R. J. J. *Macromolecules* **1998**, *31*, 8173-8182.

22. Kiefer, J.; Hilborn, J. G.; Manson, J. A. E.; Leterrier, Y.; Hedrick, J. L. *Macromolecules* **1996**, *29*, 4158-4160.

23. Kiefer, J.; Hedrick, J. L.; Hilborn, J. G. *Adv. Polym. Sci.* **1999**, *147*, 161-247.

24. Svec, F.; Peters, E. C.; Sykora, D.; Yu, G.; Fréchet, J. M. J. *J. High Resolut. Chromatogr.* **2000**, *23*, 3-18.

25. Svec, F. *LC/GC Europe* **2003**, *June (Recent Developments in LC Column Technology)*, 2-6.

26. Carlier, J.; Chuda, K.; Arscott, S.; Thomy, V.; Verbeke, B.; Coqueret, X.; Camart, J. C.; Druon, C.; Tabourier, P. *J. Micromech. Microeng.* **2006**, *16*, 2211-2219.

27. Geiser, L.; Eeltink, S.; Svec, F.; Fréchet, J. M. J. *J. Chromatogr. A* **2007**, *1140*, 140-146.

28. Svec, F.; Fréchet, J. M. J. *Ind. Eng. Chem. Res.* **1999**, *38*, 34-48.

29. Gu, C.; Lin, L.; Chen, X.; Jia, J.; Ren, J.; Fang, N. *J. Chromatogr. A* **2007**, *1170*, 15-22.

30. Van De Meent, M. H. M.; De Jong, G. J. *Anal. Bioanal. Chem.* **2007**, *388*, 195-200.

31. Zhang, L.; Ping, G.; Zhang, L.; Zhang, W.; Zhang, Y. *J. Sep. Sci.* **2003**, *26*, 331-336.

32. Širc, J.; Bosáková, Z.; Coufal, P.; Michálek, J.; Guryča, V. *Materials and Manufacturing Processes* **2008**, *23*, 591-596.

33. Qu, Q.; He, Y.; Gan, W.; Deng, N.; Lin, X. *J. Chromatogr. A* **2003**, *983*, 255-262.

34. Qu, Q.; Qu, R.; Xu, Q.; Wang, Y.; Wang, X.; He, Y. *J. Sep. Sci.* **2004**, *27*, 725-728.

35. Podgornik, A.; Barut, M.; Štrancar, A. *Anal. Chem.* **2000**, *72*, 5693-5699.

CHAPTER 4 PREPARATION OF MONOLITHIC STRUCTURES IN SACRIFICIAL LAYER, PLANAR MICROFLUIDIC DEVICES

4.1 Introduction

Microchips used for the separation of biological molecules have gained much attention due to their distinct advantages, such as fast analysis, small sample consumption, separation and detection in a single device, etc.[1] Separation processes mainly based on electrophoresis have been performed in open microchannels for biomolecular separations.[2, 3] Since chromatography is the most versatile and reliable method for protein separations, much effort has centered on introducing stationary phases in the channels. Packing the channel with particles and fabricating retaining frits in a chip is extremely difficult.[4] Chromatography in open channels with surface polymerized channel walls suffers from low surface area and, hence, low loading capacity.[3] Preparation of polymeric monoliths in chips for electrochromatography and pressure-driven chromatography can provide separations approaching those based on capillaries.[5-9]

The major interest in biological analysis is protein separation and identification, since proteins are related to many biological functions, such as cellular conditions, disease states, and environmental conditions (e.g., temperature, stress, medicines, and nutrients). Protein misfolding leads to a large number of known diseases such as Alzheimer's disease, phenylketonuria, Parkinson's disease, familial neurohypophyseal diabetes insipidus, and short chain acyl-CoA dehydrogenase deficiency.[10, 11] Thus, studying targeted proteins is becoming important for clinical

assays and pharmaceutical development. Unfortunately, protein analysis is challenging because of the complex dynamic nature of proteins. The current, popularly used method for protein separation is two-dimensional gel electrophoresis,[12] which is labor intensive, difficult to automate, and impossible to interface directly with mass spectrometry. Therefore, a critical need for new techniques still exists for the separation of complex protein mixtures.

As introduced in Chapter 1, silicon,[13] polymers[14] and glass[15] are the three major substrate materials used for microfabrication. The early microdevices were fabricated from silicon because of its widespread use in the microelectronics industry, and successful fabrication techniques were established. However, because silicon is not transparent to visible or UV wavelengths for optical detection, it is used very infrequently for the fabrication of microchip separators today. Polymeric materials are popular for microfabrication since they offer attractive mechanical and chemical properties, low cost, ease of fabrication, biocompatibility, and high flexibility. However, most of the commercial polymers can adsorb biomolecules through hydrophobic, electrostatic or other interactions, leading to sample loss, analytical irreproducibility, and poor separation. This leaves glass as the dominant material for microfluidic device fabrication with good optical, mechanical, electrically insulating and thermal properties. Moreover, glass surfaces are easy to modify because surface chemistries have been well-established. Thermal bonding is usually used for glass microchip fabrication to seal a cover plate to a micromachined substrate for channel enclosure.

Peeni et al.[16, 17] developed a method using standard micromachining procedures and thin film technology to create open channel microfluidic devices on glass or quartz substrates, avoiding the very difficult step of sealing a cover plate on the substrate for channel enclosure. Capillary electrophoresis (CE) separations of amino acids and peptides in the sacrificial layer, planar (SLP) microchannel were reported. However, more advanced separations, e.g., capillary electrochromatography (CEC) would be possible if appropriate stationary phases could be prepared in the SLP channels.[18-30]

In this chapter, a negatively charged polymer monolith based on butyl methacrylate (BMA), ethylene glycol dimethacrylate (EDMA) and 2-acryloylamido-2-methylpropanesulfonic acid monomer (AMPS), was successfully prepared in glass SLP microchannls. Extraction of FITC (fluorescein 5-isothiocyanate) labeled phenylalanine was achieved with the monolithic SLP microfluidic device. CEC separation of FITC labeled glycine and FITC was demonstrated using the same monolithic stationary phase. Laser induced fluorescence (LIF) was used for detection.

4.2 Experimental

Channel fabrication. Figure 4.1 shows the basic steps used to create sacrificial layer, planar microchips in a true bottom-up fabrication procedure.[16, 31] First, glass wafers (Precision Glass & Optics, Santa Ana, CA) were coated with silicon dioxide layers using plasma enhanced chemical vapor deposition (PECVD; SHS Equipment, Milpitas, CA) at approximately 250 °C. Then, a thin layer of sacrificial material,

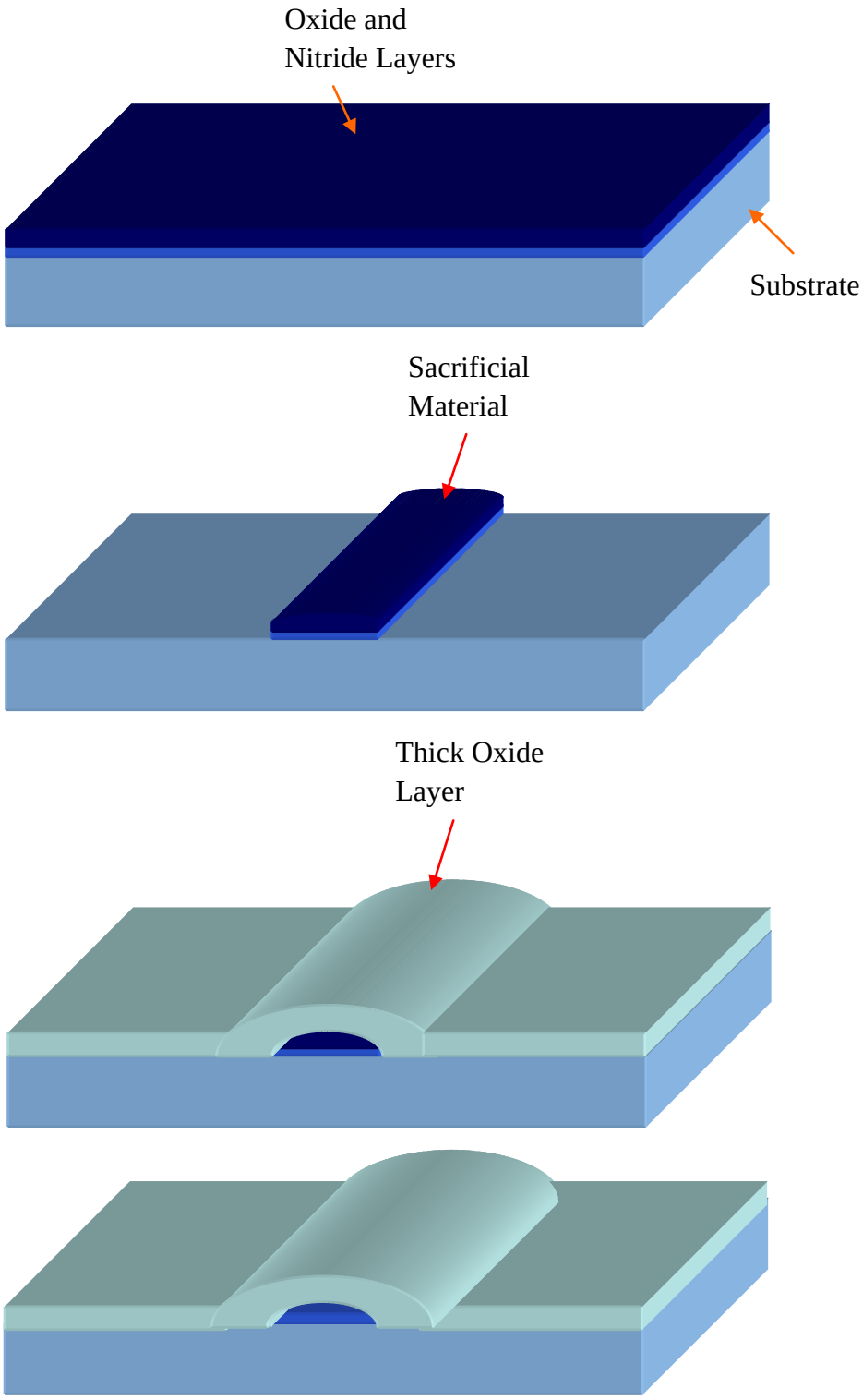

Figure 4.1. Fabrication steps used to create microfluidic channels based on removal of a sacrificial core.

aluminum, was deposited and defined into a thin layer using photolithography and etching. Third, a layer of PECVD deposited silicon dioxide was coated over the sacrificial material. The final step involved removing the sacrificial material in 2:1 HCl/HNO_3 at 80 °C for ~ 60 h and the remaining photoresist in Nano-strip (Rockwood Electronic Materials, Fremont, CA) for 2-3 h at 60 °C. As a result, a hollow tube with silicon dioxide walls was created. The resultant hollow channels with off-set cross fluid structure, 3.5 ~ 4 μm in height and 8 ~ 9 μm in width, are shown in Figure 4.2 from the top view. Once the channels were prepared, reservoirs were created by cutting cylinders of 2.1 mm internal diameter from a 1/4 inch poly(methylmethacrylate) (PMMA) sheet using a laser cutter (Universal Laser Systems, Scottsdale, AZ). Because the PMMA sheet had already been attached with double-stick tape (3M, Canoga Park, CA) before cutting, the created cylinders could be attached to the surface at the ends of the channels as reservoirs to provide access for sample injection and voltage application during experiments. A schematic of the separation device is shown in Figure 4.3.

Surface modification. Monoliths cannot be attached to the surface of the glass channels unless they are modified. Before surface treatment, a procedure to clean the glass microdevices was used. The microchips were placed in hot piranha for 4 h, then in hot water for approximately 4 h. After drying with air pressure, they were placed in 5 M acetic acid for approximately 1 h, then in deionized water overnight and finally dried with air pressure. A solution containing 0.4% TPM in a 50:50

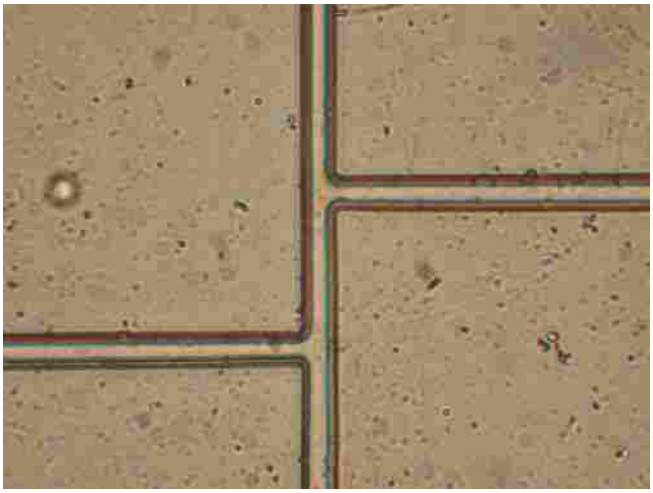

Figure 4.2. Top view optical micrograph of off-set cross fluidic channel structure built using sacrificial core etching.

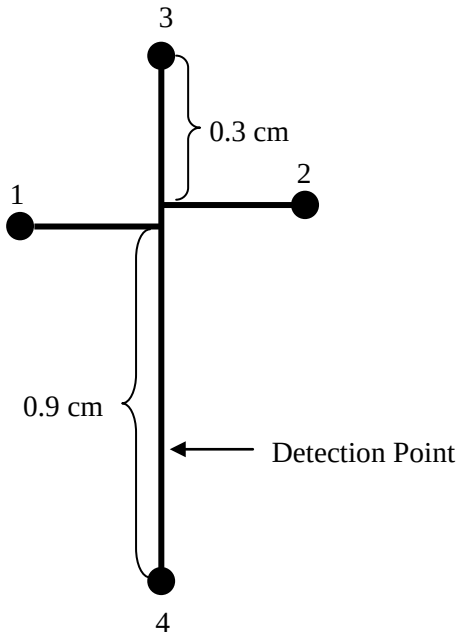

Figure 4.3. Schematic of an SLP separation device (the height of the channel was between 3.5 ~ 4 μm and the width was between 8 ~ 9 μm).

mixture of H_2O/ethanol was introduced to react with the Si-OH groups on the channel walls to produce double bonds.

Preparation of monolithic structures. The components in the prepolymer solution to synthesize the monolith and their concentrations were 0.40 % DMPA (2,2-dimethoxy-2-phenyl-acetophenone), 15.9 % EDMA, 22.9 % BMA, 1.00 % AMPS, 5.98 % Tris buffer (50 mM, pH 8.2), 23.9 % methanol, and 29.9 % 1-propanol. Generally, to prepare the monolith, all components were mixed together, degassed for approximately 30 s until the mixture was clear, and introduced into the surface functionalized microchips by capillary action (or vacuum or pressure). Then the microchip was exposed to UV light for approximately 10 min for polymerization with four aluminum caps covering the reservoirs to preventing monolith formation in the reservoirs. High voltage (600 V) and a buffer with 1:9 acetonitrile/50 mM phosphate (pH 7.5), were applied to flush the porogens, methanol and 1-propanol, and prepolymer residues from the channels. As a result, a negatively charged polymeric monolith was synthesized in the microchannel.

Amino acid extraction. Phenylalanine (Phe) was fluorescently labeled using fluorescein-5-isothiocyanate (FITC). A 200 µL volume of 6 mM FITC in dimethyl sulfoxide (DMSO) was combined with 600 µL of a 3 mM aqueous solution of Phe. The solution was maintained in the dark at room temperature for 4 days. A single separation channel was used to demonstrate extraction. First**,** fluorescein sodium salt was used to evaluate the flow in the through pores. Then, 10 µL of FITC-labeled Phe diluted to 870 µM in 1:9 acetonitrile/50 mM phosphate buffer (pH 7.5) was extracted.

Phosphate buffer was used to flush the microchannel for approximately 1 h, and finally 7:3 acetonitrile/50 mM phosphate buffer (pH 7.5) was applied to elute the extracted analyte.

Amino acid elution. Glycine (Gly) was fluorescently labeled with FITC based on the same procedure for Phe. The sample was prepared from 10 μL of FITC-labeled Gly diluted to 870 μM in 1:9 acetonitrile/50 mM phosphate buffer (pH 7.5). An SLP device as shown in Figure 4.3 was applied to perform CEC. A mixture of FITC-labeled glycine and FITC was separated using the negatively charged monolithic channel.

4.3 Results and Discussion

Reservoirs. Although a cover plate was not required with the SLP microfluidic devices, matching reservoirs were required to provide access for sample injection and voltage application. Several approaches were tried to find appropriate reservoirs for SLP devices. Considering that substrates for SLP devices are typically quartz or glass, a method to chemically bond glass reservoirs on the devices was investigated. Glass tubes with 2.0-5.0 mm inner diameters and 4.0 mm in height were prepared. Both glass tube and glass microdevice surfaces were first cleaned with acetone and placed in 0.2 M NaOH and then 0.2 M HCl for maximizing the concentration of hydroxyl groups. These hydroxyl groups were reacted with 3-(trimethoxysilyl)propylmethacrylate (TPM) to provide double bonds on the glass surface. A monomer, 1,1,1-trimethylolpropane trimethacrylate, was finally

polymerized between the reservoir and the glass surface under UV light for approximately 10 min. Figure 4.4 shows a microdevice with strongly bonded reservoirs which resisted most organic solvents, such as ethanol, acetone and toluene. This method provided strong reservoirs for devices; however, careful attention was required to avoid sealing the openings of the channels during polymerization. Hence, an easier method, i.e., PMMA cylinders and double-stick tape, for attaching reservoirs to glass devices that can be used with aqueous solutions and a variety of organic solvents was preferred. When PMMA reservoirs were attached to quartz substrates, the substrate was placed on a hot plate and a little acetonitrile was introduced around the base of each reservoir to enhance adhesion.

Morphology of monolithic structures. The recipe for the monolith that was to be introduced into the SLP channels was first studied in 75 and 5 μm i.d. fused silica capillaries. After a desirable monolith structure was obtained in a 5 μm i.d capillary, the procedure was then transferred to SLP microchannels. Figure 4.5 shows an SLP microchannel filled with the negatively charged monolith. Due to the magnification limitation of the microscope, a clear structure of the monolith cannot be seen. SEM images were obtained after the channel was carefully cut and the cross section was exposed. As is clearly shown in Figure 4.6, a monolith with canal-like micrometer-sized through-pores were formed and well attached to the walls of the SLP microchannel.

Choices of polymer monoliths. Before performing any separations, I investigated the theory of LC separations with the SLP devices based on an equation

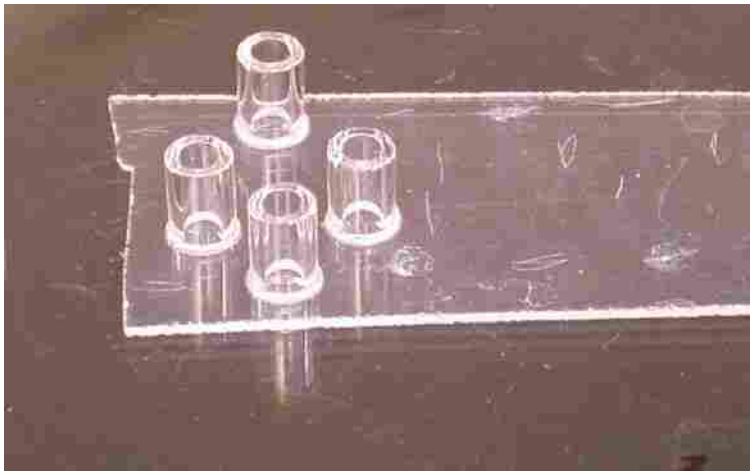

Figure 4.4. Glass reservoirs bonded on a glass microchannel device.

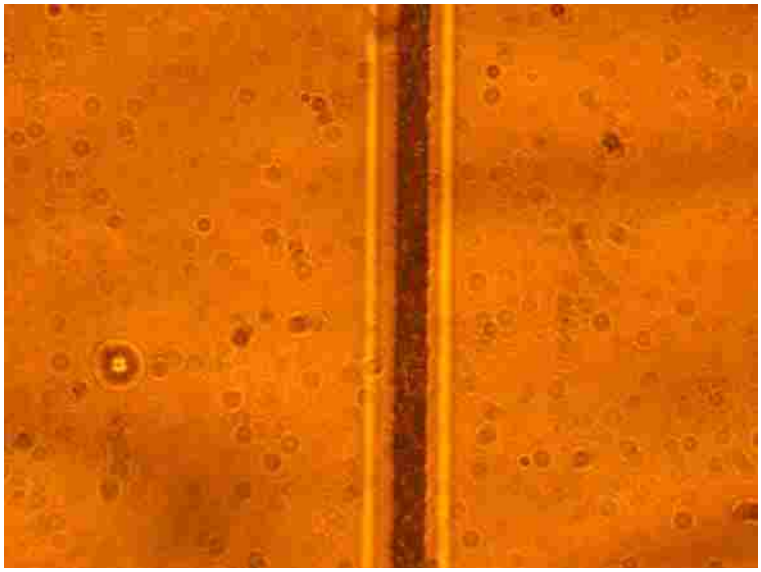

Figure 4.5. Microchannel filled with a negatively charged monolith on a glass substrate.

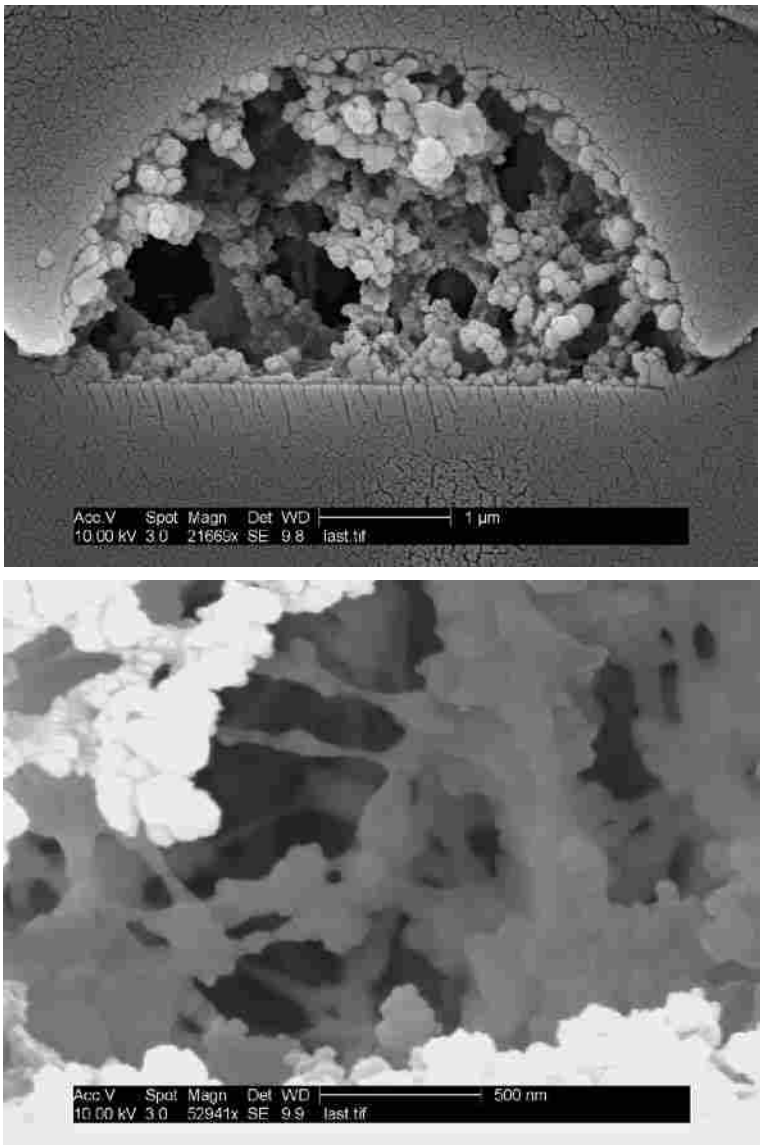

Figure 4.6. Scanning electron micrographs of a negatively charged monolith in the sacrificial layer, planar mcirochannels on a quartz substrate: (A) 21669× magnification; (B) 52941× magnification.

developed by Jorgenson et al. for LC in open-tubular columns (OTC):[32]

$$N_{\max} = \left[\frac{3P(1+k)t}{8\eta(1+6k+11k^2)} \right]^{\frac{1}{2}} \tag{4.1}$$

where N is the number of theoretical plates attainable with pressure and time restrictions, P is the applied pressure, k is the solute's retention factor, t is the retention time of the solute in the column, and η is the mobile phase viscosity. Also,

$$P_{\mathrm{OTC}} = \frac{8\eta \mathrm{L} \upsilon}{r^2} \tag{4.2}$$

where L is the column length, υ is the mobile phase velocity, and r is the column radius, and,

$$t = \frac{L}{\upsilon} \tag{4.3}$$

If we assume $k = 0$, then

$$N_{\max} = (\frac{3Pt}{8\eta})^{\frac{1}{2}} \tag{4.4}$$

Combining equations (4.2), (4.3) and (4.4), Equation (4.5) can be obtained:

$$N_{\max} = \sqrt{3}\frac{L}{r} \tag{4.5}$$

With the estimated dimensions of the SLP microfluidic channel as 1 cm in column length and 2.99 µm in column radius, calculations based on the above equations concerning the maximum number of theoretical plates and the required applied pressure indicated that an approximately 1 cm long separation channel was too short to provide a reasonable pressure-driven LC separation. Hence, I began to focus on CEC separations in the microchannels. Because electroosmotic flow (EOF) is required to drive the mobile phase in CEC separations, a neutral monolithic stationary phase would not work. When the pH of a solution is higher than 2, AMPS

(Figure 4.7) is ionized, producing sulfonic acid groups with negative charges. Therefore, AMPS was added to the prepolymer solution containing BMA and EDMA to add negative charges to the monoliths. The final optimum recipe was given in the experimental section. A simple CEC assembly as shown in Figure 4.8 was used to measure the flow rate of the mobile phase generated by the EOF. When a voltage of 1000 V was applied, a flow rate of 0.066 μL/min was obtained, which indicated the presence of a desirable EOF in the monolith.

Amino acid extraction using monolithic microchips. Figure 4.9 illustrates that the negatively charged monolith in the microchannel was capable of extracting amino acids. Figure 4.9 (A) shows the initial image of the microchannel filled with the monolith. Fluorescein sodium salt was used to illluminate the through pores of the monolith as expected in Figure 4.9 (B). A 10 μL volume of FITC-labeled phenylalanine (FITC-Phe) diluted to 870 μM in 1:9 acetonitrile/50 mM phosphate buffer (pH 7.5), was passed through the microchannel by applying 300 V, and FITC-Phe was extracted by the monolith as shown in Figure 4.9 (C). To show that FITC-Phe was strongly held, phosphate buffer was used to flush the microchannel for approximately 1 h. As is shown in Figure 4.9 (D), FITC-Phe remained in the channel. However, when eluent buffer was introduced (i.e., 7:3 acetonitrile/50 mM phosphate buffer, pH 7.5) to flush the microchannel, FITC-Phe was completely removed in approximately 30 min. All of the above experiments indicated that this monolith was able to successfully extract FITC-Phe with this type of microchip device. They also indicated the possibility of using monolithic microchannels to

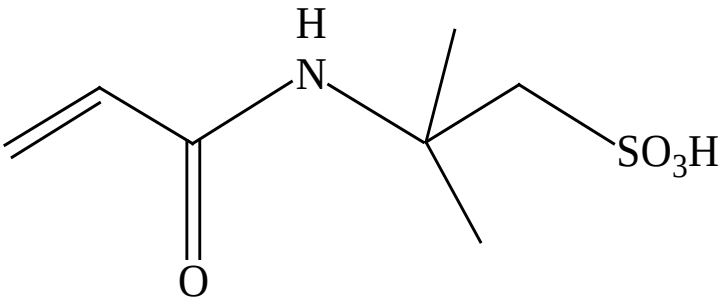

Figure 4.7. Chemical structure of AMPS.

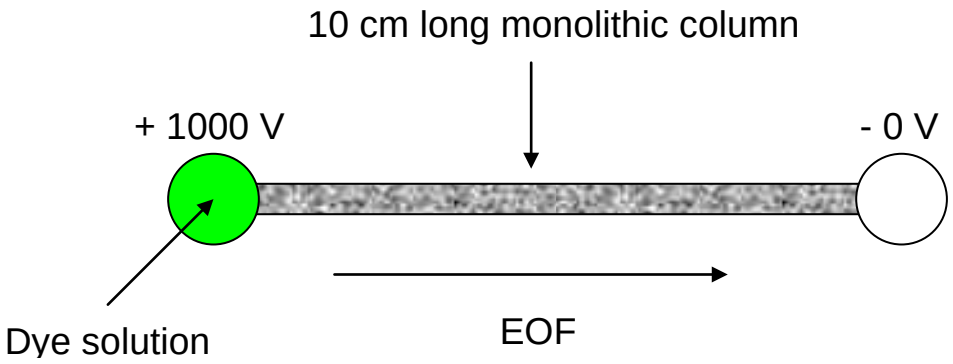

Figure 4.8. Schematic of a simple assembly for measuring the EOF of negatively charged monolithic columns (75 µm i.d.) based on BMA, EDMA and AMPS.

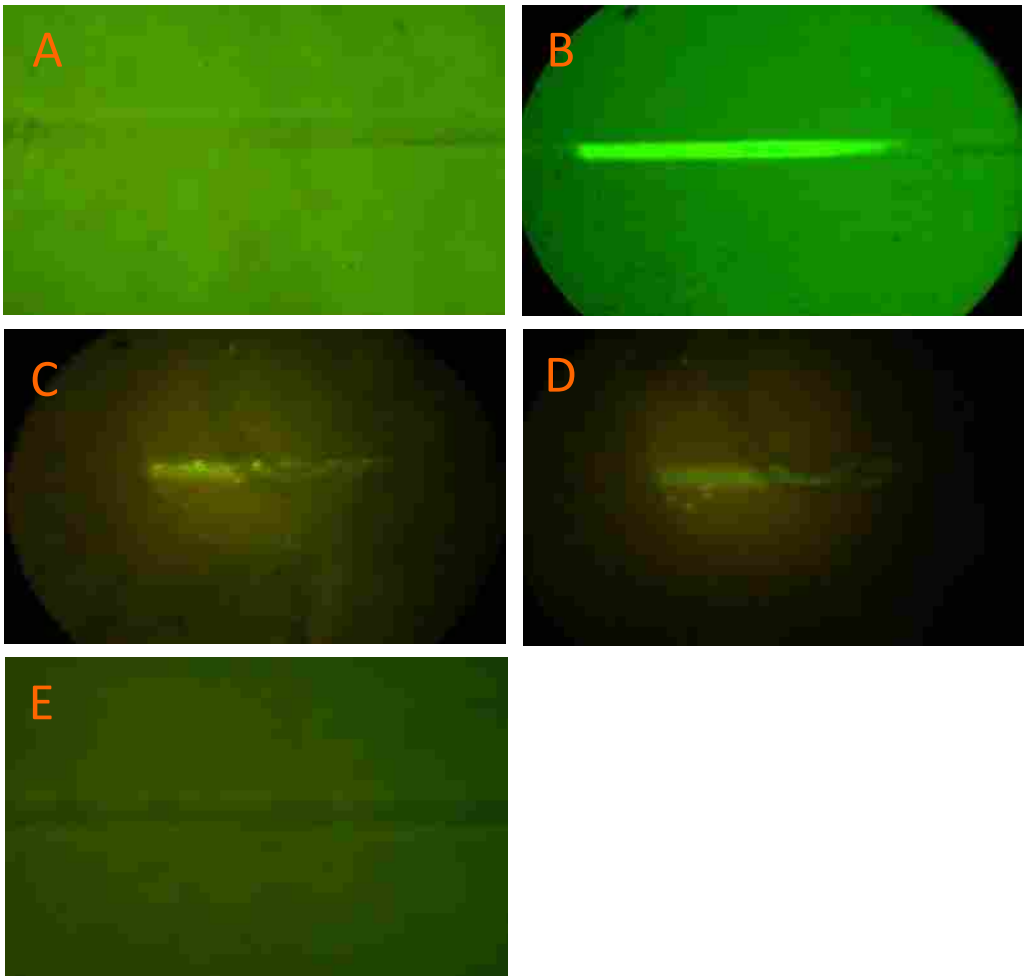

Figure 4.9. Photographs showing the extraction of FITC-labeled phenylalanine by a negatively charged monolith in a microchannel. (A) Initial image of the microchannel filled with the monolith, (B) buffer containing fluorescein sodium salt to illuminate the through pores of the monolith, (C) following the passage of 10 μL volume of FITC-labeled phenylalanine (Phe) diluted to 870 μM in 1:9 acetonitrile/50 mM phosphate buffer (pH 7.5), (D) Phe remaining in the channel following flushing with phosphate buffer for approximately 1 h, and (E) after complete removal of Phe after flushing with eluent buffer (i.e., 7:3 acetonitrile/50 mM phosphate buffer, pH 7.5) for approximately 30 min.

separate peptides and proteins.

Amino acid separation. Voltage schemes as shown in Figure 4.10 were applied to separate FITC-labeled glycine and FITC. Reservoir 1 was filled with sample solution, while reservoirs 2, 3 and 4 were filled with buffer solution. To inject the sample into the channel, reservoirs 1, 3, 4 were grounded and -600 V was applied to reservoir 2. Figure 4.11 shows a fluorescence image of the sample in the injection mode. The loaded sample was then separated by applying -600 V to reservoirs 1 and 2, -1000 V to reservoir 4, and grounding reservoir 3. Figure 4.12 presents the fluorescence image of the sample caught by LIF as the sample moved through the separation channel. Figure 4.13 shows a separation obtained using the SLP device. However, the background noise was high and the signal was relatively weak. Possible reasons for this are too low sample concentration, photobleaching, low PMT sensitivity, or the shape and position of the focused spot in the channel.

4.4 Conclusions

Sacrificial layer, planar microchips were successfully fabricated on glass substrates through photolithographic techniques. Different methods for attaching plastic or glass reservoirs on the microchips to provide access for sample injection and voltage application were studied. Due to the presence of silanol groups on the silica glass surface, the walls of the glass microchip were able to be treated with TPM to provide double bonds for monolith attachment. AMPS was added to neutral monolith reagents to generate negative sulfonic acid groups to provide electroosmotic flow, which avoided the requirement of exceptionally high pressure

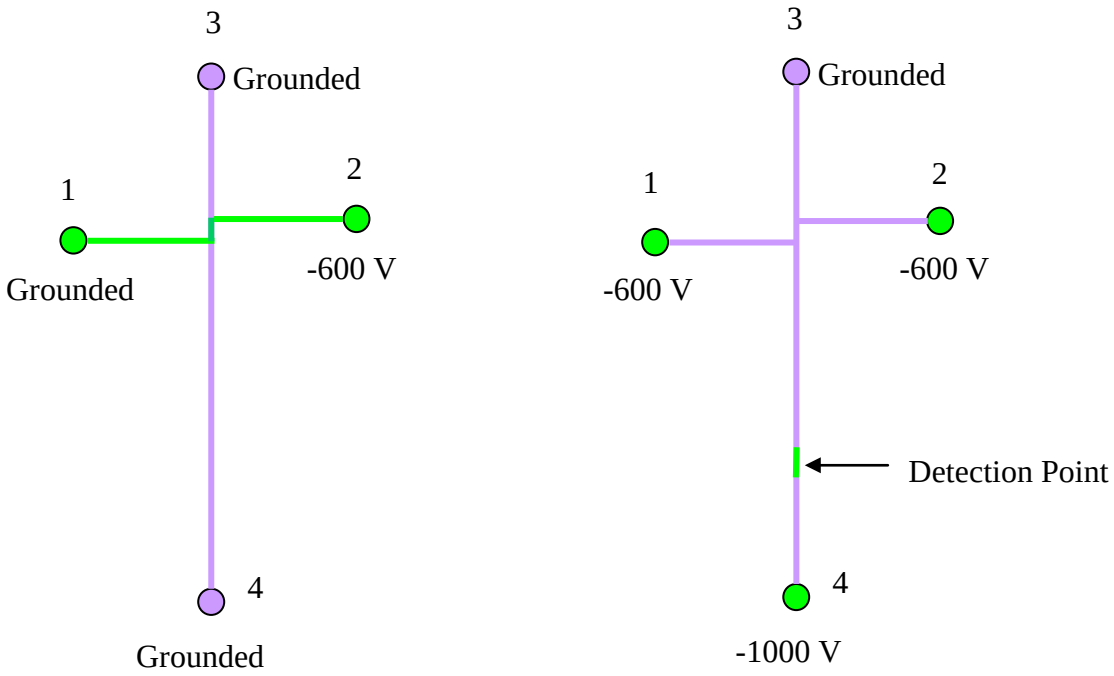

Figure 4.10. Applied voltage schemes for sample injection mode (left) and separation mode (right).

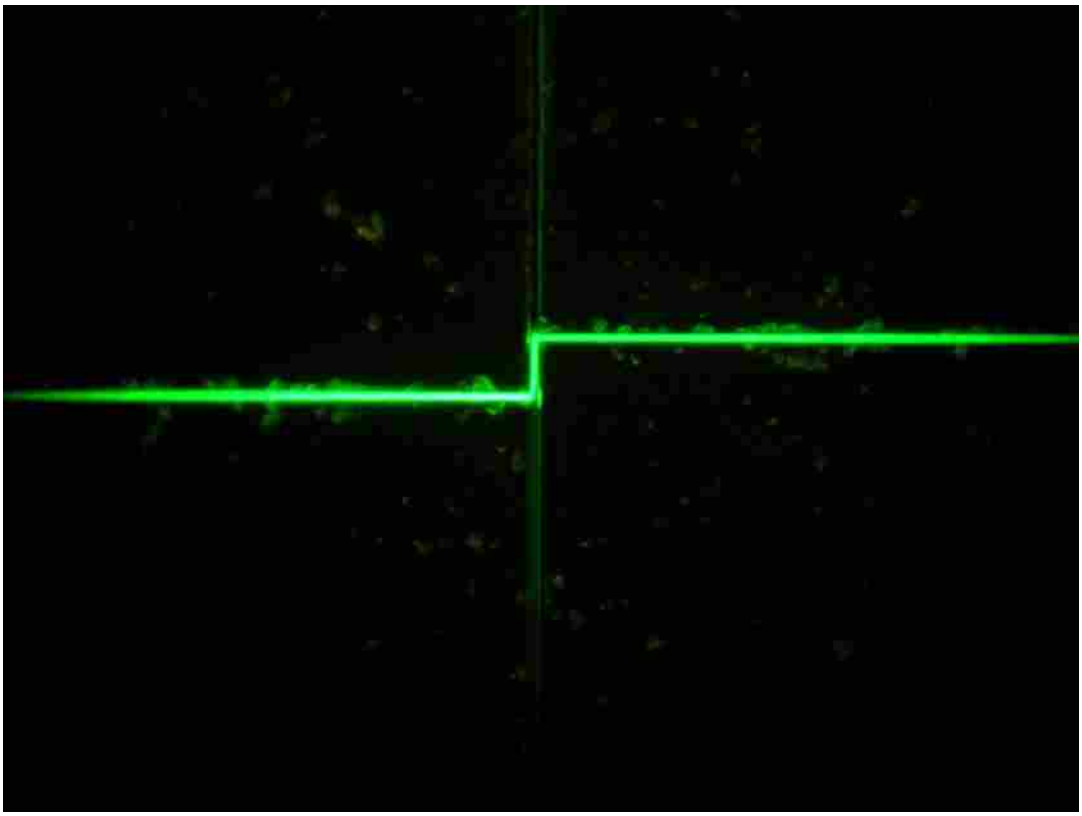

Figure 4.11. Fluorescence image of the sample in the injection region.

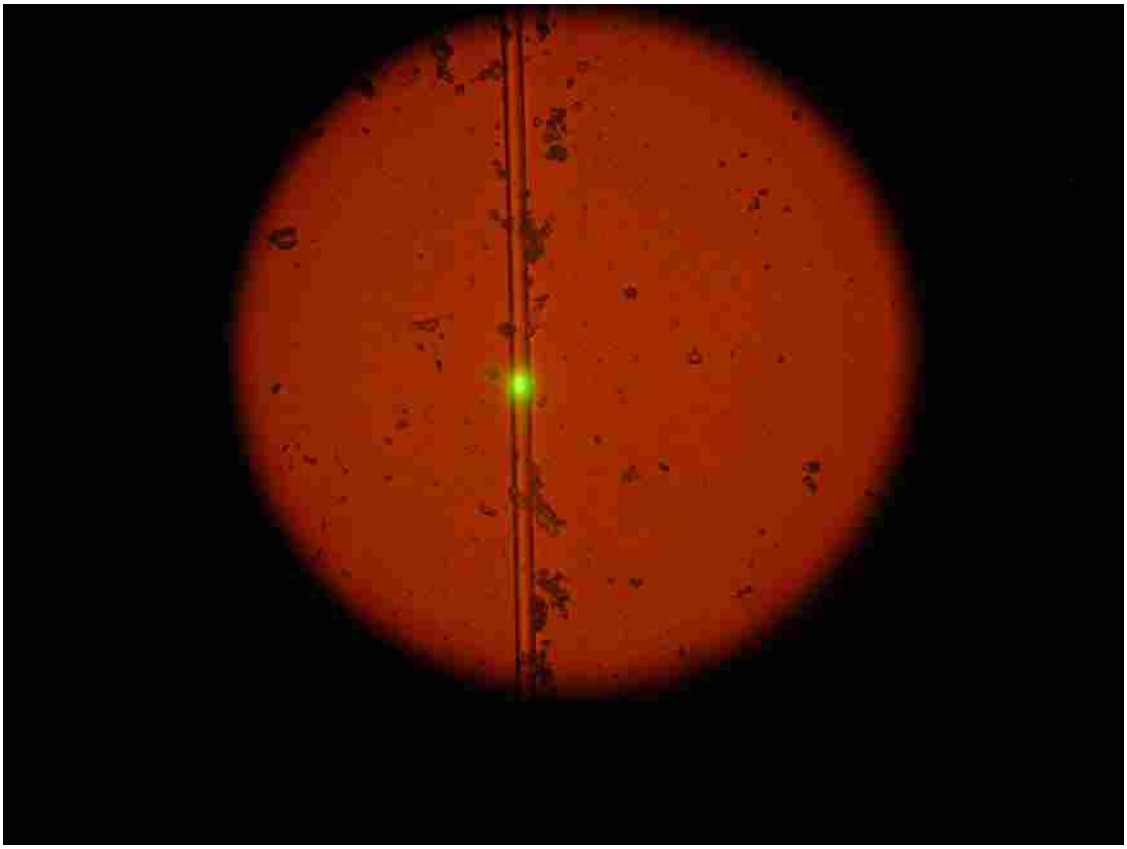

Figure 4.12. On-device point detection using laser induced fluorescence (LIF).

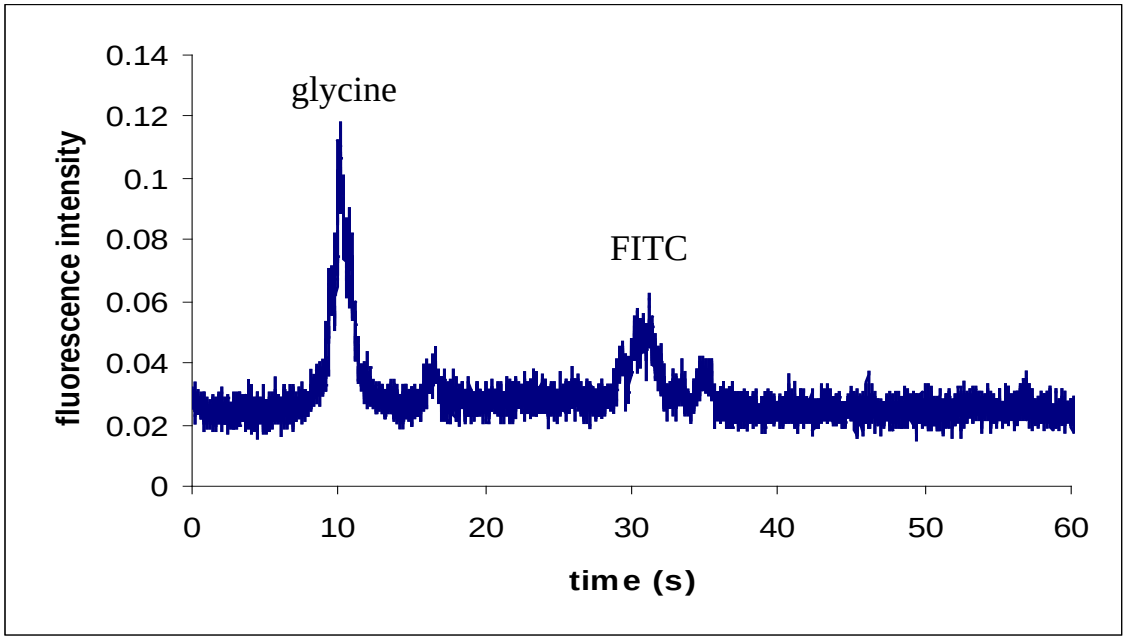

Figure 4.13. CEC separation using a monolithic SLP microchip [1:9 v/v CH_3CN/phosphate buffer (50 mM, pH 7.5)].

to force the mobile phase through the small dimension microchannels. The extraction of Phe using this monolithic channel illustrated the possibility of further separations. A preliminary CEC separation of a mixture of FITC-labled Gly and FITC was achieved. Further optimization of experimental conditions should allow advanced separations on more complicated systems using sacrificial layer, planar microchip channels filled with negatively charged methacrylate monoliths.

4.5 References

1. Reyers, D. R.; Iossifidis, D.; Auroux, P. A.; Manz, A. *Anal. Chem.* **2002**, *74*, 2623-2636.
2. Jacobson, S. C.; Hergenrőder, R.; Koutny, L. B.; Ramsey J. M. *Anal. Chem.* **1994**, *66*, 2369-2373.
3. Gottschlich, N.; Jacobsen, S. C.; Culbertson, C. T.; Ramsey, J. M. *Anal. Chem.* **2001**, *73*, 2669-2674.
4. Ocvirk, G.; Verpoorte, E.; Manz, A.; Grasserbauer, M.; Widmer, H. M. *Anal. Methods Instrum.* **1995,** *2*, 74-82.
5. Ericson, C.; Holm, J.; Ericson, T.; Hjerten, S. *Anal. Chem.* **2000**, *72*, 81-87.
6. Sun, X; Yan, J.; Yang, X.; Wang, E. *Electrophoresis* **2004**, *25*, 3455-3460.
7. Woolley, A.T.; Mathies, R. A. *Proc. Natl. Acad. Sci. USA*, **1994**, *19*, 11348-11352.
8. Xie, J.; Miao, Y.; Shih, J.; He, Q.; Liu, J.; Tai, Y.; Lee, T. D. *Anal. Chem.* **2004**, *76*, 3756-3763.
9. Stachowiak, T. B.; Mair, D. A.; Holden, T. G.; Lee, L. J.; Svec, F.; Fréchet, J. M. J. *J. Sep. Sci.* **2007**, *30*, 1088-1093.
10. Bucciantini, M.; Giannoni, E.; Chiti, F.; Baroni, F.; Formigli, L.; Zurdo, J.; Taddei, N.; Ramponi, G.; Dobson, C. M.; Stefani, M. *Nature* **2002**, *416***,** 507-511.
11. Iberer, G.; Hahn, R.; Jungbauer, A. *LC-GC* **1999**, *17*, 998-1005.

12. Gorg, A.; Obermaier, C.; Boguth, G.; Harder, A.; Scheibe, B.; Wildgruber, R.; Weiss, W. *Electrophoresis* **2000**, *21*, 1037-1053.

13. Lambertus, G.R.; Fix, C.S.; Reidy, S.M.; Miller, R.A.; Wheeler, D.; Nazarov, E.; Sacks, R. *Anal. Chem.* **2005**, *77*, 7563-7571.

14. Liu, J., Sun, X., Lee, M. L. *Anal. Chem*. **2005,** *77*, 6280-6287.

15. Harrison, D. J.; Manz, A.; Fan, Z.; Ludi, H.; Widmer, H. M. *Anal. Chem.* **1992**, *64*, 1926-1932.

16. Peeni, B. A.; Conkey, D. B.; Barber, J. P.; Kelly, R.; Lee, M. L.; Woolley, A. T.; Hawkins, A. R. *Lab on a Chip*. **2005**, *5*, 501-505.

17. Peeni, B. A.; Lee, M. L.; Hawkins, A. R.; Woolley, A. T.; *Electrophoresis* **2006**, *27*, 4888-4895.

18. Fields, S. M. *Anal. Chem.* **1996**, *68*, 2709-2712.

19. Minakuchi, H.; Nakanishi, K.; Soga, N.; Ishizuka, N.; Tanaka, N. *Anal. Chem.* **1996**, *68*, 3498-3501.

20. Dulay, M. T.; Kulkarni, R. P.; Zare, R. N. *Anal. Chem.* **1998**, *70*, 5103-5107.

21. Asiaie, R.; Huang, X.; Farnan, D.; Horvath, C. *J. Chromatogr. A* **1998,** *806*, 251-263.

22. Tang, Q.; Lee, M. L. *J. High Resolut. Chromatogr*. **2000**, *23*, 72-80.

23. Hjerten, S.; Liao, J. L.; Zhang, R. *J. Chromatogr*. **1989,** *473*, 273-275.

24. Svec, F.; Frechet, J. M. *Anal. Chem.* **1992**, *64*, 820-822.

25. Ro, K. W.; Liu, J.; Knapp, D. R. *J. Chromatogr. A* **2006,** *1111*, 40-47.

26. Ngola, S. M.; Fintschenko, Y.; Choi, W. Y.; Shepodd, T. J. *Anal. Chem.* **2001**, *73*, 849-856.

27. Palm, A.; Novotny, M. V. *Anal. Chem.* **1997**, *69*, 4499-4507.

28. Rohr, T.; Hilder, E. F.; Donovan, J. J.; Svec, F.; Fréchet, J. M. J. *Macromolecules* **2003**, *36*, 1677-1684.

29. Vidič, J.; Podgornik, A.; Štrancar, A. *J. Chromatogr. A* **2005,** *1065*, 51-58.

30. Courtois, J.; Szumski, M.; Byström, E.; Iwasiewicz, A.; Shchukarev, A.; Irgum, K. *J. Sep. Sci.* **2006,** *29*, 14-24.

31. Schemidt, H.; Yin, D.; Barber, J. P.; Hawkins, A. R. *IEEE Journal of Selected Topics in Quantum Electronics*. **2005**, *11(2)*, 519-527.

32. Jorgenson, J. W.; Guthrie, E. J. *J. Chromatogr.***1983**, *255*, 335-348.

CHAPTER 5 FUTURE DIRECTIONS

5.1 Effect of Column Diameters Larger than 250 μm on Pore Properties of Polymeric Monolithic Capillary Columns Determined by CFP

The structure of a monolith highly depends on the irradiation UV light wavelength and intensity (for organic polymeric monoliths), polymerization temperature and the initial composition of the prepolymer mixture. The initial composition of the prepolymer mixture decides the basic properties of the monolith. The UV light and/or temperature controls the decomposition rate of the initiator and, as a result, the pore properties of the monolith. In addition, polymerization is typically an exothermic process and heat is released during preparation of monoliths even if initiated by UV radiation. Better heat dissipation is obtained in smaller inner diameter columns. Therefore, larger pore size forms in columns with smaller inner diameter. This phenomenon is well known as the temperature effect in monolithic polymerization.[1]

However, as reported in Chapter 3, while a butyl methacrylate (BMA) and poly(ethylene glycol) diacrylate (PEGDA) based monolith was prepared in capillary columns with inner diameters from 50 to 250 μm, similar pore size distributions were determined using CFP. Similar pore morphologies were visualized from their SEM images as well. This is due to only a very moderate temperature effect on pore size in columns with inner diameters in the μm dimensions, as indicated in Figure 3.3.

Theoretically, the temperature effect should become more significant as the inner diameter of the columns increase. To determine the extent of this potential problem,

BMA and PEGDA based monoliths should be prepared in columns with inner diameters larger than 250 μm, and their pore size distributions determined using CFP. The columns tested should extend beyond the capillary dimensions, since larger diameter monoliths are useful in conventional LC. Testing larger diameter columns with CFP should not be a problem since the home-made CFP is flexible and can be adapted to tubes with different diameters.

So far, it is still not completely conclusive that different prepolymer reagents have the same curve shapes as shown in Figure 3.3, or the same temperature at which the temperature effect starts to be significant. Hence, a comparison should be made for a variety of polymeric monoliths with different inner diameters. CFP should be applied to obtain their respective pore size distributions.

Studies described in the previous chapters demonstrated that SEM images are not reliable for determining the detailed differences in pore properties of monoliths. However, in some cases, differences could be directly visualized when they were obvious; for example, the SEM images of silica monoliths synthesized in capillaries and in bulk shown in Figure 2.10. The silica monoliths prepared in bulk could be considered as prepared in a column with unlimited inner diameter. Because there was a large dimensional difference between the capillaries and the unlimited diameter bulk monoliths, the temperature effect was very significant. Theoretically, similar SEM images should be observed for polymeric monoliths prepared in capillaries and in bulk. This is a study that should be pursued in detail, since on one hand it would verify the temperature effect in the polymerization of polymeric monoliths, and on the

other hand, it would further prove that representative results cannot be provided on the pore properties of a monolith when determined in bulk using BET or MIP.[2-4]

5.2 Construction of an Automatically Controlled CFP System

As introduced in Chapter 2, a micro-flow meter made from a glass pipette was successfully used in CFP measurements. The detectable gas flow was as low as 10^{-6} mL/s, which was useful for initial pore size characterization of packed and monolithic capillary columns. However, an automated porometer would be much more practical for routine use.

For an automated CFP system, the flow meter should be electronically driven. Various flow meters are commercially available, however, one for measuring the gas flow rate from a short section of monolithic capillary should be very sensitive to extremely low flow rate, e.g., in the range of 10^{-6} ~ 10^{-3} mL/s. To date, I have not found a commercial flow meter that can reach this low range. This was found to be the main problem with a commercially available capillary flow porometer,[5] which resulted in its inability to characterize the pore size characteristics of capillary columns. Therefore, a low flow measurement device from a commercial supplier is desirable for the development of an advanced CFP system.

Software specifically written for a CFP instrument is necessary to automate the system. Automation would produce more reliable determinations. At the same time, the possibility of damaging the parts of the device by frequent handling would be avoided. The software could be used to automatically organize data in different formats, and compute the final results.

The software should basically include three components. One component would control the operation of the instrument. Users would set up the experimental conditions, including the determination method, e.g., dry up/wet up or dry up/wet down, etc.,[6] which kind of gas to provide flow, the specific wetting liquid and its surface tension parameters, the location where data will be saved, and in what format the data will be reported. The second component would be designed to set up the parameters of the device, and to reflect the electronic state of the device. The final component will be mainly for data manipulation and reporting.

The "Alicat" digital pressure controller as described in Chapter 2 was chosen as the pressure controller for the home-made CFP. Based on my extensive experience with this controller, I found that its speed, stability and repeatability are excellent, and its operation is very easy.

When the instrumentation is totally integrated together, it will need to be evaluated for accuracy, stability and repeatability.

5.3 CEC Separations of Amino Acids and Proteins in Monolithic Microchips

It was shown in Chapter 4 that the sacrificial layer, planar microchip filled with negatively charged polymeric monolith could be used for the extraction and separation of amino acids. This monolithic device should be applied for separation of more complicated samples, such as peptides and proteins.

However, preparing a perfect monolith in the silica microchannel is still a major challenge. The conditions for monolith growth should be optimized, including surface modification, photopolymerization time, flushing voltage, etc. The polymerization

time for synthesizing the negatively charged monolith was 10 min. Inhomogeneous monolith structures were observed at the ends of the column for both the capillary and microchip device due to porogen evaporation during the relatively long polymerization time. To avoid this problem, the monolith recipe should be adjusted to shorten the polymerization time by changing the porogens.[7] Actually, I have already found that only 3 min polymerization time is needed after decreasing the percentages of methanol and 1-propanol in the prepolymer mixture.

This sacrificial layer, planar microchip device with negatively charged monolith has two advantages: a unique, tiny micro-channel and an advanced, monolithic stationary phase for proteomics research. If this monolithic microchip could provide μCEC separations,[8-12] it would represent a significant advance in miniaturized separation systems.

5.4 References

1. Svec, F., Tennikova, T.B., Deyl, Z. Monolithic Materials: Preparation, Properties and Applications; Elsevier: Amsterdam, 2003.
2. Jr., F. V. W.; Bidlingmeyer, B. A. *Anal. Chem.* **1984**, *56*, 950-957.
3. Urban, J.; Eeltink, S.; Jandera, P.; Schoenmakers, P. J. *J. Chromatogr. A* **2008,** *1182*, 161-168.
4. Thommes, M.; Skudas, R. Unger, K. K.; Lubda, D. *J. Chromatogr. A* **2008,** *1191*, 57-66.
5. Jena, A. K.; Gupta, K. M. *J. Power Sources* **1999**, *80*, 46-52.
6. Gigova, A. *J. Power Sources* **2006**, *158*, 1054-1061.
7. Gu, B.; Li, Y.; Lee, M. L. *Anal. Chem.* **2007**, *79*, 5848-5855.
8. Throckmorton, D. J.; Shepodd, T. J.; Singh, A. K. *Anal. Chem.* **2002**, *74*, 784-789.
9. Matsuda, R.; Hayashi, Y.; Suzuki, T.; Saito, Y. *Fresenius J Anal. Chem.* **1993**, *347*, 225-229.
10. Logan, T. C.; Clark, D. S.; Stachowiak, T. B.; Svec, F.; Fréchet, M. J. *Anal. Chem.* **2007**, *79*, 6592-6598.
11. Zhang, L.; Ping, G.; Zhang, L.; Zhang, W.; Zhang, Y. *J. Sep. Sci.* **2003**, *26***,** 331-336.
12. Qu, Q.; Qu, R.; Xu, Q.; Wang, Y.; Wang, X.; He, Y. *J. Sep. Sci.* **2004**, *27***,** 725-728.